Anti-icing Properties of Polymer Composite Films
and
Aqueous Polymer Solutions

by

Bilge Ercan

A Thesis Submitted to the

Graduate School of Engineering

in Partial Fulfillment of the Requirements for

the Degree of

Master of Science

in

Materials Science and Engineering

Koç University

July 2013

Koç University

Graduate School of Sciences and Engineering

This is to certify that I have examined this copy of a master's thesis by

Bilge Ercan

and have found that it is complete and satisfactory in all respects,
and that any and all revisions required by the final
examining committee have been made.

Committee Members:

_____

A. Levent DEMİREL, Ph. D. (Advisor)

_____

Seda KIZILEL, Ph. D.

_____

Alkan KABAKÇIOĞLU, Ph. D.

Date: _____

"Knowledge may give weight, but accomplishments give luster, and many more people see than weigh."

-- Lord Chesterfield

To my parents,

Kudret Ercan & D. Ali Ercan

Abstract

Anti-icing solutions and coatings have been in great demand in applications which stimulated scientific studies to develop new material systems having anti-icing functionality and to understand their anti-icing mechanisms. Water soluble polymers are effective anti-icing agents for aqueous solutions. Nanoparticle/polymer composite coatings are good candidates for effective anti-icing functionality provided that they are hydrophobic and have surface roughness at different length scales.

We investigated the freezing and melting behavior of aqueous solutions of poly (ethylene glycol) (PEG) and poly (2-ethyl-2-oxazoline) (PEOx) by differential scanning calorimetry. The effect of polymer concentration (1-80 g/L) and molecular weight (2,000 – 400,000 g/mol) on the freezing/melting of aqueous solutions was reported. The melting of bound water was observed at ~ – 11 °C in PEG solutions. Higher molecular weight PEG samples were more effective in decreasing the onset temperature of melting of ice at 0 °C and in forming more frozen bound-water that melted around ~ – 8 °C. Bound water was also present in aqueous PEOx solutions, but did not freeze down to – 60 °C. A glass transition was observed at ~ – 26 °C in aqueous PEOx solutions which confirmed that bound water was not frozen. The strong amide dipoles of PEOx and the resulting strong hydrogen bonds between water molecules and PEOx are expected to be responsible for the observed phenomena.

In the second part of the thesis, hydrophobic silica nanoparticle/styrene-butadiene-styrene (SBS) block copolymer composites were prepared and the anti-icing functionality of their coatings was tested as a function of nanoparticle concentration. Nanoparticles caused surface morphology and surface wettability of SBS coatings to change gradually up to ~ 43% by mass above which the morphology and wettability were rather constant. The water droplets showed the longest freezing times on composite coatings whose composition was close ~ 43%, corresponding to the transition in surface morphology and wettability. The coating containing 43 % by mass nanoparticle showed the longest freezing delay of 3718 s and 980 s at – 4 °C and – 8 °C surface temperatures, respectively. The composite material was added into bitumen to give anti-icing functionality to bitumen. Modified bitumen coatings containing 20-30% nanoparticles also showed delayed freezing of water droplets on them at surface temperatures of – 8 °C and – 10 °C. The laboratory results are promising for obtaining modified bitumen that has anti-icing functionality and better mechanical properties.

Özet

Buzlanmayı engelleyen çözeltiler ve kaplamalar, yeni malzemelerin geliştirilmesini teşvik eden ve bilimsel çalışmalarca beslenen uygulamalarda çok önemli bir yer tutmaktadır. Suda çözünen polimerler etkili buzlanmayı engelleyen ajanlardır. Nanoparçacık/polimer kompozitler hidrofobik ve pürüzlü olmaları sayesinde buzlanmayı engelleyici kaplamalar için uygun adaylardır.

Suda çözünen polimerlerden polietilen glikol (PEG) ile poli (2-etil-2-oksazolin)'in (PEOx) suyun donma ve buzun erime davranışına olan etkisi diferansiyel taramalı kalorimetre (DSC) ile incelenmiştir. Polimer derişimi (1-80 g/L) ile molekül ağırlığının (2,000 – 400,000 g/Lmol) etkisi rapor edilmiştir. Polimere bağlı olan suyun erime sıcaklığı yaklaşık – 11 C'de gözlenmiştir. Yüksek molekül ağırlıklı PEG çözeltilerinin buzun donma noktasını geriye çekmede etkili oldukları ve de daha çok su tarafından bağlandıkları ve böylece yaklaşık – 8 °C'de erime piki gösterdikleri gözlemlenmiştir. PEOx'un sulu çözeltilerinde de bağlı suya rastlanmıştır. Ancak – 60 °C'ye kadar bağlı suyun donması görülmemiştir. – 26 °C'deki camsı geçiş sıcaklığının varlığı bağlı suyun donmadığına işaret etmektedir. PEOx'da bulunan kuvvetli amit dipolünün ve su molekülleri ile PEOx arasındaki kuvvetli hidrojen bağlarının varlığının gözlenen bu durumun kaynağı olduğu düşünülmektedir.

Tezin ikinci bölümünde hidrofobik silika nanoparçacık/stiren-bütadien-stiren (SBS) üçlü blok kopolimer kompozitler hazırlandı ve bu kaplamaların buzlanmayı engelleyici özellikleri nanoparçacık konsantrasyonunun bir fonksiyonu olarak incelendi. Nanoparçacık eklenmesi, kaplamaların yüzey morfolojilerini ve ıslanabilirliklerini % 43 nanoparçacık oranına kadar değiştirdi. Bu nanoparçacık yüzdesinden sonra yüzey morfolojisi ve ıslanabilirlik kısmen değişti. Damlatılan su damlacıkları, nanoparçacık yüzdesi ağırlıkça % 43 olan yüzey üzerinde en geç dondu. Donma süreleri – 4 ve – 8 °C yüzey sıcaklığında 3718 saniye ve 980 saniyedir. Daha sonra kompozit malzeme bitümen içine katılarak modifiye bitümen yüzeyler hazırlandı ve buzlanmayı geciktirici özellikleri incelendi. % 20-30 nanoparçacık içeren modifiye bitümen yüzeylerde de donma gecikmesi – 8 °C ve – 10 °C yüzey sıcaklıklarında görüldü. Bu laboratuar sonuçları buzlanmayı engelleyen ve daha iyi mekanik özelliklere sahip modifiye bitümen için umut vericidir.

ACKNOWLEDGEMENTS

Many individuals and friends have helped me in making this project a success. Pivotal in this role, was my advisor Prof. A. Levent Demirel who taught me literally being skeptic and helped me to develop the scientific thinking. His delicate balance of guiding the students without transforming them into order-taking robots always impressed me. I feel very lucky to have met him and have the opportunity to work with him.

I had pleasure to spend two years with my group members. We had very enjoyable moments together in the office. I thank them very much. Especially, H. Enis Karahan taught me the laboratory skills that would take years if I was alone. Without his assistance, my evolution would not be so fast. I also would like to thank Dr. Sanjay Latthe to show me how a person can be revolutionist of our times. Atilla Oğuz never showed a sign of displeasure when I gave him not-so-enjoyable-works. He always helped me whenever I needed him that's why I thank him a lot. Dr. Barış Yağcı was always eager to help when it comes to using instruments in KUYTAM. Yasemin Yar helped me to calibrate DSC. Caner Nazlı introduced me the basics of rheology and the usage of rheometer. I thank them all for their assistance.

I cannot skip my lifelong friend, Zeynep Ekicioğlu, for her support especially in my last year. Her joy of living and quick problem-solving ability motivated me and made daily problems easier to overcome. I thank her just being here.

TABLE of CONTENTS

LIST of TABLES

LIST of FIGURES

CHAPTER I

INTRODUCTION

1.1 Motivation and Objectives

Anti-icing coating is the term that is used for coatings capable of delaying and/or preventing ice formation on solid surfaces. Superhydrophobic surfaces have recently been proposed as anti-icing coatings [1], [2], [3], [4], [5], [6], [7]. These coatings have extremely high water repellency and this leads to rolling off water droplets on tilted surfaces. Since water cannot stay on the surface, ice cannot form easily at sub-zero temperatures. There is controversy on the relation between superhydrophobicity and icephobicity of coatings [8], [9]. Therefore, elucidating the factors such as humidity, surface and air temperature that affect icing on surfaces and finding the surface morphology-icing relation is of great importance to combat ice formation.

Inhibition of ice crystallization on surfaces is a recently proposed and passive method. There are more effective anti-icing mechanisms for aqueous solutions. In 1960's it was found that some proteins in Antarctic fishes' blood inhibit the growth of ice nucleation [10], [11]. Since that time other natural polymers have been found, analyzed [12], [13] and also the protein-like polymers have been synthesized [14], [15], [16]. However, the effect of synthetic polymers on the melting and freezing behavior of water is a rather new research area. Thus, elucidation of the effect of polymer addition on the freezing and melting behavior of water is of great importance to understand the icing mechanism.

In the light of these factors, the objectives of this project are

- To prepare polymer/nanoparticle composite coatings and characterize their anti-icing property,
- To develop test routes that are applicable for possible anti-icing coatings,
- To apply the coating to bitumen, main ingredient of road pavement,

- To study the melting and freezing behavior of water for two model systems such as aqueous solutions of PEG and PEOx.

1.2 Scope of the thesis

In Chapter 2, relevant literature will be reviewed. In Chapter 3, the materials, sample preparation methods and instruments will be described. In Chapter 4, the DSC investigation of aqueous solutions of PEG and PEOx, two model systems, in regard to their effect on melting and freezing will be discussed. The polymer/nanoparticle composites with and without bitumen inclusion and their anti-icing effect will be reported in Chapter 5. The conclusions of the thesis results will be presented in Chapter 6.

CHAPTER II

LITERATURE REVIEW

2.1 Anti-icing in Water

Ice formation is inhibited and/or delayed in water with various ways. The most traditional method is using salts and small molecules as freezing point depression agents. These agents decrease the freezing point by decreasing the chemical potential of water. The more solutes that are present in the liquid phase the more chemical potential of liquid decreases. As a result, lower temperatures are required to equate the chemical potential of the liquid and solid phases. The properties which do not depend on the identity of solute but the amount are called colligative properties.

In nature, animals and plants have developed ways to combat cold environments. Some specified serum proteins in Antarctic fishes' blood have been found to inhibit ice crystallization [10], [11], [17], [18], [19], [20], [21]. These proteins named as antifreeze proteins, AFPs, and antifreeze glycoproteins, AFP(G)s, depending on the chemical structure differences. Figure 2.1.1 shows the secondary structures of four types of AFPs and the primary structure of AFGP. As a primary protein structure of AF(G)Ps, the backbone is composed of an alanyl-alanyl-threonyl sequence with a disaccharide moiety attached to each threonyl residue [22]. On the other hand, AFPs can be divided into four groups; Type I, Type II, Type III and Type IV. Type I is an alanine-rich, α-helix protein: Type II has disulfide bridges and Type III does not have any distinguishing features of secondary structure or amino acid sequence. For Type IV, the elucidation of the structure has not been completed yet; however, it is almost certainly predicted to be a helix-bundle [23].

The mechanism of action of AFPs differs from freezing point depression caused by small molecules. AF(G)Ps specifically binds to the prism planes of ice and inhibits the growth of ice crystals whereas the addition of small molecules in water delays ice formation by decreasing the chemical potential of water. Figure 2.1.2 shows two mechanisms that have been proposed to elucidate binding to ice surface. They both have energy considerations but

differ in geometrical details. The step pinning model has been proposed by Raymond and Devries [19]. In this model AFPs bind across the ice surface. However in the Mattress model proposed by Knight and Devries [17], AFPs pin to ice surface perpendicularly and therefore inhibit the growth normal to the surface [17]. No matter how the pinning of AF(G)Ps on ice surfaces occurs, the depression of the freezing point of water is explained by the Kelvin effect. Because of the adsorption of AF(G)Ps on ice surfaces, the formation of ice is forced to grow between adsorbed AF(G)Ps. Increased curvature causes a higher ice/water interface area and consequently, increased interfacial tension determines lower cooling temperature than equilibrium freezing temperature. Since the AF(G)Ps do not affect the internal disintegration of ice, the melting point of ice stays unchanged (T_m). The difference between the melting point of ice (T_m) and the freezing point of water (T_f) is called as thermal hysteresis and is the primary manifestation of non-colligative freezing point depression [24]. Figure 2.1.3 shows the difference in colligative and non-colligative freezing point depression mechanism. Black line shows the melting and freezing temperatures in pure water. They are same and at 0 °C. Purple line shows colligative freezing point depression. The melting and freezing temperatures are again same however lower than 0 °C. Green line shows non-colligative freezing point depression. Because of AF(G)Ps' mechanism of action, the freezing point temperature decreases. However, the melting temperature is not affected. The gap between the melting and freezing temperatures are known as thermal hysteresis and shown as shaded area.

a)

b)

c)

d)

e)
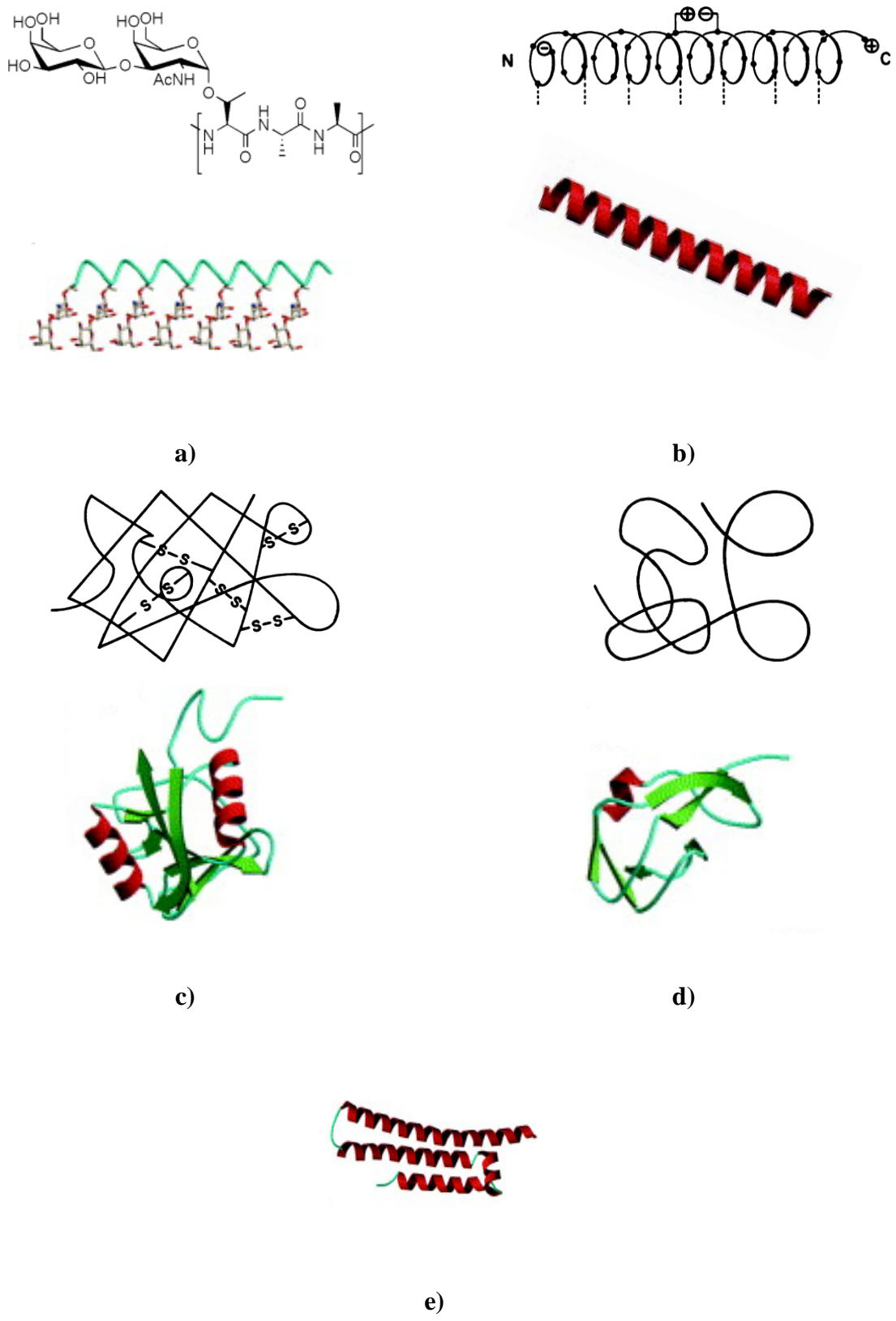
Figure 2.1.1 a) Primary protein structure of fish antifreeze proteins. AF(G)Ps [25] ,b) Type I AFP, c) Type II AFP, d) Type III AFP [13] and e) Type IV. Molscript illustrations were taken from [23].

a)

b)
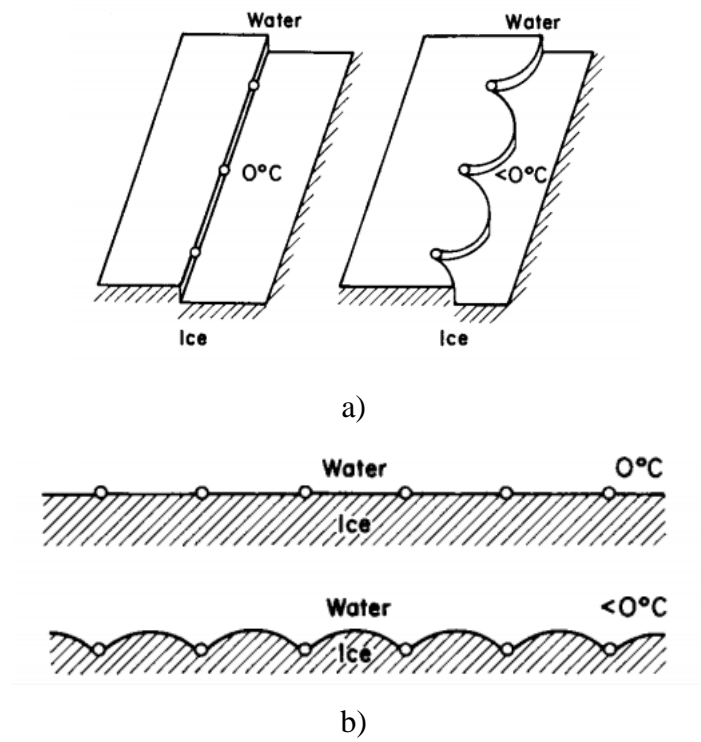
Figure 2.1.2 The mechanism of action of AF(G)Ps. a) Step pinning model and b) Matress model [17].
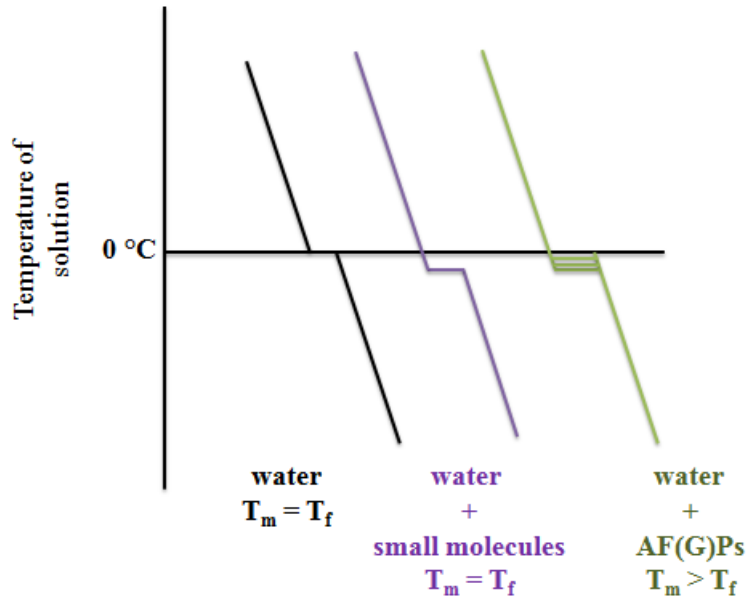
Figure 2.1.3 The melting point of ice and freezing point of water is same in water. Addition of small molecules decrease freezing and melting point temperature of water whereas AF(G)Ps only affect freezing point of water. Shaded area shows thermal hysteresis gap.

Although AF(G)Ps are very effective in terms of inhibiting the propagation of ice crystallization, purification and large scale preparation limit the possible application areas. Therefore synthetic water soluble polymers have been in use as synthetic ice blocking agents in cryopreservation, frozen foods and biological tissues [26][27]. On the contrary to salt mechanism to action, these polymers are thought to interact with water in a non-colligative manner as AFPs do. Succeeding titles will introduce the previous works on anti-icing property of water soluble polymers.

2.1.1 Aqueous solutions of synthetic polymers

Polyethylene glycol (PEG) is a water soluble, nonirritating, biocompatible and biodegradable polymer with low toxicity. Interaction of PEG with water at low temperatures has attracted great interest because of possible application areas such as food industry and pharmaceutics [28][29]. Anti-ice nucleation property of PEG has been recently reported only by one group [30].
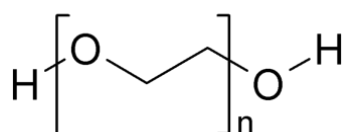
Figure 2.1.1.1 Chemical structure of polyethylene glycol

Huang et al. [31] investigated PEG-water interaction by differential scanning calorimetry, DSC, and compared solution properties of different molecular weight PEGs such as 400, 1540 and 70K . Samples were cooled to -120 °C and heated to 60 °C with 1 min/°C ramp time. At heating cycle step like deviation is observed for all molecular weights and attributed to glass transition. They have found that the peak temperature of melting endotherm is independent of system composition. They concluded that for the aqueous solutions of low molecular weight of PEG secondary endotherm is seen at much lower temperatures such as − 120 °C. Hydration number for EG units have been found as 1.6, 2.4 and 3.3 for samples with molecular weights of 400, 1540 and 70K, respectively. The reason of forming not stable PEG-water complex is that 1.6 water molecules per EG unit is smaller than the minimum hydration number of 2 for forming strong steric constraints.

In aqueous solutions of medium molecular weights of PEG it is assumed that helical structure of PEG is retained and it helps to form PEG-water complex. For the high molecular weights of PEG, most of the ordered crystalline structures are preserved and therefore PEG-water complex becomes stronger.

PEG is believed to decrease the nucleation temperature of ice because of its effect on diffusional motion of water [32]. In order to understand this Hilgren et al. [28] studied the aqueous solutions of PEG-6K at concentrations having 0.05-160 g/L by DSC. It has been found that moderate cooling rate and slow heating rate at DSC experiments revealed the most stable PEG-water complex. It also has been found that enthalpy of PEG-water complex at − 15 °C is dependent on the heating rate but not the cooling rate. They also calculated the amount of bound water for PEG-6K having > 10 g/L concentrations. It has been found that 1.7-2.7 water molecules bind to polymer at concentrations > 10 g/L. The melting temperatures of PEG-water complex have been found to decrease with increasing polymer concentration on the contrary to findings of Huang et al.

Vringer et al. [33] studied the aqueous solutions of PEG 1550 by DSC. The samples were cooled down to − 60 °C from 25 °C with 5 °C/min cooling rate and subsequently heated to 90 °C with 5 °C/min. For the PEG 1550 aqueous solutions the secondary melting endotherm was seen around − 16 °C. They concluded that two water molecules per ethylene glycol unit do not freeze until − 60 °C because they are bounded to etheric oxygen via hydrogen bonds.

2.2 Anti-icing on Surfaces

The development of the coatings which can impede or delay ice accretion on surfaces has been a challenge since ice affected human activity. It has been thought that water repellent coatings might be the solution to this problem. However, surface topography and the chemistry of these coatings differ from each other significantly and this leads to different mechanisms to impede ice formation and ice adhesion. In other words, these coatings show different behaviors in case of frost/ice formation and ice adhesion. While some papers separate frost from ice and evaluate the problem in this way, others merge these two terms and use "anti-ice/frost" to describe the properties of desired coating. Since people approach the icing problem from different perspectives it is appropriate to classify the cases into two groups. Those approaches mainly aim to impede frost/ ice formation and ice adhesion. In

succeeding titles we will point out the contradictions between findings and highlight pivotal experimental conditions.

2.2.1 Frost formation and droplet freezing

Frost is a form of ice that is formed when water vapor from saturated air deposit onto solid surfaces which have temperatures below the freezing point of water. Liu et al. [34] compare paraffin coated copper plate and bare copper plate. Static water contact angles of these surfaces are 133° and 63°, respectively. The researchers investigated different air, surface temperatures and relative humidity conditions. While large water droplets occur on hydrophilic surface, the first observable water droplets on hydrophobic surface are small. When room and surface temperature is 24 °C and -8 °C and the air relative humidity is 62%, water droplets on a hydrophobic surface become smaller and droplets freeze 60 s later than on a plain copper surface. When only the surface temperature is decreased, the freezing time of droplets decreases to 35 s from 60 s. Explanation for this phenomenon is that critical nucleate radius of ice will be smaller when the surface temperature is lower. This will lead to small potential barrier to exceed.

Even if there might be a difference in the freezing delay of droplets, once the frost formation begins and covers the whole surface, there is no difference between hydrophobic and hydrophilic surfaces. The surface chemistry is limited to initial period of frost formation. These findings are reasonable since homogenous nucleation theory says crystal will grow when its size is greater than critical radius. Potential barrier that must exceed is given as [34]

$$\Delta G_{c,vs} = \left[-\frac{4\pi r_{c,vs}^3 k T_w}{3\Omega_s ln\left(\frac{p}{p_{vs}}\right)} + 4\pi r_{c,sv}^2 \sigma_{vs} \right] f(\theta)$$

Where

$f(\theta) = (2 - 3cos\theta + cos^3\theta)/4$ And θ is contact angle between vapor and solid phases, σ_{vs} is interfacial energy between vapor and solid phases, Ω_s is volume of a single molecule, $r_{c,vs}$ is the critical radius , k is Boltzmann's constant, T_w is the wall temperature, p is the vapor pressure and p_{vs} is saturated vapor pressure corresponding to Tw. It is seen that water contact

angle determines the critical radius. However, it does not guarantee the complete prevention of frost on surfaces.

Liu et al. [35] investigate injected droplet behavior on superhydrophobic (obtained by fluorinated process of CF_4 plasma) and on plain copper surfaces. Contact angles of these surfaces are 162° and 72°, respectively. They perform same task as they did in [34] but now they study frost formation in detail. They observe 55 minutes freezing delay of water droplets on superhydrophobic surface. However, they are concerned mostly on formation direction of frost crystals. They found that the way that frost crystals begin to freeze is different than on a plain copper surface. Most of the frost crystals grow along the horizontal direction (dendritic grow) on a superhydrophobic surface instead of the normal vertical direction (normal to the surface) as those on the plain copper surface. The explanation for this dendritic grow is thawing of frost crystals on the upper part of the droplet. Because they can easily affect from air perturbations, frost crystals on upper part of droplets thaw. Additionally, these thawed crystals fall on lower parts and later these crystals can connect with each other and result in dendritic growth. Another proposed explanation for this peculiar growth is it may be related to the fact that water molecules are of strong polarity and the electric charge distribution is non-uniform on an isolated conductor surface. In their previous work, Lie et al. investigate the frost formation of condensed droplets. However, in this study they look at frost formation on droplets and on the surface.

Wang et al. [36] focus on the frost formation on the surfaces with different hydrophobicity. $CaCO_3$ is modified with FAS-17. These nano $CaCO_3$ aggregates form micro roughness on polyacrylate, the binding agent, and FAS-17 provides hydrophobicity. The water contact angle of plain copper surface is 64° and of superhydrophobic surface is 155°. Initial frost on this surface is observed after 50 s whereas a longer time is required for forming the initial frosts on a more hydrophobic surface. When the position of coating is tilted, water droplets cannot condense on the surface and this leads to better anti-frost performance. The researchers conclude that, due to this performance, superhydrophobic coatings are suitable for anti-frost purposes. However, they point out that the plain copper surface is covered completely by irregular small dots whereas the hydrophobic surface (water contact angle is 120°), which they prepared separately from the superhydrophobic surface, is covered by large sized droplets. This observation is contradictory to the Liu et al. observations in which large droplets occur on the hydrophilic surface.

He et al. [37] find a correlation between oscillation of wettability and frost formation on superhydrophobic and hydrophobic films. The samples are superhydrophobic and hydrophobic i-PP films and static water contact angles are 155.3° and 98.1°, respectively. Freezing experiments are carried out at temperature of -10 °C and a relative humidity of 50%. They observed that due to the merging process of droplets, the droplet size increases more than those on hydrophobic surface. Additionally, the condensed droplets on the superhydrophobic surface freeze later. The authors point out that, the water contact angle decreases steadily with the growth of the condensed droplet on the hydrophobic surface whereas oscillatory behavior shows on superhydrophobic surfaces. Since both films are made of i-PP, this peculiar behavior cannot be explained by surface chemistry. The hydrophobic film has a flat surface. When the temperature is -10 °C, beside large condensed droplets, many micro droplets are formed on the surface as seen in Figure 2.2.1.1. These micro droplets can coalescence with condensed drop. As this coalescence continues the volume of the coalesced droplet cannot be large enough to keep its constant CA.
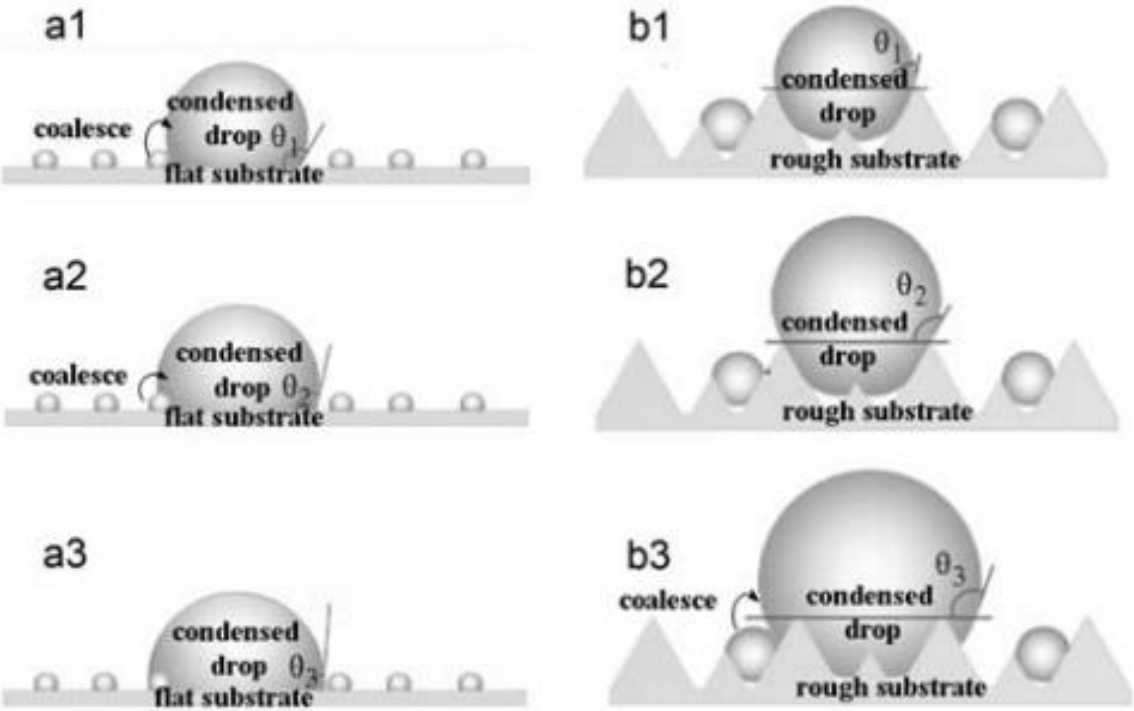
Figure 2.2.1.1 Coalescence behavior of hydrophobic and superhydrophobic films. [37]

Since superhydrophobic film has surface composed of micro and nano asperities micro droplets cannot coalescence with condensed drop until it becomes large enough to meet them. The process from b1 to b3 in Figure 2.2.1.1 results in oscillation in the water contact angle. The three phase line which also affects contact angle hysteresis of surfaces are different from each other. The hydrophobic surface has an unstable three phase line whereas the three phase line of superhydrophobic surface is metastable which leads to freezing delay.

He et al. [3] prepare ZnO nanorod arrays and investigate both macro and micro sized droplets on these surfaces below freezing point. Most superhydrophobic surfaces lose their ability when the temperature is below the freezing point due to water condensation. Condensed water layers formed on tops of asperities and some liquid penetrates into air gaps among nanostructures. As a result, the increment of the contact area between the measuring droplets and condensed water causes the preexisting solid-gas substrate to be converted to a solid–gas–liquid substrate, leading to a loss of super-hydrophobicity. Therefore it is important to test the surfaces at low temperatures. In this study, the growth time of ZnO nanorods determines their size. As the growth time of ZnO nanorods increase, the size of nanorods increases. With increasing size, surface area of nanorods also increase (Figure 2.2.1.2). Droplets maintaining the liquid state increase with the decrease of the growth time of ZnO nanorods. Since less growth time provides a small surface area and therefore more trapped air between asperities, trapped air can behave like a heat insulator.
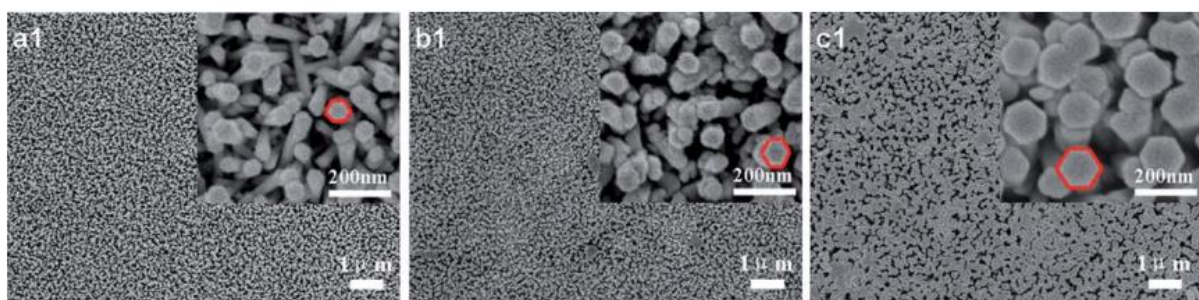
Figure 2.2.1.2 From left to right growth time increases. Surface area of nanorods increases with growth time. Static water contact angles are 170.9°, 166.1°, and 165.8°, respectively. [3]

The authors conclude that superhydrophobic surfaces can delay frost/ice formation and there is a correlation between surface wettability (i.e. water contact angle) and frost formation. Moreover, the researches prepare a superhydrophobic coating which does not lose its property at low temperatures.

Cao et al. [38] investigate the effect of roughness on anti-icing and find that there is a critical particle diameter which is necessary to impede ice formation. They prepare nanoparticle-polymer composites with different particle sizes ranging from 20 nm to 20 μm. Although composites made with particles up to 10 μm in diameter are all superhydrophobic, the anti-icing capabilities of these coatings are completely different. Ice does not form on coatings with 20 and 50 nm particles. The critical radius of nucleating crystal is found to be 21.6 nm under experimental conditions. After these particle diameters, the icing probability increases. As a result, the authors draw attention to the importance of particle size for anti-icing properties.

Yin et al. [39] prepare superhydrophilic, hydrophilic, critical, hydrophobic and superhydrophobic films and investigate the correlation between wettability of surface and ice formation. Because of condensed water between asperities, static water contact angle of superhydrophobic surfaces decrease when temperature decrease to freezing point and below. In this study same phenomenon is observed. Static water contact angle values of the superhydrophobic surface are *ca.* 165° at 20 °C but they fall to 155.9 ± 1.7° and then to 145.8 ± 3.2° when the surface temperature decreased to 10 °C and to − 10 °C, demonstrating increment of wettability of the surface at low temperatures. Water condensation also affects the hydrophobic surface, on which the static water contact angle fall from 114.0 ± 4.9° to 104.1 ± 2.2° when the surface temperature went down from 10 °C to − 10 °C. However, the influence of condensed water is weaker comparing to superhydrophobic surface since there exists only microstructures on the surface. Authors conclude that surfaces with static water contact angle is smaller than 90° is not affected by the change of surface temperature in arrange between −10 °C and 40 °C under relative humidity larger than 80%. Another important conclusion of this article is that ice formation (kinetics of ice) mostly depends on surface topography rather than surface wettability. Similar conclusion was made by Cao et al. [38] as they propose critical particle diameter to prevent ice nucleation. Superhydrophobic surfaces have advantage in terms of rolling of the droplet at the initial stages of freezing. If water droplet can be rolled before freezing completes, superhydrophobic surfaces can be solution of icing/frosting problem.

So changing of static water contact angle near freezing point temperatures needs to be elucidated since superhydrophobic surfaces lose their ability around this temperature region. In this purpose Karmouch et al. [40] prepare polished silicon, polished aluminum, roughened silicon, gold, high density polyethylene, PTFE (polytetrafluoroethylene), and PMMA samples and investigate possibilities that may affect water contact angle decrease. Roughness effect is investigated with rough and flat silicon surfaces and no contact angle hysteresis is found. Later, oxidation effect is investigated and Al_2O_3 is compared to Au film. Again no contact angle hysteresis is found. Polyethylene and Polytetrafluoroethylene is compared and no contact angle hysteresis is found even if the initial static water contact angle values are different from each other. Lastly, nanostructured PTFE, nanostructured PMMA and HIREC-100 which is super water-repellent coating blended with TiO_2 is compared and contact angle hysteresis is found. Humidity in air is condensed on the asperities in these nanostructured samples when the temperature drops down to 0 °C. As a result, if superhydrophobic coatings are desired not to lose their property near freezing point, formation of primary water vapor condensation should be avoided.

Alizadeh et al. [41] has been investigated ice nucleation and delayed freezing on superhydrophobic surfaces recently. As samples, Silicon-PEG, Si-Fluorine and single, double textured are used. Room temperature droplets are impinged on −20 °C substrates. Different from other papers, they use IR thermometry to observe phase transition of water droplet. As seen in previous papers, authors also observe later freezing of droplet on fluorinated silicon than PEGylated silicon. They suggest, as already been explained by others [7], that air trapped between protrusions behave like heat insulators and ice nucleation rate on the superhydrophobic surfaces is also affected due to a reduction of water−substrate interfacial area and increase in the free energy barrier to forming a critical nucleus at the interface. This explanation, however, is suggested by Cao et al. As superiority, they use high-speed photography to determine interfacial areas. It is seen that, delayed freezing is observed when interfacial area decreases (figure 3). Since water-substrate interfacial area is a function of temperature, at lower temperatures of substrate, water-substrate interfacial area does not play a role in terms of delayed freezing. In conclusion, ice nucleation under low humidity conditions can be delayed through control of surface chemistry and texture. As opposed of Yin et al., this paper addresses the importance of both surface texture and surface chemistry to prevent ice nucleation at low humidity conditions.
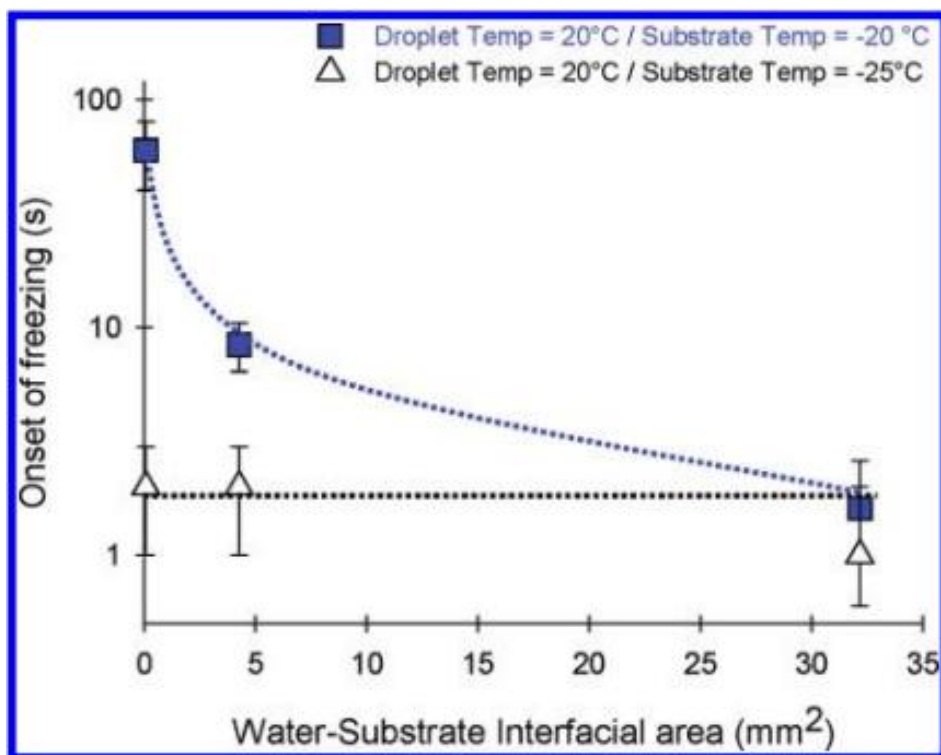
Figure 2.2.1.3 Freezing delay time increases with decreasing interfacial area [41].

Suzuki et al. [42] observed the freezing behavior of supercooled water on self assembled monolayers (SAMs) of various silanes such as 1H, 1H, 2H, 2H-Perfluorodecyltrimethoxysilane (FAS-17), trifluoropropyltrimethoxysilane (FAS-3) and, octadecyltrimethoxysilane (ODS) with high speed camera. Later, freezing temperatures of supercooled droplets were investigated by differential scanning calorimetry (DSC) and found -22 .7 °C, -22.4 °C and, -19.9 °C for FAS-17, FAS-3 and ODS, respectively. Interestingly they have found that, although contact angle of FAS-3 surface is lower than that of ODS, FAS-3 exhibits lower freezing temperatures. The explanation for this observation is related to chain freedom of alkyl groups of ODS and FAS-3. Since ODS has longer alkyl chains that FAS-3, water molecules on ODS surfaces can have more freedom. Freedom of water molecules leads to quick rearrangement compared to water molecules on FAS-3 and leads to faster nucleation.

Zheng et al. [43] functionalized SWCNTs with acetone to attain low surface energy. Obtained SWCNT films both had surface roughness due to the intrinsic property of CNTs to form bundles and low surface energy as a result of functionalized with acetone. Supercooled water droplets with temperature of – 8 °C were impinged on these 30° tilted films (substrate

15

temperature is − 8 °C) and observed whether the droplets stick on surface or not. On the contrary to unfunctionalized SWCNT films and bare substrates, droplets bounce off from the surface. Nonstick nature of acetone-functionalized SWCNT films might be a solution for combating ice on surfaces.

Since there are multiple voices on the effect of wettability on ice nucleation and delayed freezing, a recently published paper [9] says that surfaces with nanometer scale roughness and higher wettability display unexpectedly long freezing than typical superhydrophobic surfaces with larger hierarchical roughness and low wettability. Hydrophobic surfaces display higher resistance to icing than rough hydrophilic surfaces whereas hydrophilic surfaces with roughness values close to the critical nucleating radius display higher icephobicity. In contrast to previous papers, neither surface chemistry nor surface topography impedes ice/frost formation by itself. There should be optimum design of these two competing influences.

This desired optimum design can be found in nature. Mei et al. [44] discover multi-level micro-/nanostructures of the wing of *Morpho nestira* butterfly. These butterfly wings consist of oriented step arrangements in arrays of stripes and overlapping scales. Unusual orientation of steps effectively retard wetting, and achieve water repellency at low temperature and at changeable humidity conditions. Until now, all superhydrophobic coatings have failed at wide range of humidity conditions. They were mostly active at low humidity conditions. Thus this novel orientation can be successful for preparing anti-icing coatings.
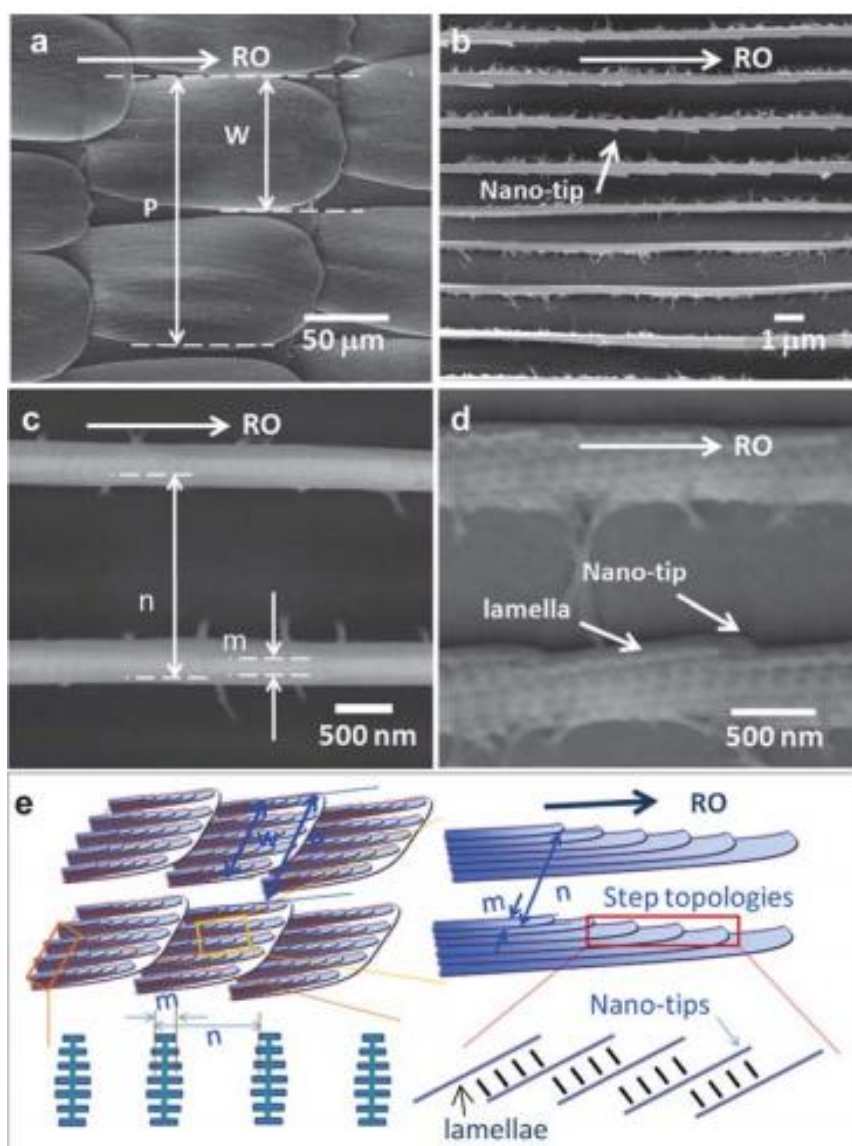
Figure 2.2.1.4 Multi-level micro-/nanostructure of Morpho nestira butterfly. [44]

Inspired from novel natural design of *Morpho nestira* butterfly wings, Guo et al. [45] prepare mechanically worked ZnO nanohairs with ratchet arrays. MN-surfaces, N-surfaces, M-surfaces and S-surfaces can be achieved (MN indicates micro-nano, M and N indicates micro and nano, respectively. S is smooth surface). Contact angle hysteresis of MN surface is very low at -10 °C comparing to other surfaces. Again at -10 °C delay time of MN-surface is 7220 s whereas 1740 s of N-surface, 1260 s of S-surface and 30.5 s of M-surface.
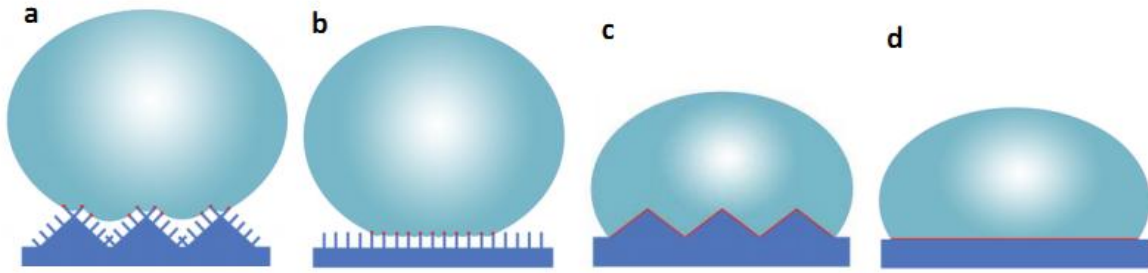
Figure 2.2.1.5 Illustration of anti-icing/ice-phobic properties on MN-, N-, M-, S-surface. [46]

Drops can be suspended up by the micro-/nanostructure due to discontinuous three phase contact line on MN-surface and high trapped air appears on MN-surface. As for N-surface, it generates the more solid contact than MN-surface. The M-surface increases the solid-liquid contact more than S-surface and the contact line of M-surface can be longer than S-surface.

2.2.2 Ice adhesion strength

Another approach to the icing problem is decreasing the adhesion strength of ice on surfaces. Basically, this solution requires small contact area between water and substrate. In this purpose Meuler et al. [47] prepare surfaces with relatively low average roughness of polymer coatings. They find that ice adhesion strength correlates more strongly with rolling angle or/and practical work of adhesion strength of water rather than static water contact angle. Good correlation between water wettability and low ice adhesion is found. Authors conclude that icephobicity of smooth surfaces can be predicted by measuring receding contact angle of droplets rather than static water contact angle. However, Dotan et al. [48] finds correlation between static contact angle of water and low adhesion of ice. They do not investigate roughness levels of coatings in this study.

Other groups [49] cannot find correlation between static contact angle of water with ice adhesion too. They use same surface chemistry with different surface roughness coatings. Contact angle hysteresis is highly dependent on substrate-water contact area. Therefore low contact angle hysteresis rather than static water contact angle is required to low ice adhesion.

Mishchenko et al. [50] study the dynamic wetting of supercooled water droplets and ice accretion by combining high speed imaging with modeling of nucleation, heat transfer, and wetting dynamics. The high speed imaging reveals that water droplets dropped from a height

of 10 cm completely retracts from tested superhydrophobic surfaces when the substrate temperature is greater than 20 °C. Colder surface leads to freezing of the impinging water during retraction processes. Furthermore, the authors note that, when water freezes on the superhydrophobic substrates, the adhesion of the accreted ice was lower than it was on chemically equivalent smooth surfaces. This findings are consistent with [48]. However, Cao et al. [6] have reported that there is a critical radius of crystal is 21.6 nm which is significantly different from Mishchenko et al. [50] have used.

Many other groups show correlation between superhydrophobicity (surface chemistry and surface roughness) and low ice adhesion [5], [51], [52]. Varanasi et al. [53] discuss both frost formation and its effect on ice adhesion strength. From ESEM images it is seen that frost forms indiscriminately all over the superhydrophobic surface texture including post tops, sidewalls, and valleys without any particular preference. This leads to increased ice-surface contact area so increased ice adhesion strength.

Some other scientists also discuss the durability of superhydrophobic surfaces [54], [55] .These coatings are tested icing/de-icing cycles and seen whether they lose their property. Kulinich et al. [54] show that superhydrophobic surfaces lose anti-icing properties since the asperities are distorted during icing/de-icing circles. Also they investigate these coatings at high humidity conditions and conclude that adhesion strength of ice is increasing.

CHAPTER III

MATERIALS, METHODS AND TECHNIQUES

There are two main sections in this chapter. The first section will introduce the materials and methods in the study of interaction of hydrophilic polymers with water/ice at subzero temperatures. The second part will introduce the materials and methods that we used to prepare polymer/nanoparticle composite films as possible anti-icing coatings.
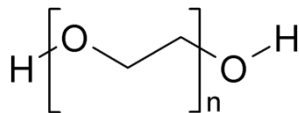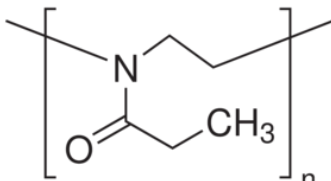
3.1 Interaction of Hydrophilic Polymers with Water/Ice at Subzero Temperatures

3.1.1 Materials

Hydrophilic polymers that were used in this study are tabulated with their chemical structure and molecular weight (Table 3.1.1.1). We have chosen Polyethylene glycol, PEG because polyglycols have been proved to display anti-freeze property. Moreover, glycols such as ethylene and triethylene glycol have been used as anti-freeze agents in cars, air conditioners and radiators. Secondly, we have chosen Poly(2-ethyl-2-oxazoline), PEOx. As described in Chapter 2, some specified polymers in Antarctic fishes' blood inhibit ice crystallization. Because of its structural similarity to anti-freeze proteins, PEOx may show the same characteristics.

The diverse selection of these water soluble polymers was made in order to understand how different chemical structures influence the anti-freeze property and interaction with water/ice.

Table 3.1.1.1 Water soluble polymers that are used in this study with their specifications

Polymer	Weight average molecular weight (M_w)	Chemical structure	Company
PEG	2K		Merck
	10K		
	100K		
	200K		
	400K		
PEOx	5K		Alfa Aesar
	50K		Aldrich

3.1.2 Sample Preparation

All polymer aqueous solutions were prepared in glass vials. Glass vials were used after rinsing with distilled water. Solution concentrations were changed between 1-80 mg/mL. After preparing polymer solutions, they were left in the shaker at least one night in order to mix well and reach thermodynamic equilibrium.

3.1.3 Characterization

3.1.3.1 Differential Scanning Calorimetry (DSC)

Differential scanning calorimetry measurements were performed on TA instruments Q200 under continuous nitrogen atmosphere. Calibration was done with water and indium. Samples were taken from glass vials via syringe and dropped in hermetic aluminum pans. Sample amounts varied between 5-20 mg. Later, pans were sealed and put in a DSC cell. Each sample was first equilibrated at 20 °C. The temperature was decreased to subzero temperatures with various ramp times and samples were kept isothermally at these temperatures. We studied the effect of ramp time and isothermal treatment time on interaction of hydrophilic polymers with water.

Polyethylene glycol solutions were cooled to -30 °C and heated to 20 °C with 5 °C/min. Samples were kept at -30 °C isothermally for 3 minutes. Poly(2-ethyl-2-oxazoline) solutions were cooled to -35 °C and heated to 20 °C with 5, 2.5, 0.5 °C/min. Samples were kept at -35 °C isothermally for 3 minutes. To stay on the safe side, we changed the isothermal treatment temperature because we observed a glass transition at − 28 °C.

3.2 Polymer/Nanoparticle Composites for Anti-icing Applications

3.2.1 Materials

Styrene-butadiene-styrene (SBS) triblock copolymer with number average molecular weight of 140,000 g/mol was kindly supplied by Arçelik company, SBS (A) and D1101 linear SBS block copolymer with 30% polystyrene content was bought from Kraton, SBS (K). Hydrophobic silica nanoparticles with different hydrophilicity were supplied by Degussa. The codes of the nanoparticles used in this study are R974 and R816 which are hydrophobic and semi-hydrophilic, respectively. Hydrophobic nanoparticles have methyl groups attached to silica core whereas semi-hydrophilic nanoparticles also have hydroxyl groups. Bitumen 50/70 grade was kindly supplied by Turkish Petroleum Refineries Co.
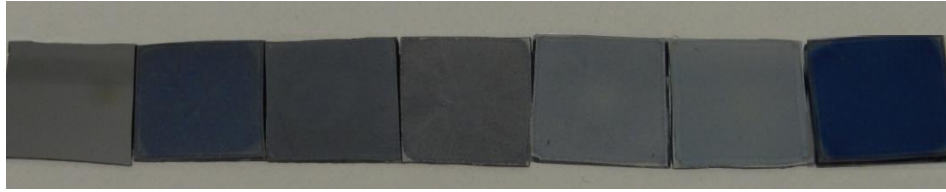
3.2.2 Sample Preparation

3.2.2.1 SBS with hydrophobic silica nanoparticle (R974) inclusions

SBS (A) was dissolved in chloroform and 1 % (w/v) stock solutions were prepared. Hydrophobic silica nanoparticles (R974) were weighted to make 10-66 % (w/w) nanoparticles in a polymer solution. After SBS completely dissolved in the chloroform, 10 mL of polymer solution was added to falcon tubes filled with weighted nanoparticles. Each falcon tube was left in the shaker at 200 rpm for 30 minutes. Immediately after, tubes were sonicated using Ultrasons-H, SELECTA for one hour at 10 °C to avoid solvent evaporation due to extreme heating. Obtained dispersions were homogenous and clear. Later, to see the effect of polymer concentration 2 % (w/v) SBS (A) solution was prepared in chloroform. Nanoparticle fraction varied from 5 to 43 % (w/w). Thin films from these dispersions were prepared by the spin-coating method. For solvent cast films, SBS (A) dissolved in chloroform to prepare 2 % (w/v) polymer solution. Hydrophobic silica nanoparticle fraction varied from 5 to 43 % (w/w). The dispersion procedure was applied as same as described above for both spin and solvent cast films.

3.2.2.3 Thin film preparation

Thin films of SBS alone, SBS (A)/hydrophobic silica, SBS (A)/semi-hydrophilic silica and SBS (K)/hydrophobic silica nanoparticles were prepared by the spin coating and solvent casting method. Spin-casting method is done by dispensing an appropriate amount (depending on substrate size) of polymer solution/dispersion on flat substrate and rotating the substrate at specified time [56]. Undoped silicon wafers were cut as 0.5 x 0.5 inch^2 and 2 x 2 cm^2 depending on the experiments they were used. For 0.5 x 0.5 inch^2 substrates 200-250 µL and for 2 x 2 cm^2 substrates 300-350 µL liquids were dispensed on these surfaces. Substrates were rotated at 2000 rpm for one minute. For SBS (A)/hydrophobic silica nanoparticles, homogenously dispersed thin films were obtained. However, semi-hydrophilic silica nanoparticles were not uniformly dispersed on the surface. Figure 3.2.2.4.2 shows photographs of SBS (A)/hydrophobic silica nanoparticle.

 We dispensed polymer solutions on 2 x 2 cm^2 silicon wafers and waited in oven at 70 °C for 30 minutes to obtain solvent cast films.

Figure 3.2.2.3.1 Photographs of SBS (A)/hydrophobic silica nanoparticle thin films. **a)** From left to right; bare Si wafer, 10, 20, 33, 50, 66 % (w/w) nanoparticles and 1 % (w/v) SBS thin films.

3.2.2.4 Sample preparation for Rheology measurements

Bitumen and 5 % by weight SBS were mixed by IRA 20 RW high shear mixture. Bitumen and SBS mixture was heated up to 100 °C and mixed at 1000 rpm for two hours. After the samples were cooled down, rheology measurements were conducted.

3.2.3 Characterization

3.2.3.1 Ellipsometer

Ellipsometer is one of the techniques used in surface science to analyze film thickness ranging from 1 nm up to several microns. In this technique, monochromatic light is polarized and directed onto the surface. Light polarized parallel and perpendicular to the surface is reflected differently [57]. Amplitude and phase change differently at the interface. Film thickness is determined by measuring the phase shift of the incident and the reflected beam (Δ) and the amplitude ratio of parallel and perpendicular polarized light (Ψ).
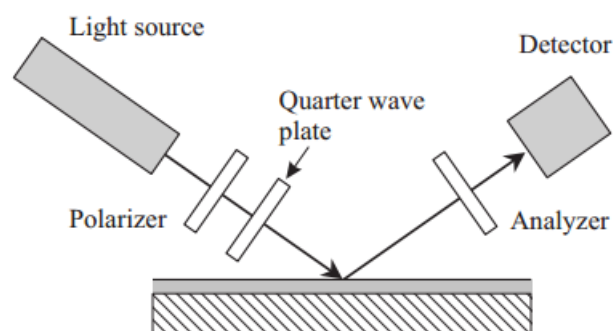
Figure 3.2.3.1.1 The configuration of ellipsometry [57]

We used EL X-01R high precision ellipsometer from Micro Photonics Inc. to analyze film thicknesses of polymer films. The wavelength of Helium-neon laser was 632.8 nm. The thickness of the films was measured by averaging the thicknesses from five different points. The refractive index of SBS (A) was taken as 1.5.

3.2.3.2 Optical microscopy

Surface morphology analysis of obtained coatings was carried out by using DAS Mikroskop Leica DM LM model with lowest 10x and highest 50x magnification.

3.2.3.3 Water contact angle measurements

We used OCA 20 optical contact angle measuring device from DataPhysics to analyze wettability of coatings. In room temperature measurements, plate temperature was held constant at 22 °C and droplets with 3 μL volumes were placed onto substrates. We used the average values of 3 and 4 droplets' contact angle degree for 0.5 x 0.5 inch^2 and 2 x 2 cm^2 substrates, respectively to obtain statistically meaningful values.

89 ± 0.71 °	146 ± 1.94 °
a)	b)
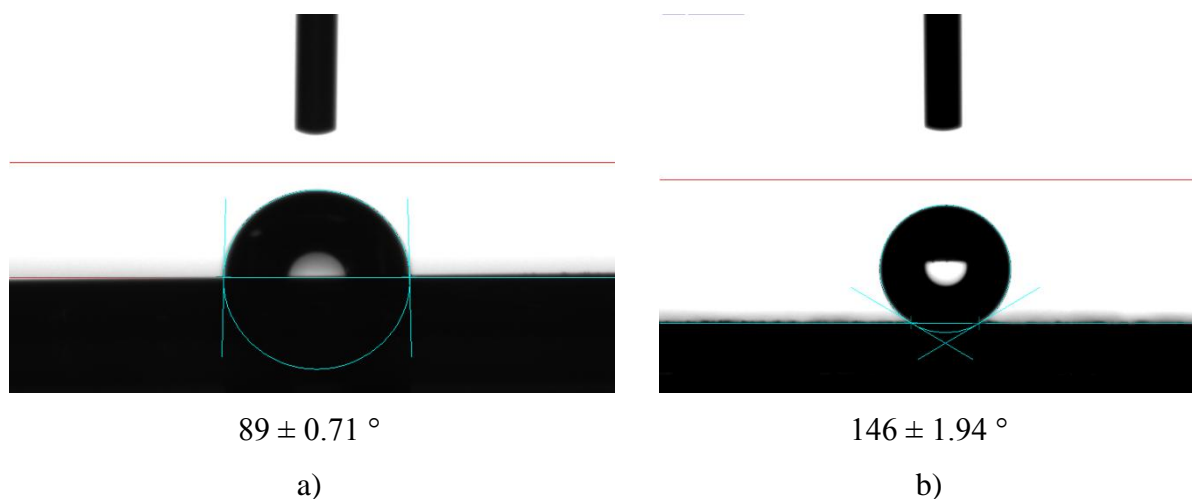
Figure 3.2.3.3.1 Water contact angles on solvent cast films of a) 2 % (w/v) SBS coating, b) SBS (A)/hydrophobic silica nanoparticle coating with 43 % (w/w) nanoparticle content. Addition of hydrophobic silica nanoparticles increase water contact angle.

We studied the effect of temperature on the wettability of coatings with the same device. All samples were put in a device cell at the same time to avoid cell temperature differences. The

procedure in Figure 3.2.3.3.2 was applied to measure the water contact angles of all samples at different plate temperatures at once. At first, the plate temperature was decreased to 15 °C from 20 °C. Substrates were placed in the cell and left at 15 °C for five minutes. At the end of the fifth minute, droplets were dispensed on substrates and water contact angles were measured. Impinging of droplets and measuring water contact angles took ten minutes at every step. Substrates were taken out from the cell and dried with nitrogen gas after measuring the water contact angles. Drying with nitrogen gas before every step is crucial because otherwise the remaining condensed water from the previous measurement can adversely affect the measurement.
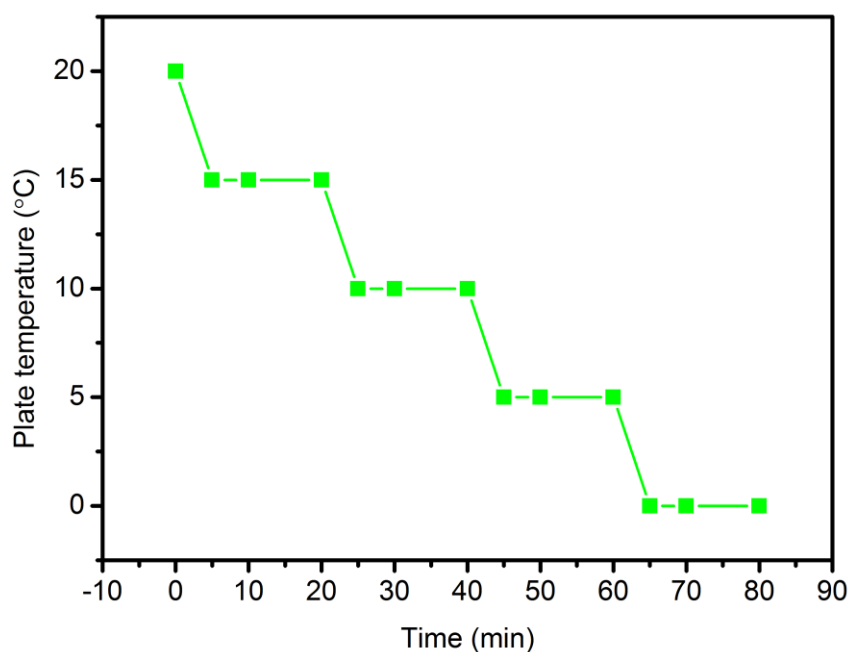
Figure 3.2.3.3.2 Procedure to investigate effect of temperature change on water contact angle of coatings. Plate temperature was decreased to 15 °C from 20 °C and stayed there for five minutes. Droplets were dispensed at the end of fifth minute and water contact angles were measured. Substrates were taken out from the cell after measurement and dried with nitrogen gas. Same procedure was followed till the end of experiment.

3.2.3.4 Freezing Experiments

We carried out freezing experiments in two different instruments. Figure 3.2.3.4.1 shows the procedure followed in OCA 20 optical contact angle measuring device from DataPhysics. We tested anti-icing property of coatings at two different temperatures, separately. The plate temperatures were decreased to -4 and -8 °C from 20 °C in five minutes.

We placed samples in the cell at the end of fifth minute and then left in the cell for ten minutes. We dispensed water droplets at the end of ten minutes and recorded the time that is required for freezing. Air temperature and relative humidity were roughly controlled by pumping nitrogen gas in the cell.
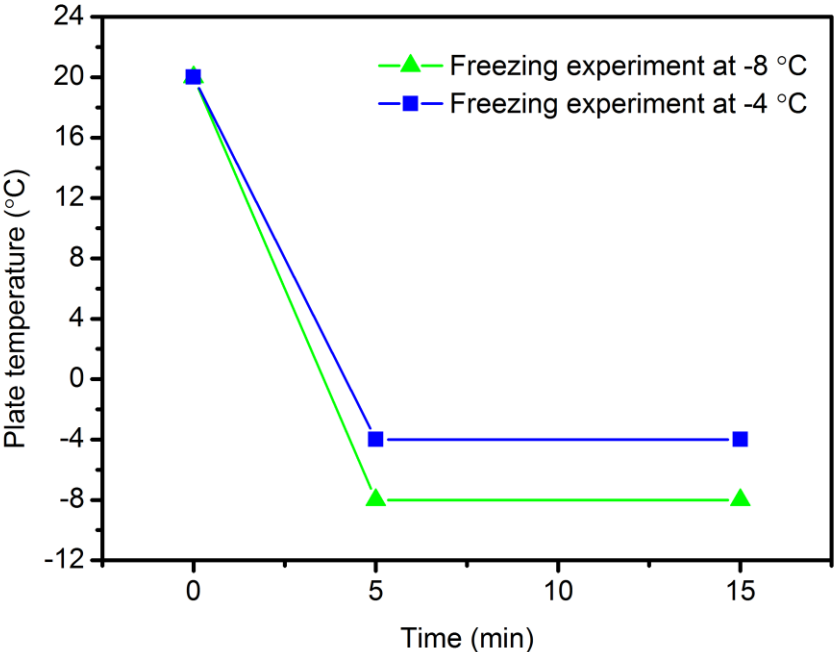
Figure 3.2.3.4.1 Freezing experiment at -4 °C and -8 plate temperature. First, plate temperature was decreased to -4 °C from 20 °C in five minutes. Samples were placed in cell at fifth minute and stayed for ten minutes to ensure to avoid temperature difference between plate and sample. Required time for freezing was recorded.

Secondly, we used temperature and humidity control cell manufactured by Teknofil Co. In this instrument, the samples were placed in the cell at room temperature. The temperature and relative humidity were decreased to the desired values. The time was recorded when the plate temperature reached the desired value.

3.2.3.5 Rheometer

DHR hybrid rheometer by TA instruments was used to analyze the effect of composite on mechanical properties of bitumen.

CHAPTER IV

ANTI-ICING EFFECT OF AQUEOUS POLYMER SOLUTIONS

Interactions of hydrophilic polymers with water change freezing and melting behavior of water. In this chapter, we investigated aqueous solutions of polyethylene glycol (PEG) and poly(2-ethyl-2-oxazoline) (PEOx) in terms of their anti-icing effect by differential scanning calorimetry. It is known that addition of solute particles depress the freezing point of water which is a colligative effect independent of the type of solute particles [58]. In addition to colligative effect, polymers with specific backbone and side chain groups can further lower freezing point due to specific interactions with water. We chose polyethylene glycol because of its flexible backbone that helps it to undergo conformational changes [59] and etheric oxygen that is able to make hydrogen bonds with water. Poly(2-ethyl-2-oxazoline), on the other hand, has C-C-N backbone and strong amide dipole that are able to interact with water [60]. These two polymers, because of their molecular structures, are good model systems to study the freezing phenomenon of water and interpret it at molecular basis. Moreover, these polymers can be included in a hydrophobic matrix and let diffuse into water to act as a freezing point depressant. In conclusion, the knowledge gained from these studies will be helpful in understanding the requirements for anti-icing effect and preparing novel anti-icing coatings.

4.1 Overview of DSC experiments

Differential scanning calorimetry (DSC) is a useful tool to monitor thermal changes in materials. Since it detects the heat capacity associated with a phase transition water freezing/melting behavior can be probed. Figure 4.1.1 shows typical DSC heating and cooling curves of pure water and 40 g/L PEOx-5K aqueous solution. Two transitions are seen in the thermograms. The exothermic peak at lower temperature refers to crystallization of supercooled water whereas the endothermic one at higher temperature shows the melting peak of ice. It is seen that crystallization peak of the water shows irregular shape. When supercooled water crystallizes suddenly, a large amount of heat is given off and temperature of the DSC cell begins to increase. Since cooling run continues and instrument tries to decrease the cell temperature, crystallization peaks become irregular in shape.
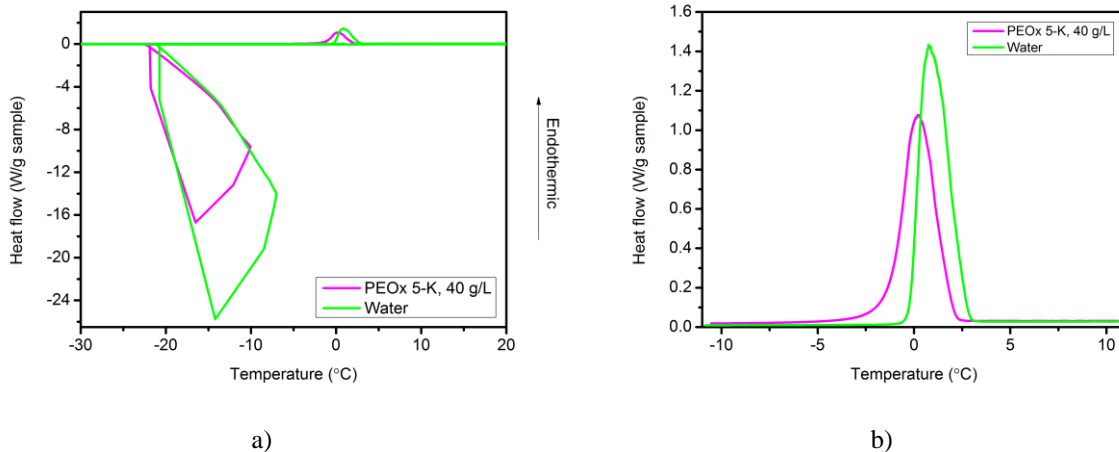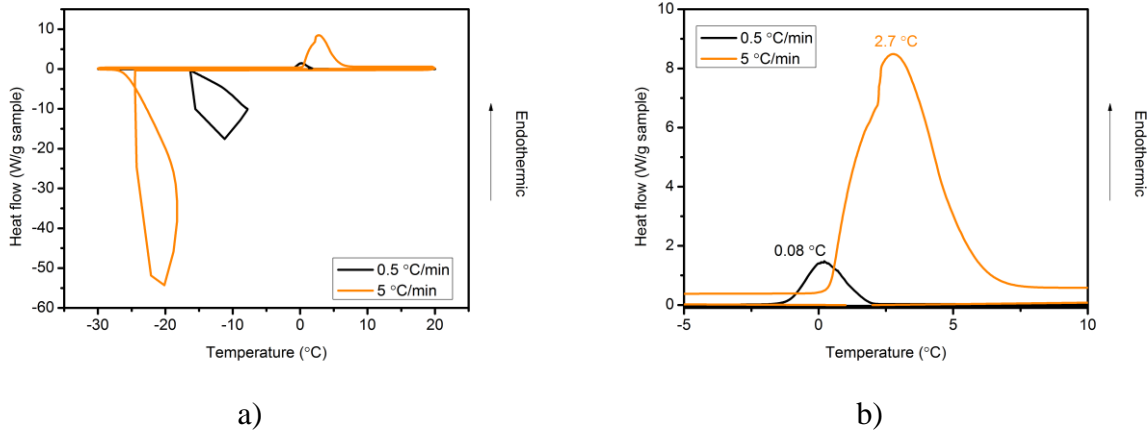
Figure 4.1.1 DSC curves of double distilled water and 40 g/L PEOx-5K. Exothermic peak refers to crystallization of supercooled water. Endothermic peak indicates the melting of ice. Heating and cooling rates are 0.5 °C/min. a) Complete view of DSC curves, b) Melting peaks were magnified.

The interesting point in the graph b) is the difference in melting points of ice and aqueous PEOx-5K solution. Addition of 4 % (w/v) PEOx-5K resulted in the depression of melting point of ice. It also decreased freezing point of supercooled water. In succeeding sections, the concentration and molecular weight effects on melting points of ice will be discussed.

4.1.1 Effect of heating and cooling rates on peak temperatures of transitions

In order to obtain the most reasonable results, we studied the effect of heating and cooling rates of water and PEOx-5K aqueous solutions. The importance of heating and cooling rates on baseline correction in aqueous solutions was reported before [61] but the effect on peak temperatures was not discussed. Figure 4.1.2 shows the DSC result of distilled water with heating and cooling rate of 5.0 °C/min (orange line) and 0.5 °C/min (black line). In graph a) it is seen that the crystallization peak was shifted to higher temperatures at 0.5 °C/min. Furthermore in graph b) it is seen that melting temperature of ice is 2.7 °C when the heating and cooling rate are 5 °C/min and decrease to 0.08 °C when the rates are 0.5 °C/min. Furthermore, the baseline was not affected in case of low heating and cooling rates whereas high rates resulted in a change of the baseline slope.

Figure 4.1.2 a) DSC thermogram of double distilled water with 0.5 °C/min and 5.0 °C/min ramp times for cooling and heating cycles. There are two peaks seen in thermogram. Exothermic peak refers to crystallization of supercooled water. Endothermic peak indicates the melting of ice. b) Melting peaks were magnified in order to see melting temperatures for both cases.

In order to examine whether the heating and cooling rates also affect aqueous solutions of polymers, we analyzed three different rates for the aqueous solutions of PEOx-5K. Figure 4.1.3 shows the DSC curves of 0.5 °C/min, 2.5 °C/min and 5.0 °C/min heating and cooling rates for the 40 g/L aqueous solution of PEOx-5K. The graphs show that heating rate has effect on ice melting temperatures. With increasing heating rates melting peaks shifted to higher temperatures.
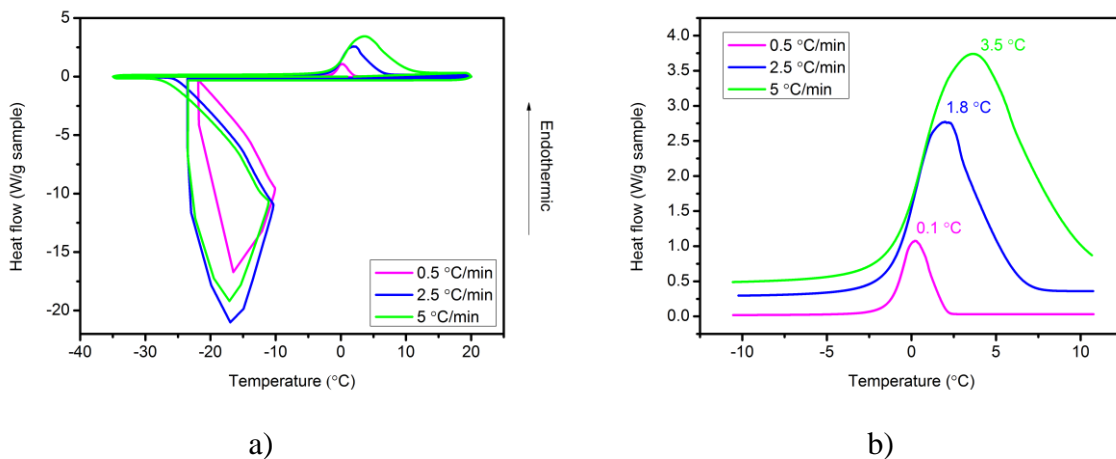
**Figure 4.1.3** Heating and cooling rate effects on the melting point of ice. Aqueous solutions of PEOx-5K show gradual decrease with heating and cooling rate. a) Complete view of DSC curves of 40 g/L PEOx-5K for the heating and cooling rates of 0.5 °C/min, 2.5 °C/min and 5.0 °C/min. b) Magnified melting peaks. Melting temperatures are 0.1 °C, 1.8 °C and 3.5 °C for 0.5 °C/min, 2.5 °C/min and 5.0 °C/min, respectively.

In the light of these findings, the heating and cooling rates were decreased where needed to minimize kinetic effects and therefore melting peaks of pure ice approached to 0 °C.

4.2 Aqueous polyethylene glycol (PEG) solutions

In this section we have investigated the anti-icing effect of two different molecular weights of PEG namely PEG-2K and PEG-10K and its concentration dependence. It is known that chain entanglement increases with the molecular weight and this prohibits rapid dissolution of the polymer [62]. Since these polymers are potential anti-icing agents we chose low molecular weights to overcome the slow dissolution problem.
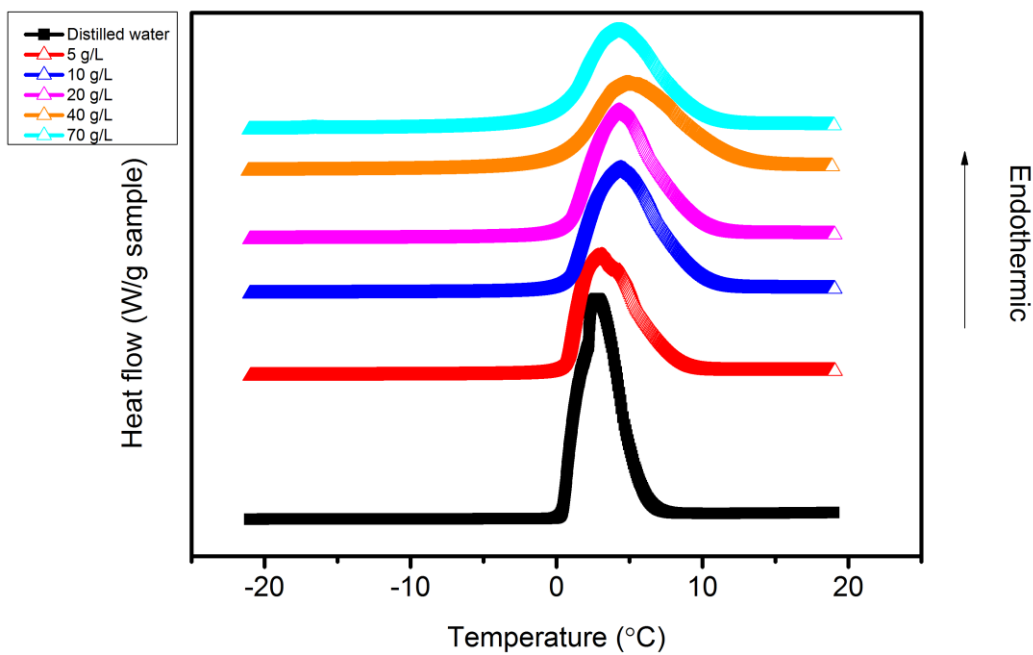
Figure 4.2.1 shows heating curves of PEG-10K aqueous solutions with 5 °C/min heating rate. Two endotherms are seen in DSC curves of PEG-10K. The one closer to 0 °C is attributed to the melting peak of ice formed by the freezing of bulk water. The melting temperatures of ice are seen to range between 3.7 °C and 5.25 °C. The peak temperatures of low-T endotherms are between − 10.7 °C and − 11.2 °C and do not change reasonably with the polymer concentration. In order to analyze further, low-T endotherms were magnified. Figure 4.2.2 shows the magnified versions of low-T endotherms for PEG-10K aqueous solutions. It is seen that there is a lower limit in polymer concentration for second endotherms to appear. The lower limit for PEG-10K is 10 g/L which equals to 1 % (w/v) polymer solution. The low-T endotherms are thought to be the melting of ice in hydrated polymers, that is water molecules bound to polymer chains [63][64]. In order to see whether smaller polymer can affect the freezing behavior of water, aqueous solutions of PEG-2K were analyzed. Figure 4.2.3 shows heating curves of PEG-2K aqueous solutions with heating rate of 5 °C/min. The melting temperatures of ice ranged between 2.9 °C and 5.5 °C for the solutions of PEG-2K. Magnification of Figure 4.2.3 also revealed low-T endotherms. Figure 4.2.4 shows other very weak endothermic peaks at around − 16.5 °C for PEG-2K solutions. For the case of PEG-2K solutions the lower limit for hydration of polymer chains is 15 g/L which is 1.5 % (w/v). Table 4.1 summarizes the melting temperatures of ice and low-T endotherms for aqueous solutions of PEG-2K and PEG-10K.
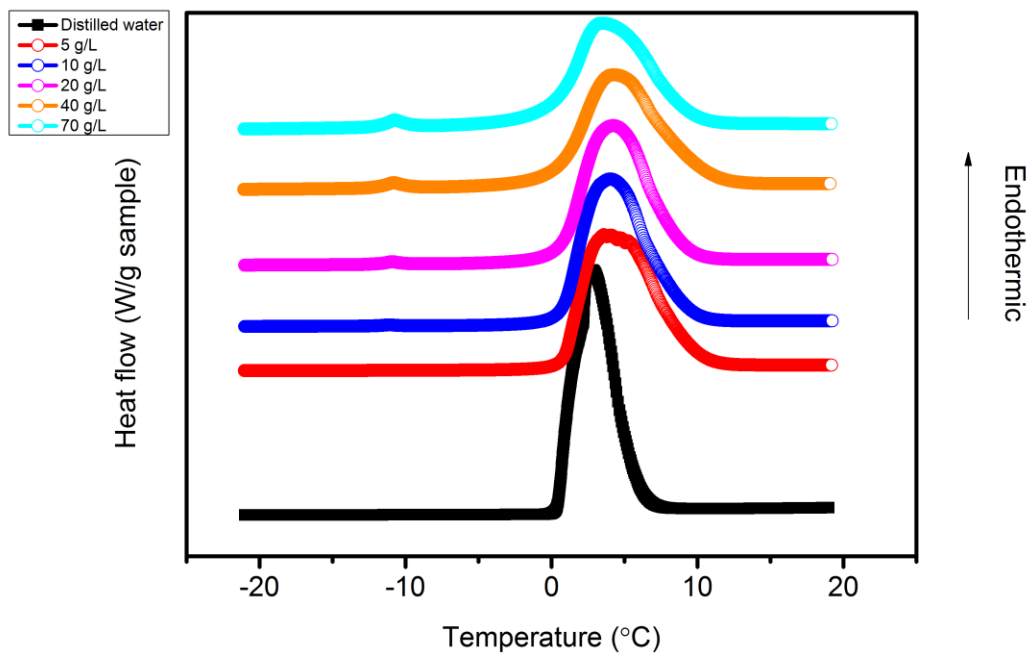
Figure 4.2.1 DSC heating curves of PEG-10K aqueous solutions. Heating rate is 5 °C/min.
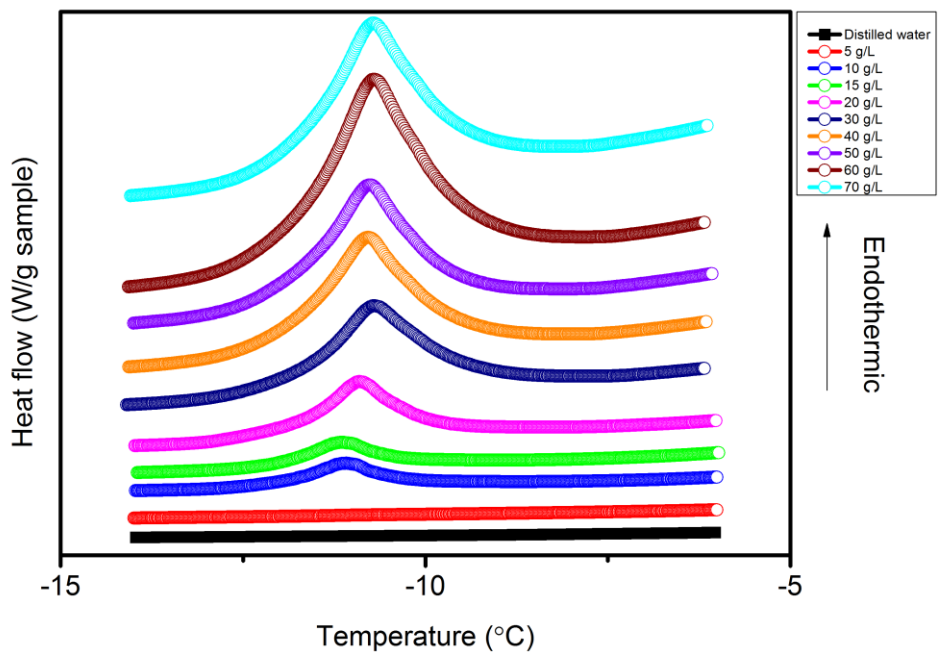
Figure 4.2.2 Magnified version of DSC heating curves of PEG-10K. Heating rate is 5 °C/min. Low-T endotherms are thought to be the melting of hydrated polymers resulting from bound water.
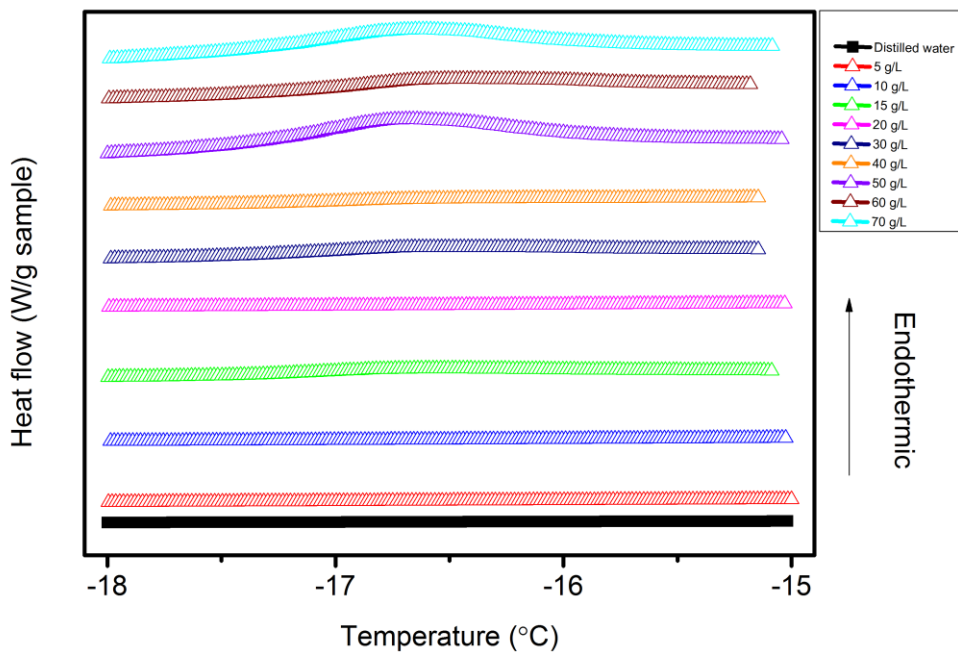
Figure 4.2.3 DSC heating curves of PEG-2K aqueous solutions. Heating rate is 5 °C/min.

Figure 4.2.4 DSC heating curves of PEG-2K. Low-T endothermic peaks are seen at concentrations from 15 g/L to 70 g/L.

Table 4.1 Melting peaks of ice (T_m) and lower-T endotherms (T_{m2}) for PEG-2K and PEG-10K molecular weights. Heating and cooling rate is 5 °C/min.

	PEG -2K		PEG -10K	
	T_m (°C)	T_{m2} (°C)	T_m (°C)	T_{m2} (°C)
1 g/L	4.10	-	3.77	-
3 g/L	4.10	-	3.70	-
5 g/L	2.90	-	4	-
10 g/L	4.32	-	4	-11
15 g/L	4.55	-16.8	3.70	-11.2
20 g/L	4.20	-	4.12	-10.8
30 g/L	5.50	-16.7	5.25	-10.7
40 g/L	4.90	-16.7	4.31	-10.8
50 g/L	3.37	-16.7	4.10	-10.8
60 g/L	5.50	-16.6	3.84	-10.7
70 g/L	4.10	-16.7	3.65	-10.7

4.2.1 Molecular weight dependence of low-T endotherms

Two different molecular weights of PEG showed that the low-T endotherm depended on the molecular weight. In order to see molecular weight dependence clearly, three other molecular weights of PEG were also analyzed by DSC. Figure 4.2.1.1 shows the molecular weight dependence of lower-T endotherms for PEG-2K, PEG-10K, PEG-100K, PEG-200K and PEG-400K. Table 4.2 shows the melting temperatures of low-T endotherm for the aqueous PEG solutions. It is seen that with increasing molecular weight of PEG melting temperature of low-T endotherm shifts to higher temperatures. In previous works of Hilgren et al. [28] low-T endotherm of PEG-6K was found between – 11 °C and – 16 °C depending on the concentration. However, the concentration dependence of low-T endotherms is not pronounced in our case. The increasing molecular weight might be responsible for the increasing number of hydrogen bonds and therefore higher temperatures are needed to melt the polymer-water complex.
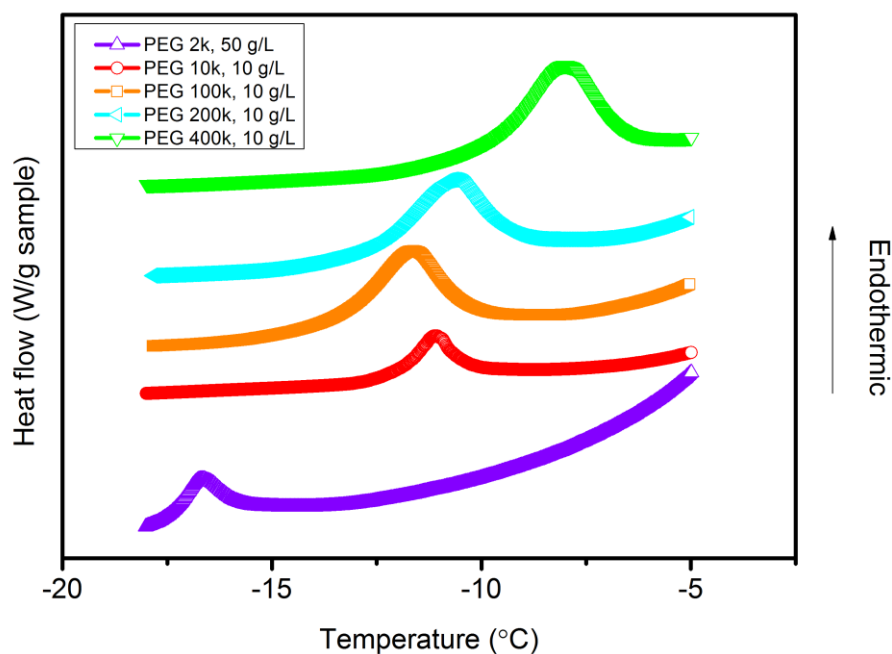
Figure 4.2.1.1 Molecular weight dependence of second endotherms. As molecular weight of PEG decreases peak temperature appears to be at lower temperatures with exception of PEG-10K.

Table 4.2 The melting temperatures of low-T endotherm for five different molecular weights of PEG.

	PEG-2K	**PEG-10K**	**PEG-100K**	**PEG-200K**	**PEG-400K**
T_{m2} (°C)	- 16. 6	- 11.1	- 11.6	- 10.6	- 8.03

4.2.2 Refreezing experiments of aqueous solutions of PEG: Understanding melting/crystallization behavior in detail

In order to understand ice-polymer interactions we have designed a DSC procedure. In this procedure, after temperature was decreased to − 35 °C with the cooling rate of 1 °C/min, samples were heated to − 1 °C with 0.5 °C/min scan rate. By selecting very slow heating and cooling rates, we were able to eliminate kinetic effects and time-temperature lag.

After that, samples were waited at − 1 °C where ice and water coexists to allow PEG to interact with ice nucleus. After 20 minutes, samples were cooled to − 35 °C with the 1.0 °C/min rate. Heating from − 35 °C to room temperature gave as expected endothermic peaks of ice close to 0 °C. Figure 4.2.2.1 shows the exothermic peaks of the crystallization of water after keeping PEG-10K samples at − 1 °C for 20 minutes isothermally and the endothermic peaks at the end of the experiment. It is seen from the graph a) that peak temperatures of exotherms follow the concentration dependence of PEG-10K. The peak temperatures shifted to lower temperatures with the PEG-10K concentration. This delay of crystallization may point out the adsorption ability of PEG-10K onto ice surfaces that was previously reported for some natural polymers [65][10]. In graph b) the endothermic peaks of ice melting is seen. The peak temperatures scattered however the enthalpy change due to the melting of ice significantly changed with the concentration of PEG-10K. The calculation of the peak area will be given in discussion section below.
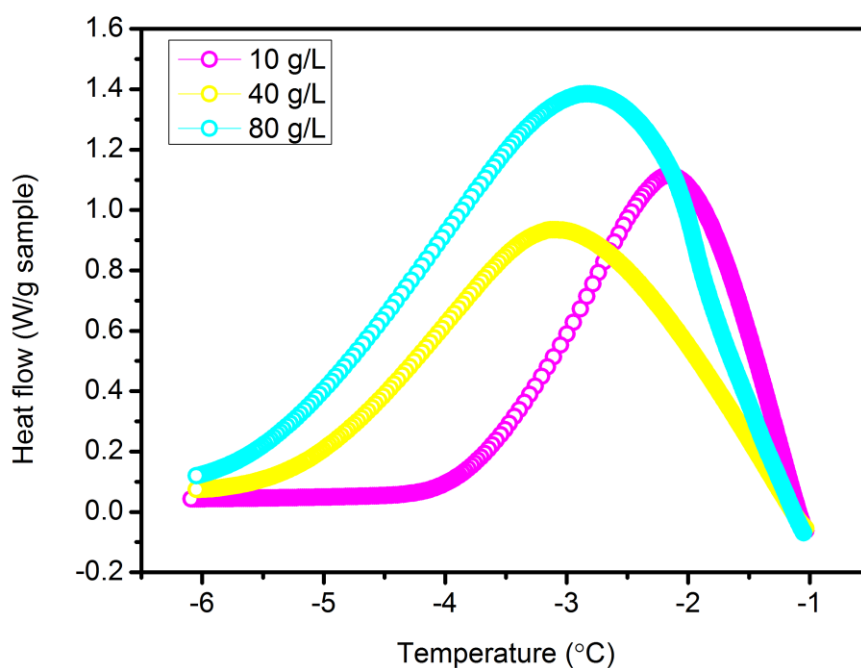

a)
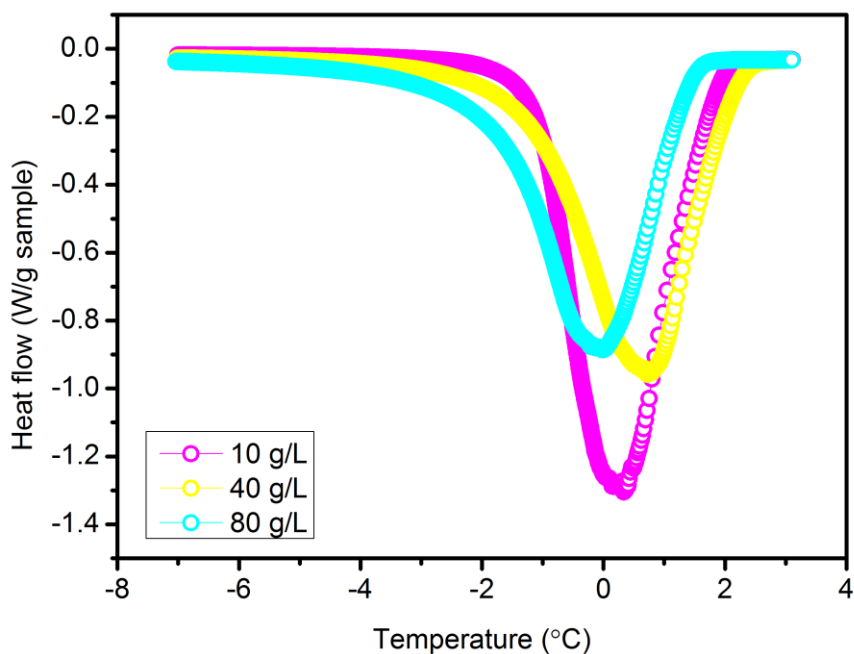
b)

Figure 4.2.2.1 Graphs of refreezing experiments for the PEG-10K. a) Exothermic peaks of ice at the end of kept at – 1 °C for 20 minutes isothermally. b) Endothermic peaks of ice at the end of the experiment.

4.2.3 Discussion

All PEG solutions with different molecular weight have secondary melting peaks at subzero temperatures. Secondary melting peak for PEG solutions is thought to be the melting of PEG-water complex. In some articles this complex is called as PEG hydrate or bound water to PEG [28], [29], [31], [66]. Three states of water is found in some water soluble polymers and polymeric membranes [28], [29], [31], [66], [67], [68], [69], [70], [71], [72], [73], [74]. First state is free water. The physical properties of free water do not differ from bulk water. Second state is unfrozen bound water. These water molecules are either confined by polymer chains or strong interactions between water and polymer makes them bound. Unfrozen water molecules do not crystallize even at - 100 °C [69]. Third and last state of water in hydrophilic polymers is frozen bound water. These water molecules makes bond with polymer chains and also interact with free water [66], [67], [69]. As a result, these water molecules do not display physical properties of bulk water. Figure 4.2.3.1 shows illustration of three different states of water and their interaction with PEG. Purple water molecules represent unfrozen bound water.

These water molecules locate in the first neighboring shell of PEG chains and therefore do not interact with other water molecules. Reds are free water molecules. They display the same physical properties as bulk water. Greens are frozen bound water molecules. These are thought to make bond with both etheric oxygen of PEG and also with other water molecules.
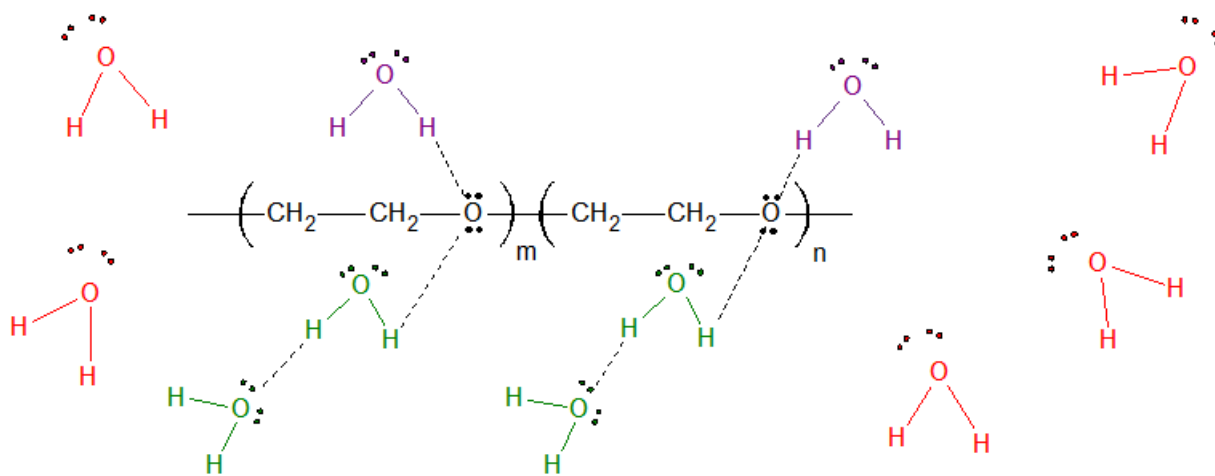
Figure 4.2.3.1 Illustration of three different states of water and their interaction with PEG. Purple water molecules represent unfrozen bound water, greens are frozen bound water and reds are free water molecules.
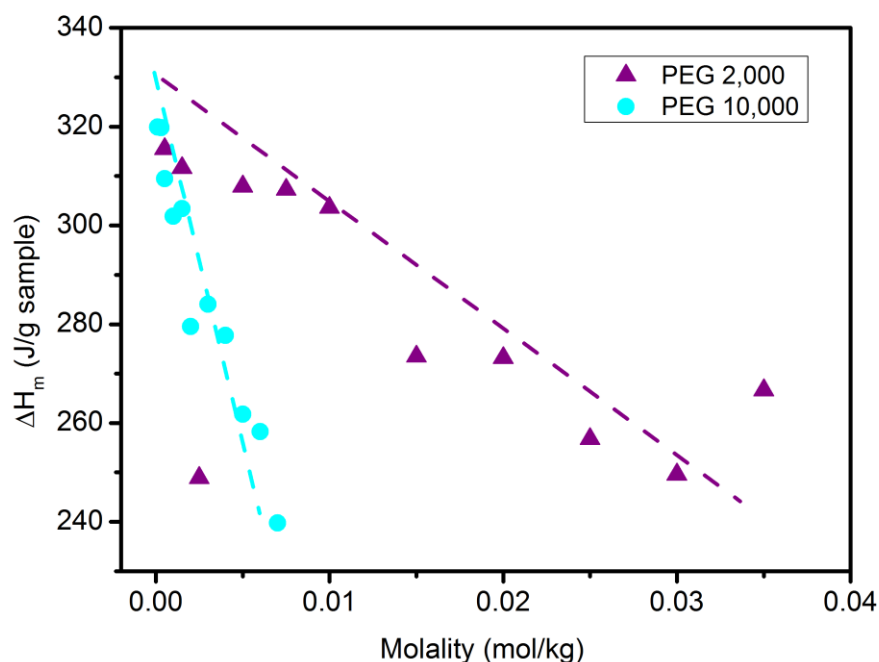

Figure 4.2.3.2 Change of melting enthalpies with molality of polymer solutions. PEG-10K addition decreases melting enthalpy of ice more dramatically than PEG-2K.

The lower-T endotherms seen at lower temperatures belong to the melting of frozen bound water molecules. Since some of the free water molecules become bound water, the amount of the free water molecules decreases. Lower amount of the free water molecules transform into lower amount of pure ice and this leads to decrease in melting enthalpies of ice at 0 °C. Figure 4.2.3.2 shows the change of the melting enthalpies of pure ice in PEG-10K and PEG-2K solutions with molality of solution. Both polymer solutions decrease enthalpy of melting with increasing molalities.

The proportion of the free water converted into ice during freezing can be calculated by the following formula

$$\% \; ice = \frac{W_w - \left(S_w + P_w + \left(\Delta H_m / \Delta H_w \right) \right)}{W_w} x \; 100$$

Where W_w is the weight of water, S_w is the weight of sample; P_w is the weight of the polymer, ΔH_m is the melting enthalpy of sample and ΔH_w is the melting enthalpy of I_h phase (most abundant phase) of ice which is 334 J/g. Calculation of % ice values are shown in Figure 4.2.3.3. It is seen that PEG-10K is more effective in terms of reducing ice formation compared to PEG-2K when it is investigated as a function of number of monomer unit. For PEG-10K, more free water molecules are able to make hydrogen bonds with PEG-10K units and therefore become bound water molecules. However, for the case of PEG-2K, less free water molecules make hydrogen bonds with etheric oxygen of PEG monomers. This leads to increment in amount of free water molecules in the polymer solution. Figure 4.2.3.4 shows the dependence of ice formation percentage on the number of polymer units. In the graph, it is seen that ice formation is not depended on the molecular weight i.e. number of monomers but the concentration of polymers.
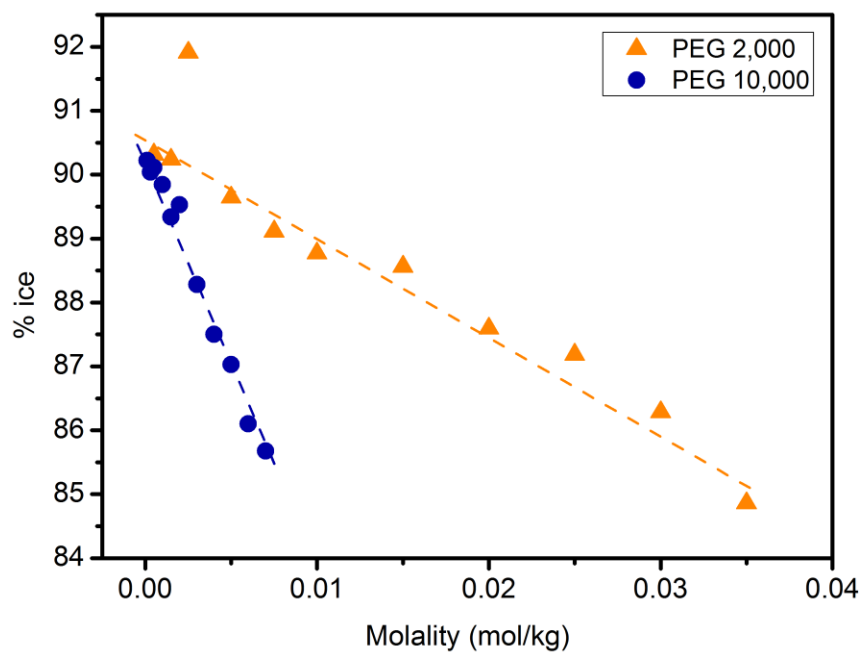
Figure 4.2.3.3 Decrease in ice formation with increasing molality of PEG. Conversion from free water to ice decreased faster in case of PEG -10K.
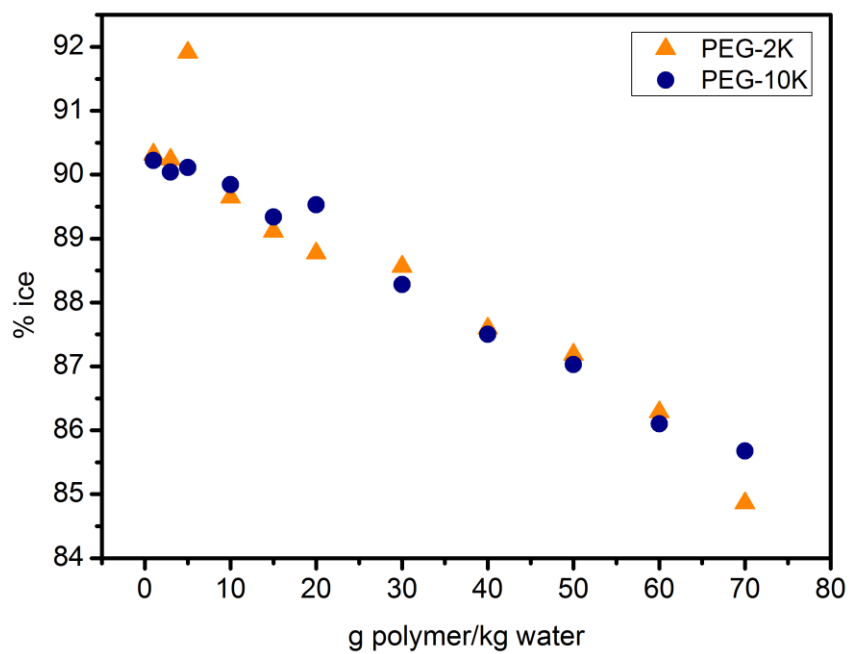

Figure 4.2.3.4 Decrease in ice formation with increasing molality of PEG. Ice formation is independent of molecular weight of PEG.

The melting of frozen bound water appears as secondary melting peaks in the thermograms. Figure 4.2.3.5 shows change in enthalpy of secondary melting peaks with molality. Addition of PEG into water increases melting enthalpy of secondary peaks. This means more free water molecules bound to polymer with addition of PEG and form a PEG-water complex as noted before [31]. Hydration possibility of polymer chain increases with molecular weight. Comparison of two different molecular weight PEG shows that PEG-10K has higher hydration possibility. Thus, even small amount of PEG addition increases melting enthalpy of PEG-water complex. Melting enthalpies of second peaks for the case of PEG-2K do not display sharp increase because of low hydration possibility. Figure 4.2.3.6 shows the concentration dependence of low-T endotherms. It is seen that with increasing polymer concentration the low-T endotherm increases for PEG-10K and PEG-2K. But, as we can see in Figure 4.2.3.5, the increase is more pronounced in PEG-10K aqueous solutions.
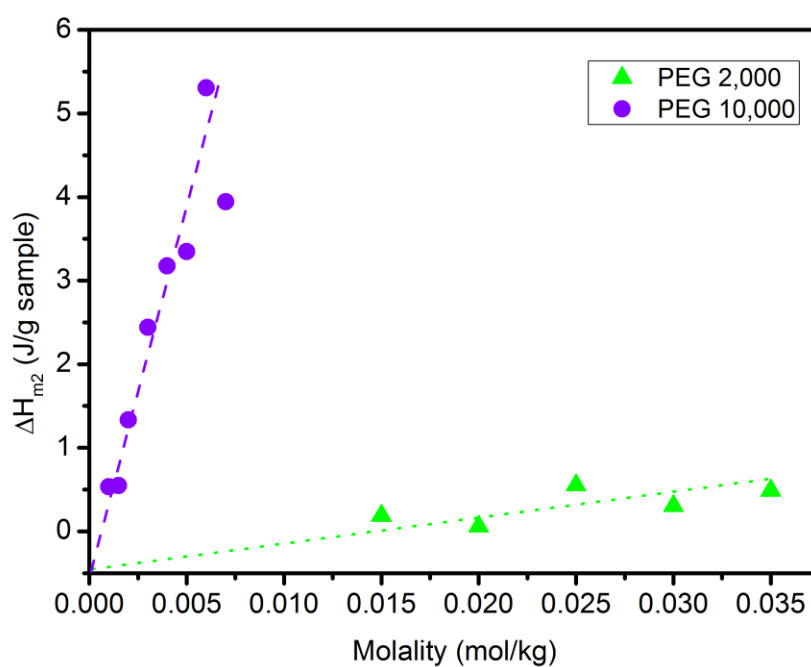
Figure 4.2.3.5 Change in melting enthalpies of secondary peaks with molality of polymer solutions. The melting enthalpies increase with molality of solutions. Increment is more dramatic for PEG -10K. Lines are guide to the eye.
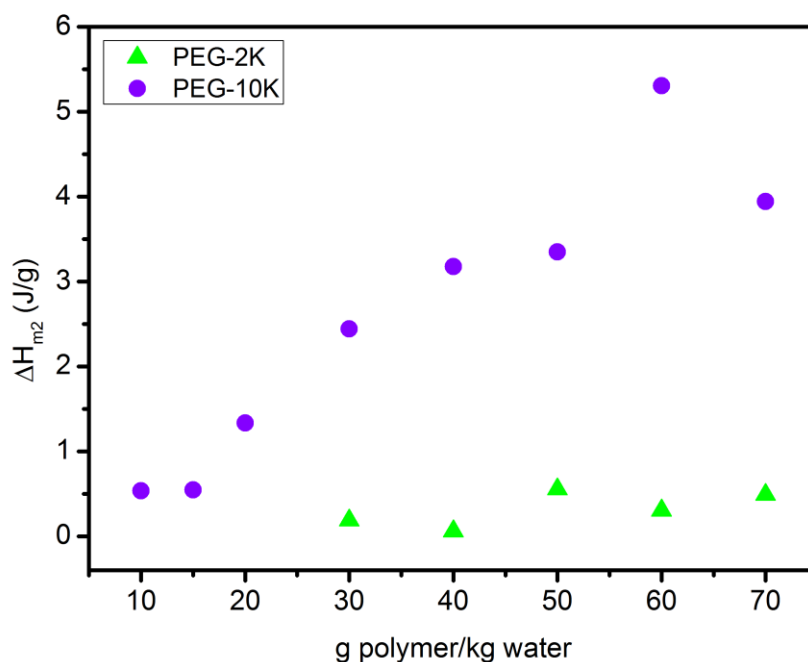
Figure 4.2.3.6 Change in melting enthalpies of secondary peaks with polymer concentration. The melting enthalpies increase with polymer concentrations for both PEG-10K and PEG-2K. Increment is more dramatic for PEG-10K.

Melting temperatures of secondary peaks differ depending on the molecular weight. Figure 4.2.3.7 shows the effect of molecular weight on melting temperatures of second endotherm. With increasing molecular weight, melting temperatures of PEG-water complex increase to higher temperatures. Previously [31] it has been calculated that PEG with molecular weights of 400, 1540 and 70K have hydration numbers of 1.6, 2.4 and 3.3, respectively. So, hydration possibility increases with molecular weight. More free water becomes frozen bound water with longer polymer chains i.e. molecular weight. With increasing hydration degree, complex becomes more stable and higher melting temperatures are required.
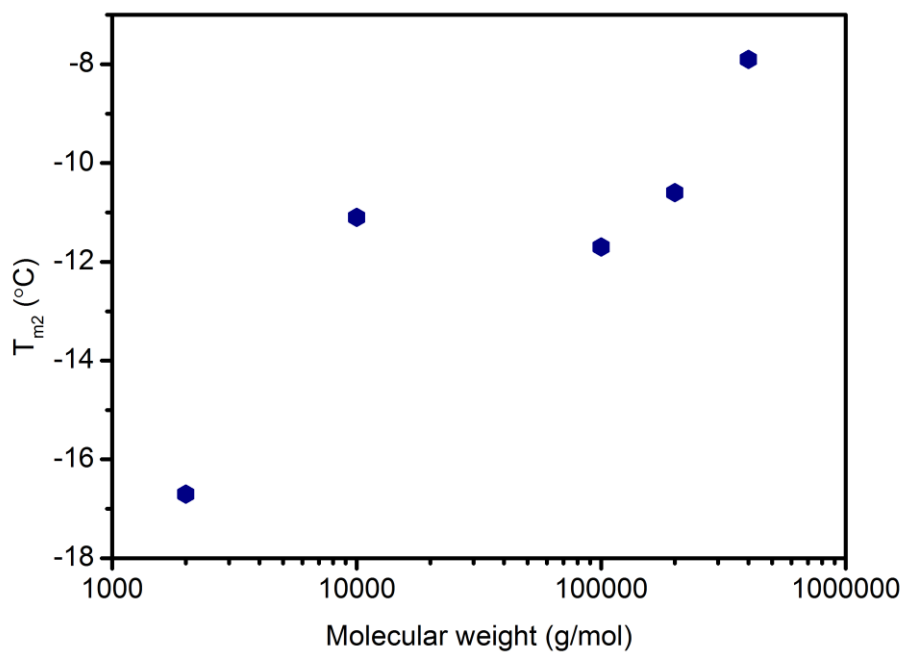
Figure 4.2.3.7 Change of melting temperatures of second endotherms with molecular weight.
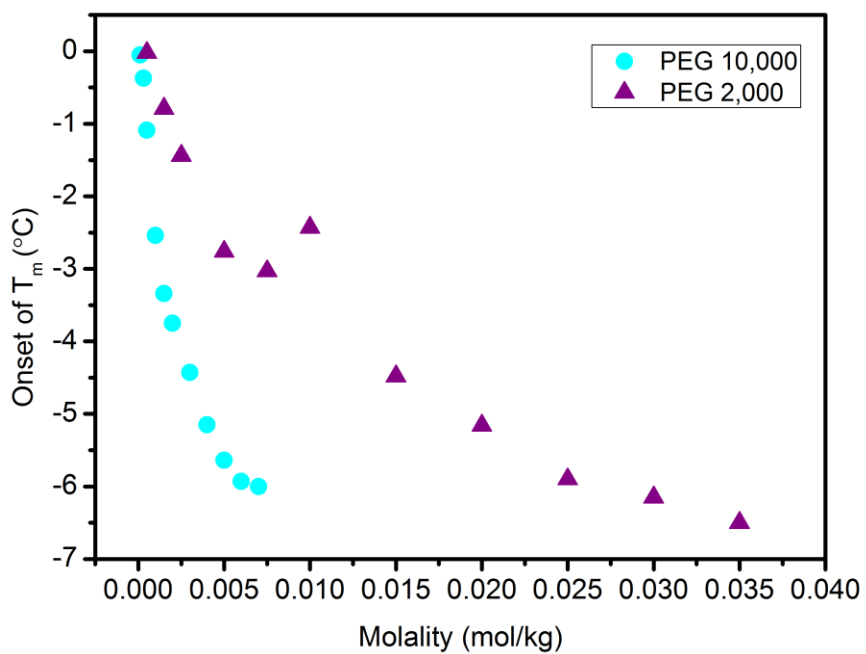
Figure 4.2.3.8 Onset points of melting temperatures for PEG-2K and PEG-10K polymer solutions.

PEG-2K and PEG-10K solutions did not show a decrease of melting temperatures of pure ice. As we pointed out previously, this is the result of high heating rate. We analyzed the onset points of melting rather than the peak points of melting to overcome this problem. Figure 4.2.3.8 shows the change in onset points of melting with molality for PEG-2K and PEG-10K solutions. Another problem we faced was baseline deviations in heat flow vs. temperature graphs. To avoid confusion and to obtain reproducible results we analyzed onset points of melting from temperature vs. time graphs. We took onset point of melting as the point where deviation from baseline starts. PEG-10K solutions decrease the onset point of melting dramatically whereas PEG-2K solutions display same temperatures at higher molalities. It means that polymer-ice or polymer-water interactions are stronger for PEG-10K solutions.
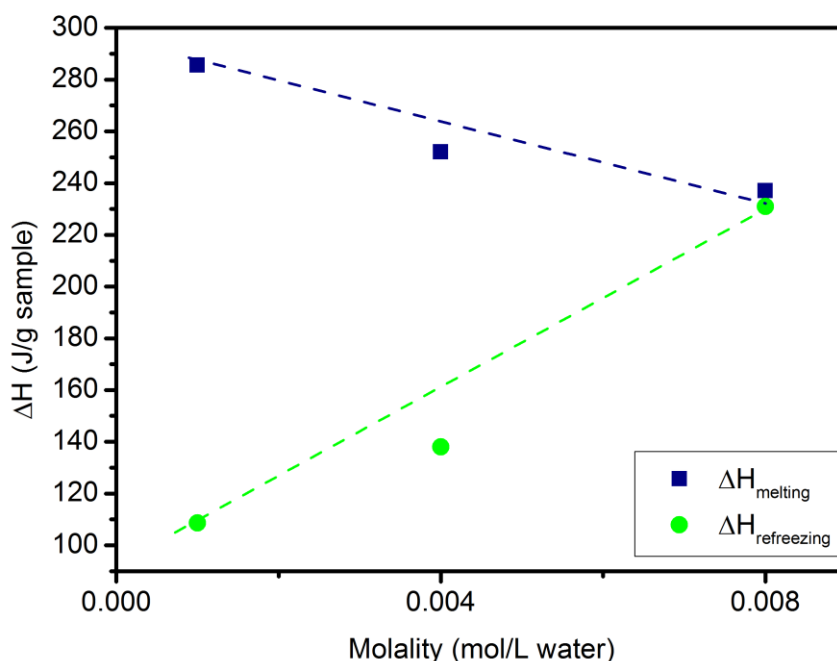
Figure 4.2.3.9 The melting and refreezing enthalpies of PEG-10K. Melting enthalpies decrease with PEG concentration whereas refreezing enthalpies increase.

Refreezing experiments of PEG-10K solutions showed that isothermal treatment at − 1 °C reveals exothermic peaks. Figure 4.2.3.9 shows the comparison of melting and refreezing enthalpies. Melting enthalpies resulted from the melting event of free water and the refreezing enthalpies resulted from isothermal treatment at − 1 °C for 20 minutes. Blue squares are melting enthalpies of free water and green dots are refreezing enthalpies of partially frozen

water. As pointed out earlier, melting enthalpies of free water decrease with polymer concentration. Enthalpy of freezing, on the other hand, increases with polymer concentration. It indicates that lesser amount of ice formed with decreasing polymer concentration. The most plausible explanation is that larger amount of ice did not melt at − 1 °C for the case of low polymer concentrations. So, refreezing of partially melted water did not give much energy and resulted in low refreezing enthalpy. However, for the case of 80 g/L PEG -10K solution, almost all ice melted at − 1 °C. So, refreezing of just melted ice gave nearly same amount of heat as melting event.

4.3 Aqueous poly (2-ethyl-2-oxazoline) (PEOx) Solutions

We investigated the molecular weight and concentration effects of aqueous PEOx solutions on ice melting behavior. Two different molecular weights namely PEOx-5K and PEOx-50K were studied. Figure 4.3.1 shows the endothermic peaks of ice melting taken at 5.0 C/min heating rate. DSC curves did not reveal low-T endotherm for PEOx-5K and PEOx-50K contrary to aqueous PEG solutions. Only melting endotherms of pure ice are seen in both graphs.
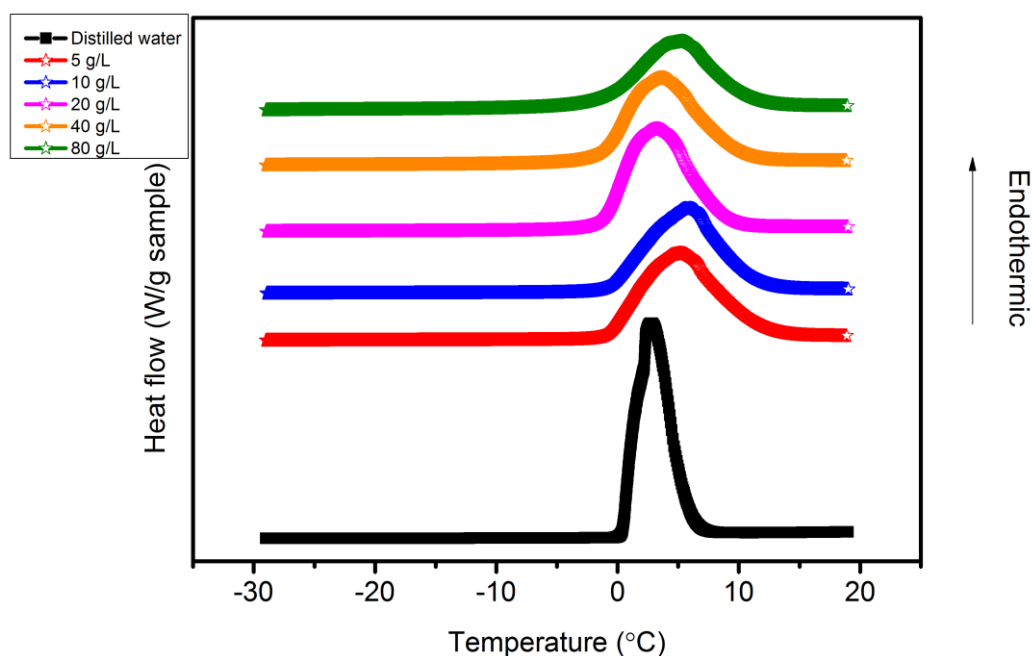
a)
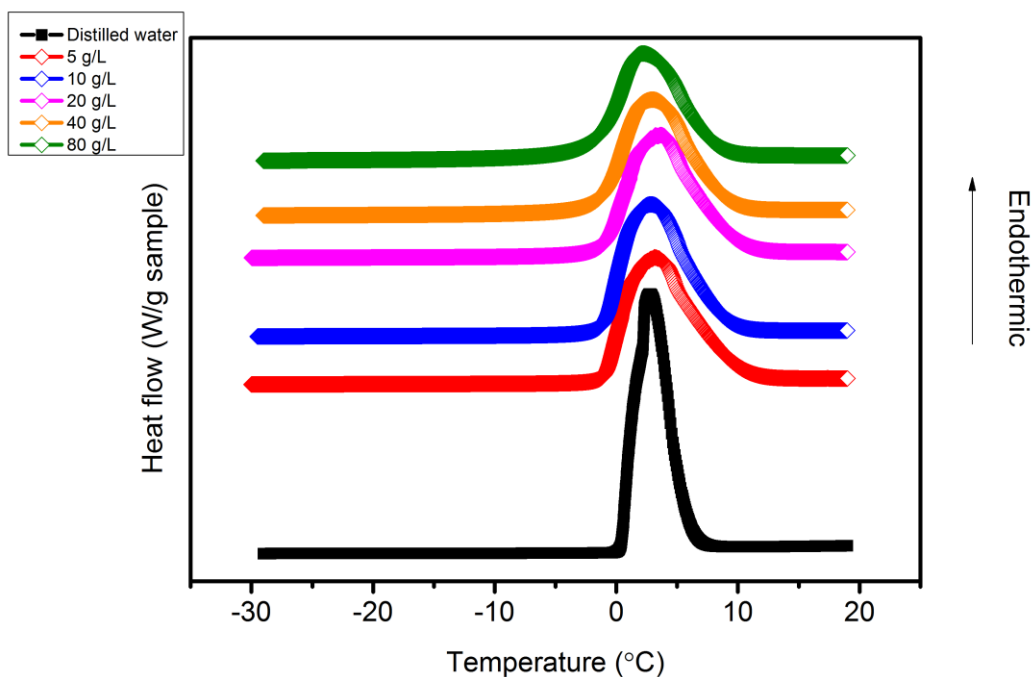
b)

Figure 4.3.1 DSC heating curves of a) PEOx-5K and b) PEOx-50K with the rate of 5 °C/min. No low-T endotherm was seen in the graphs.

Figure 4.3.2 DSC heating curves of PEOx-5K. Heating rate was decreased to 2.5 °C/min from 5.0 C/min. Still, no low-T endotherms were seen.

In order to see whether high heating rate is the responsible for not forming low-T endotherm same samples were heated and c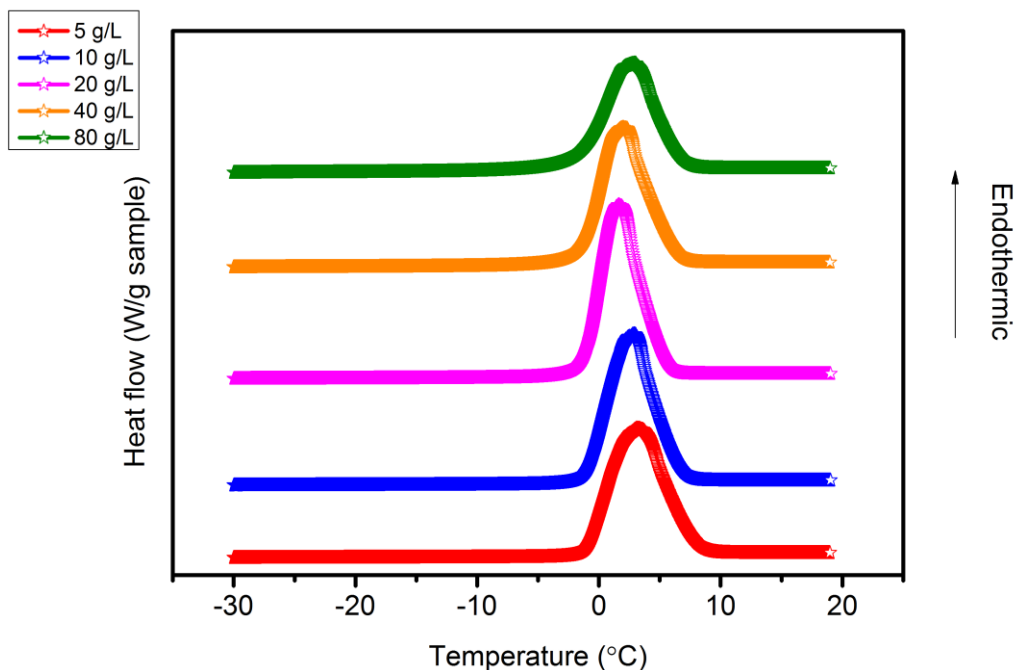ooled at 2.5 °C/min rates. Figure 4.3.2 shows the DSC heating curves of PEOx-5K solutions taken at 2.5 °C/min heating/cooling rates. Still, no low-T endotherm was seen in the graphs. Detailed investigation of the curves revealed that there is a glass transition at − 26.3 °C for PEOx-5K aqueous solutions. Figure 4.3.3 shows the glass transition temperature of 80 g/L PEOx-5K aqueous solution.
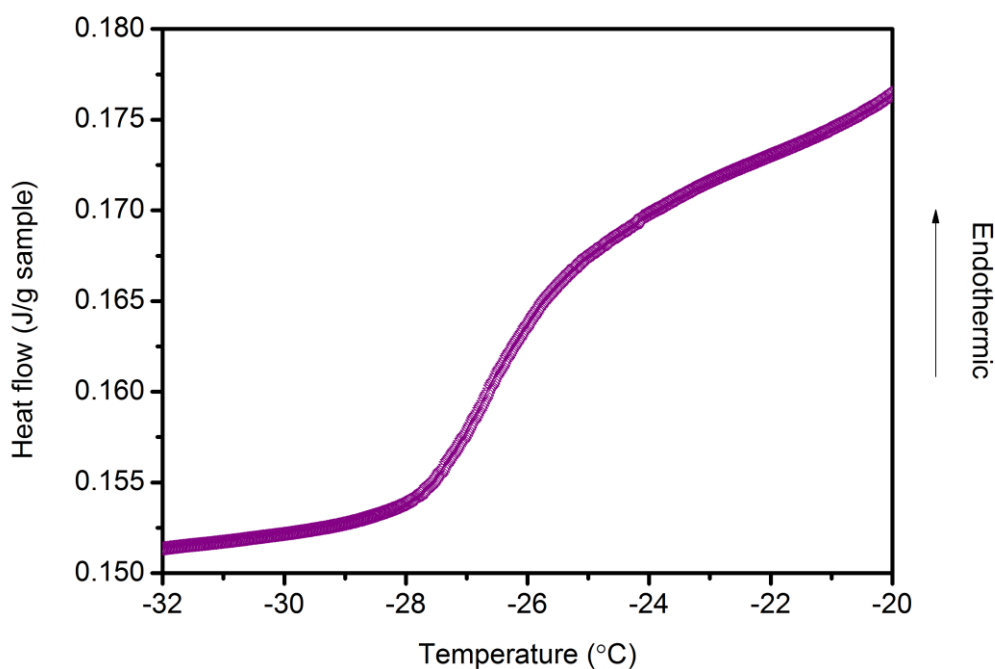
Figure 4.3.3 Glass transition temperature of 80 g/L aqueous PEOx-5K solution was found to be -26.3 °C. Polymer solution was cooled to - 60 °C and kept isothermally for one minute. Heating and cooling rate is 5.0 °C/min.

The polymer solution was cooled down to − 60 °C and isothermally waited for one minute. Bulk PEOx-500K has glass transition temperature around 60 °C [75]. It has long been known that water addition decreases the glass transition temperature because water molecules increase the chain mobility of polymer. However, the presence of unfrozen water even at − 26 °C shows that PEOx-water interaction is strong and thus water cannot freeze into ice.

To see the effect of heating rate on the glass transition temperature, samples were heated at 2.5 °C/min and 5.0 °C/min. Figure 4.3.4 shows glass transitions of polymer solutions having different concentrations measured at 5 °C/min and 2.5 °C/min scan rate. Differently, these polymer solutions were cooled to − 35 °C and isothermally kept at this temperature for three

minutes. However, isothermal treatment temperature and time did not affect glass transition temperatures for the case of 5.0 °C/min scan rate. Glass transition temperatures slightly shift to lower temperatures for 80 g/L polymer concentration when heating rate is 2.5 °C/min. In addition, DSC curve of 20 g/L polymer concentration shows deviation from baseline at − 24 °C.

a)   b)
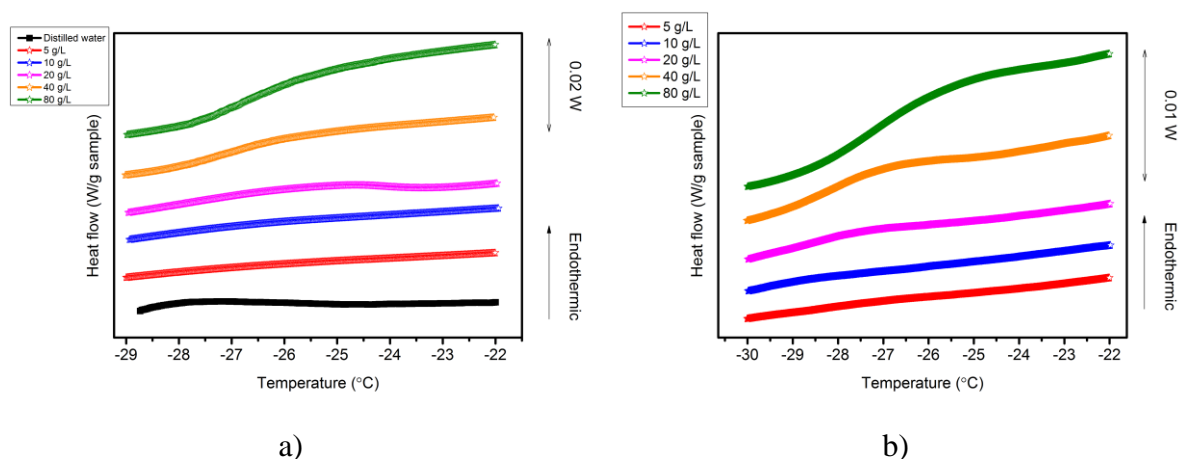
Figure 4.3.4 The effect of heating rate on the glass transition temperature of PEOx-5K. a) Heating rate is 5.0 °C/min, b) 2.5 °C/min.

Aqueous PEOx-50K solutions also displayed glass transitions. Figure 4.3.5 shows glass transitions for PEOx-50K solutions. It is seen that the glass transition temperatures of PEOx-50K solutions were same as those of PEOx-5K solutions. Again, high concentrations display significant glass transitions compared to relatively low concentrations.
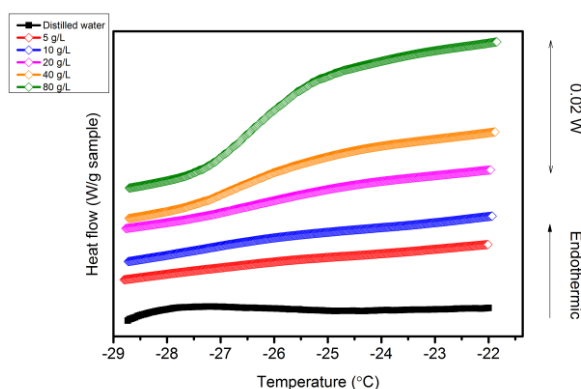
Figure 4.3.5 The glass transitions for the aqueous solutions of PEOx-50K. For the high polymer concentrations, transition is more pronounced.

This indicates that in high polymer concentrations the polymer chain is hydrated relatively more compared to low polymer concentrations. The heat change resulting from the movement

of polymer chains for the high polymer concentrations is in the range of instrument specs. Therefore, the mobility of polymer chains can be seen in the graphs for high polymer concentrations. This indirectly points out that more unfrozen water coexists with PEOx-50K in the high polymer concentrations.

Table 4.3 Melting peak temperatures of PEOx-5K solutions for 5 C/min and 2.5 C/min heating rate.

	PEOx-5K	
	5 C/min	**2.5 C/min**
	T_m (°C)	
5 g/L	5.06	3.06
10 g/L	5.63	2.55
20 g/L	2.96	1.57
40 g/L	3.67	1.71
80 g/L	4.79	2.70

4.3.1 Refreezing experiments of aqueous solutions of PEOx: Understanding melting/crystallization behavior in depth

In order to investigate ice-PEOx interaction in depth, the procedure described in 4.2.2 was applied to aqueous solutions of PEOx-50K. Briefly, samples having different concentrations were isothermally kept at − 1 °C and cooled down to − 35 °C with 1 °C/min scan rate. As expected endothermic peaks appeared when the samples were heated to room temperature with 0.5 °C/min scan rate. Figure 4.3.1.1 shows the exothermic peaks of aqueous PEOx-50K solutions after isothermal treatment at − 1 °C for 20 minutes. It is seen that peak temperatures of refreezing exotherms are likely to have concentration dependence: peak T decreases with increasing PEOx concentration. The green line did not display an exothermic peak because there was no ice nucleus that would trigger crystallization for 80 g/L PEOx-50K. Crystallization peak of supercooled water reappeared at lower temperatures for 80 g/L. Figure 4.3.1.2 shows the endothermic peaks of ice melting at the end of refreezing measurements. It is clearly seen that the melting temperatures have tendency to follow polymer concentrations. With polymer concentration the melting temperatures decrease.
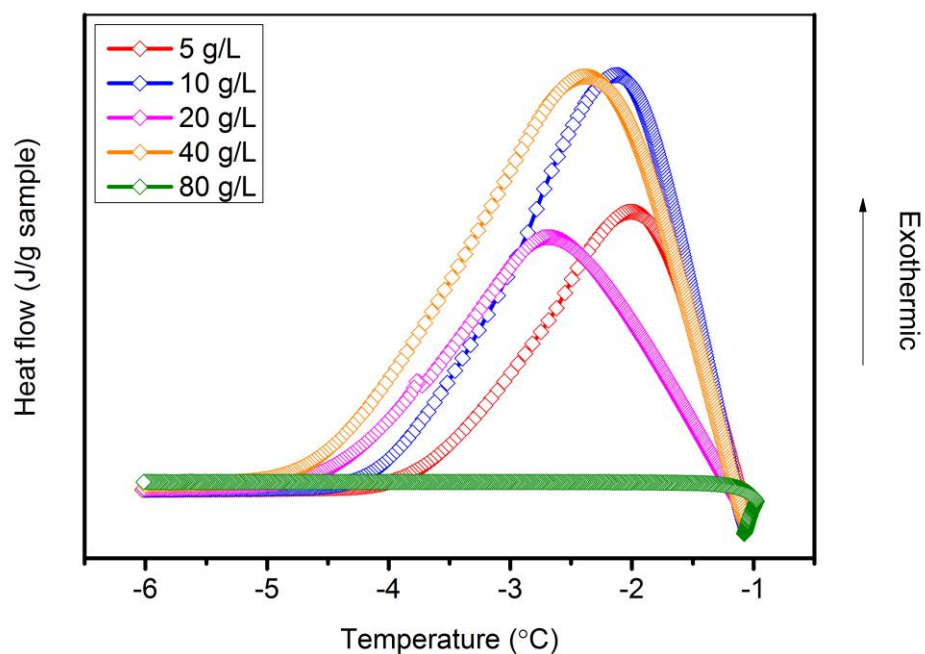
Figure 4.3.1.1 Refreezing of PEOx -50K solutions. Refreezing temperatures shifted to lower side with increasing polymer concentration except 20 g/L. Green line which represents 80 g/L does not display refreezing peak because all ice has melted at -1 °C. Cooling rate was 1 °C/min.
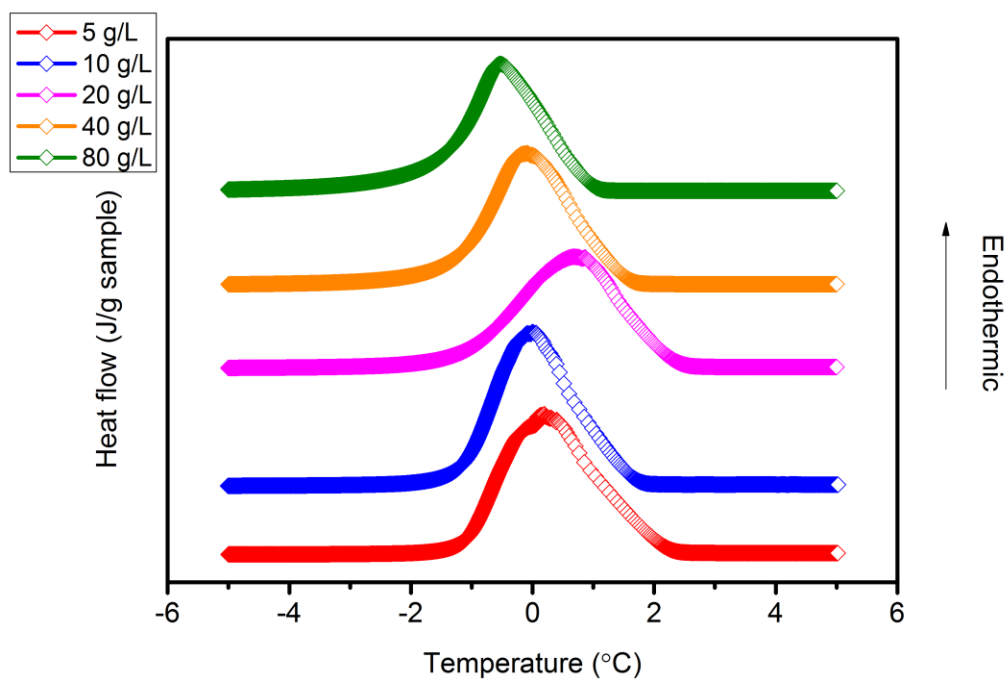
Figure 4.3.1.2 Melting peaks of PEOx-50K at the end of refreezing measurements. Heating rate is 0.5 C/min. The peak temperatures have tendency to follow concentrations.

4.3.3 Discussion

Investigation of aqueous PEOx-5K and PEOx-50K solutions showed that these solutions did not have low-T endotherm which has been observed for aqueous PEG solutions between the studied range (– 60 - 20 °C). The monomer of PEOx has carbonyl group at side chain and nitrogen on the backbone. The hydrogen-bonding capability of PEOx is shown in Figure 4.3.3.1, a). Moreover, each monomer has a strong amide dipole that gives rise to dipole-dipole interactions with water molecule.

a)   b)
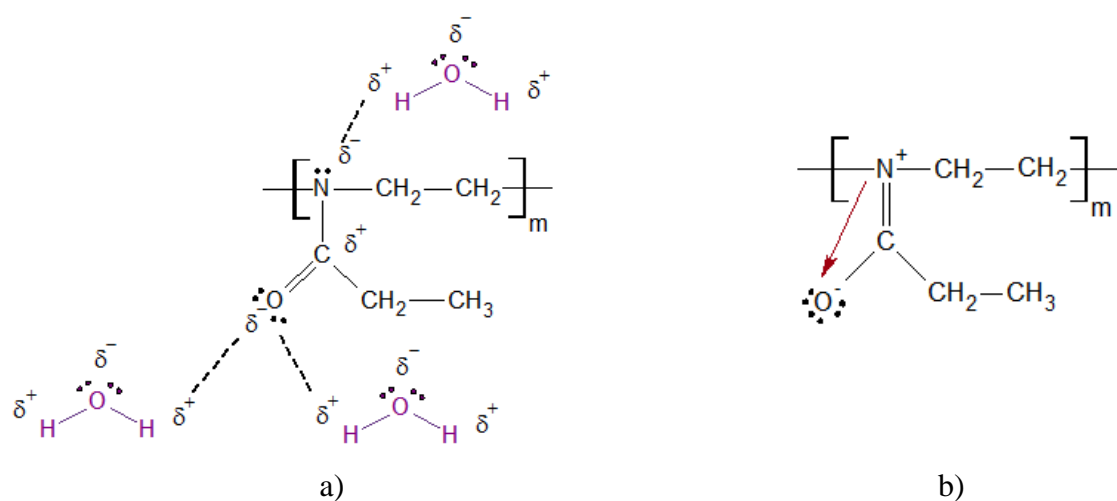
Figure 4.3.3.1 Illustrations of hydrogen-bonding capability of PEOx a) and the presence of strong amide dipole in resonance form of PEOx b) [76].

These numerous interactions hydrate the PEOx chains. The glass transition rather than melting peak of ice indicates that bound water did not crystallize but acted as plasticizer for PEOx. The strong dipole-dipole interactions might be responsible for not freezing water even until – 60 °C. The strength of PEOx-water complex might derive from the bridging water molecules between PEOx chains [76].

Figure 4.3.3.2 shows change in melting enthalpy with PEOx addition. As in the case of PEG, higher molecular weight samples decrease melting enthalpy more effectively. The explanation for this decrease is the presence of unfrozen bound water. As the polymer concentration increases unfrozen bound water amount increases. Unfrozen bound water confined in polymer chains may get frozen at temperatures lower than – 60 °C.
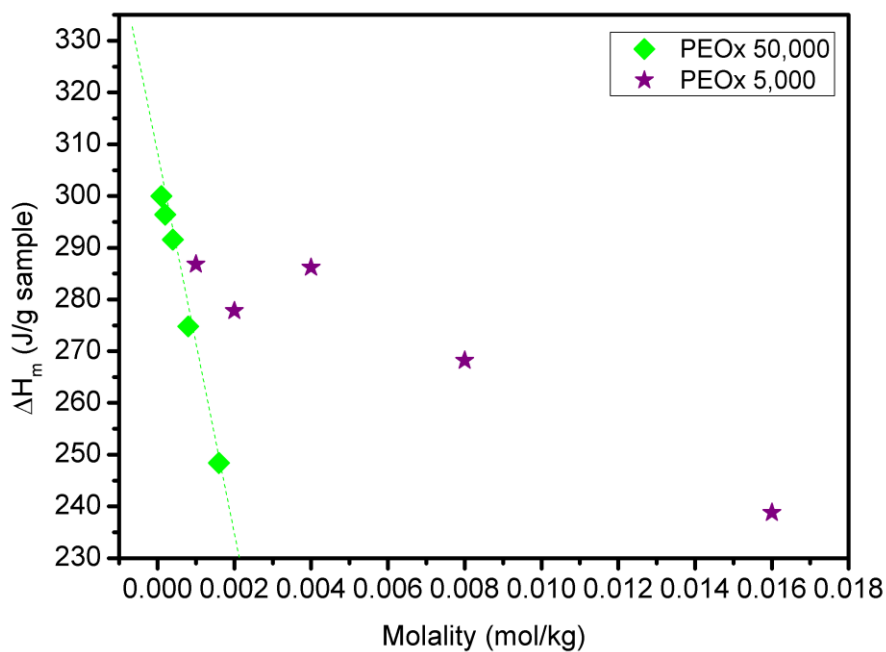
Figure 4.3.3.2 Melting enthalpy of ice decreasing with increasing PEOx concentration. Higher molecular weight sample decreases more as in the case of PEG.
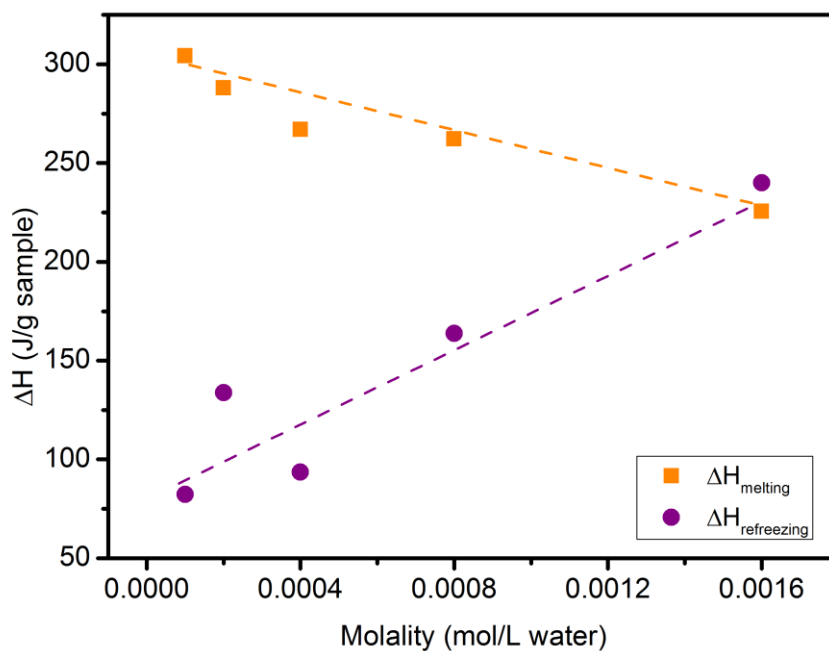
Figure 4.3.3.3 The refreezing and melting enthalpies of PEOx-50K aqueous solutions. Lines are guide to the eye.

Figure 4.3.3.3 shows the refreezing and melting enthalpies of aqueous PEOx-50K solutions at the end of refreezing experiment. It is seen that the melting enthalpy is decreasing as observed in aqueous PEG solutions. Moreover crystallization enthalpies increase with the addition of PEOx-50K which indicates more and more free water can coexist with ice.

Figure 4.3.3.4 shows melting and refreezing temperatures of PEOx-50K solutions and freezing point depression as a function molality.

a)   b)
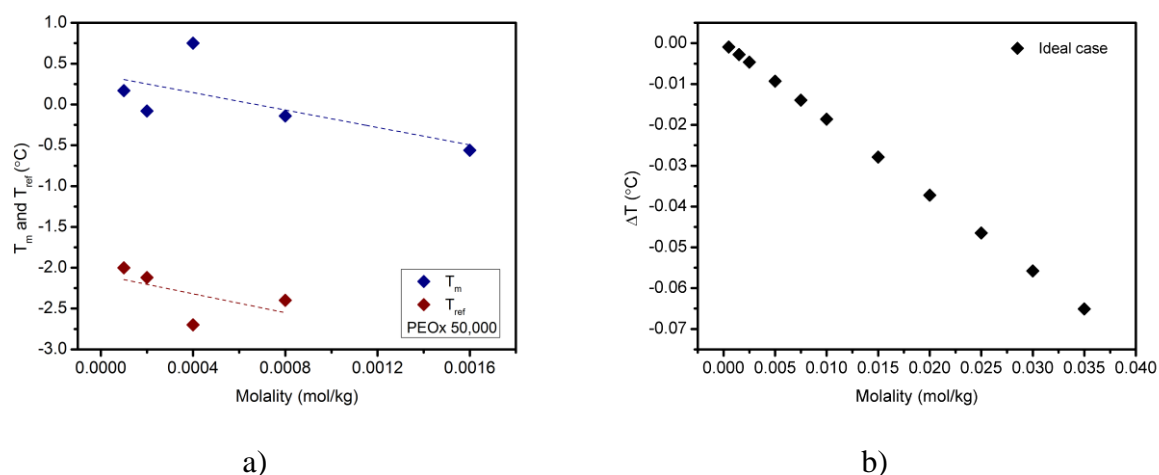
Figure 4.3.3.3 The melting and refreezing temperatures of PEOx -50K solutions, a). Colligative freezing point depression as a function of molality, b).

If the freezing point depression was the result of only amount of PEOx -50K, we would expect to see less depression (Figure 4.3.3 b). However, lower molality of PEOx -50K gives more depression in melting point. This leads to a conclusion that PEOx -50K might have freezing point depression ability due to interaction with water. Refreezing experiments support this claim. Cooling after isothermal treatment at − 1 °C gives exothermic peaks. Peak temperatures have concentration dependence. When more PEOx -50K is present the system, refreezing temperatures decrease to lower temperatures. It indicates that PEOx -50K delays the growth of ice crystals probably by adsorption onto ice crystal surfaces [12][77].

4.4 Conclusion

We have investigated the freezing and melting behavior of two water soluble polymers namely polyethylene glycol and poly (2-ethyl-2-oxazoline). Two different molecular weight of PEG showed the decrease of melting enthalpy of ice as a function of molality. Moreover, all investigated molecular weights of PEG showed second endotherm and melting enthalpy of these endotherms increase with PEG concentration. We conclude that with the addition of PEG more free water bounds to polymer chain and therefore less ice is formed. The melting temperature of second endotherm increases with molecular weight. The concentration dependence was not pronounced in our samples contrary to previous work [28]. Since the hydration degree increases with molecular weight, more free water is able to bind to polymer by hydrogen bonds. This phenomenon leads to increase of melting temperatures of low-T endotherms since the energy that is required to break the bonds increases. Refreezing experiments also revealed that less ice is reformed in concentrated PEG solutions when the samples were kept isothermally at − 1°C. In such temperatures where ice and water coexist the interaction of polymers and ice can be studied in detail. The increase of enthalpy of exothermic peaks showed that more water could coexist with ice when the polymer concentration increased.

Contrary to PEG, PEOx solutions did not show second endotherms. Nevertheless, they decreased the melting enthalpy of ice. We also observed glass transitions in PEOx solutions. Independent of heating and cooling rate glass transition temperature was found as − 26 °C. This shows that unfrozen water is confined in polymer chains and gives mobility to polymer. Although PEOx has strong amide dipole and multiple possibility of hydrogen-bonding (such as carbonyl group and the lone pairs on the backbone nitrogen) the melting event of bound water was not observed. We speculate that the lowest temperature we studied (– 60 °C) was not low enough to freeze bound water molecules. The refreezing experiments revealed that presence of PEOx delays the recrystallization of ice by decreasing the peak temperature. Furthermore, investigation of refreezing enthalpies show that the presence of PEOx chains decrease the ice re-formation. This observation might show that PEOx-ice interaction is possible and PEOx delays the growth of ice nucleus by adsorbing onto ice planes.

.

CHAPTER V

# POLYMER/NANOPARTICLE COMPOSITES

FOR ANTI-ICING APPLICATIONS

The nanoparticle incorporated polymer coatings have been considered for anti-icing surfaces. One mechanism of achieving the anti-icing property is making the surfaces superhydrophobic [1], [5], [78]. By doing this water droplets cannot stay on the tilted surface and thus ice cannot form. However, the effectiveness of these coatings on solid surfaces are still controversial [8], [9]. In order to achieve anti-icing coatings and find the factors affecting freezing of water styrene-butadiene-styrene triblock copolymer/hydrophobic silica nanoparticle composites have been prepared. The freezing times of the droplets were tested at different plate temperatures and humidity conditions in a temperature and humidity control cell. Surface morphology of the coatings was investigated by SEM and its relationship to freezing times was inferred. As an application study, SBS/hydrophobic silica nanoparticle composite was added into bitumen and modified bitumen was successfully prepared. The rheology measurements were done to see the effect of SBS/hydrophobic silica nanoparticle composite addition on the mechanical properties of bitumen.

The desired anti-icing coating consists of a polymer, SBS and hydrophobic silica nanoparticles. So, the polymer matrix which contains nanoparticles should be thick enough to disperse nanoparticles uniformly on the surface. SBS polymer can be dissolved in both chloroform and toluene. In order to understand the best solvent that gives the optimum polymer thickness as a coating, thin films of SBS were prepared from chloroform and toluene. Figure 5.1 shows the effect of two different solvents on the film thickness of polymer. SBS thin films spin-coated from chloroform solution resulted in larger thickness on silicon substrates compared to those spin-coated from toluene solution. Chloroform has lower boiling temperature than toluene. During the deposition stage of spin coating, chloroform evaporates faster, the concentration and viscosity of polymer solution increases and more polymer stays on the solid surface. Because toluene does not evaporate fast compared to chloroform, polymer dissolved in toluene is thrown out by centrifugal force at the ramp up stage. As a result, thicker polymer film forms when we dispense solution from chloroform.

Figure 5.2 shows photographs of SBS thin films deposited from chloroform and toluene. From the colors of thin films, it is seen that films grew faster when deposited from chloroform. The colors of 6 g/L SBS from chloroform and 10 g/L SBS from toluene are roughly same and thickness values for these films are both 60 nm. Other reason why we chose chloroform as solvent is its better dispersion ability. Hydrophobic silica nanoparticles disperse more homogenously in chloroform and therefore uniform composite films can be obtained.

5.1 Wettability of SBS thin films

The water contact angles of bare SBS thin films were measured first as control experiments to contrast the effect of inclusion of nanoparticles on wettability. Figure 5.1.1 shows that water contact angles for SBS thin films had slight concentration dependence. From graph it is seen that water contact angle (WCA) stays constant at value of 88°. Below the concentration of 10 g/L SBS, surface might not have been completely covered by SBS and thus the exposure of water to silicon wafer which has the contact angle of ~ 20° after hydrolization decreased the WCA. For the concentrations higher than 10 g/L surface might be covered by SBS completely and increasing the polymer concentration might slightly increase the surface roughness which increases the WCA values for hydrophobic polymers.
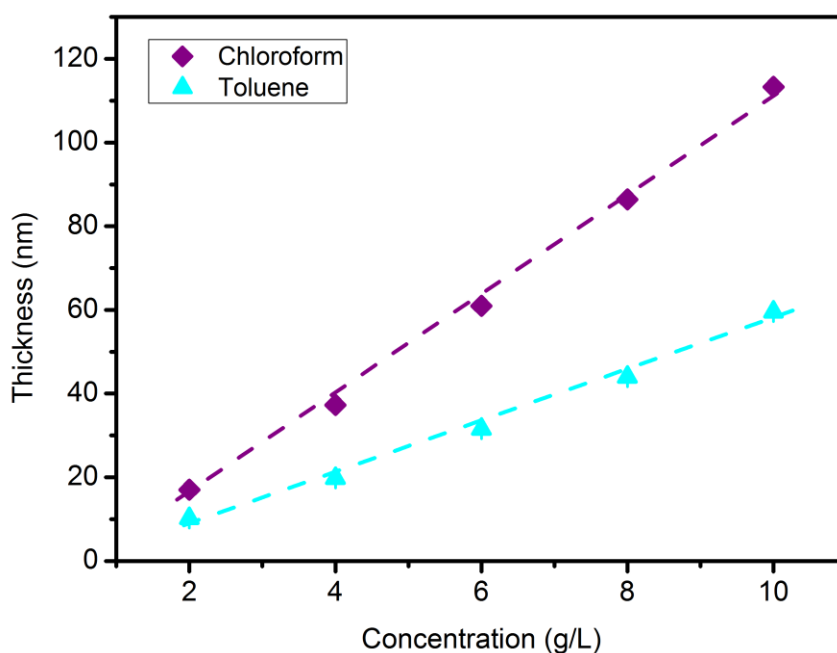

Figure 5.1 Effect of solvents on polymer film thickness. SBS thin films from chloroform displays sharper growth compared to thin films from toluene.

Another possibility of this increase might be the different surface affinity of different blocks of SBS polymer known as surface segregation. According to Young equation the contact angle of a perfectly smooth surface depends on surface tension of impinged liquid (γ_L), solid (γ_S) and interfacial energy of surface and liquid (γ_{SL}) [79]

$$cos\theta = \frac{\gamma_s - \gamma_{SL}}{\gamma_L}$$

Two different blocks of SBS, namely polybutadiene and polystyrene have different surface energies and also different mobility. The system tries to reach lowest energy state and therefore choose the lowest energy component to enrich the free surface. Since water contact angle is determined by chemistry and topology of the surfaces surface segregation affects the wettability of surfaces. Change in water contact angle as shown in Figure 5.1.1 might be the result of surface segregation of more hydrophobic component. Or by combination with surface segregation, surface reconstruction might have occurred [80]. Modification of surface chemistry by segregation and reconstruction changes water contact angle. By considering these issues we continued our experiments with constant 10 g/L SBS concentration.
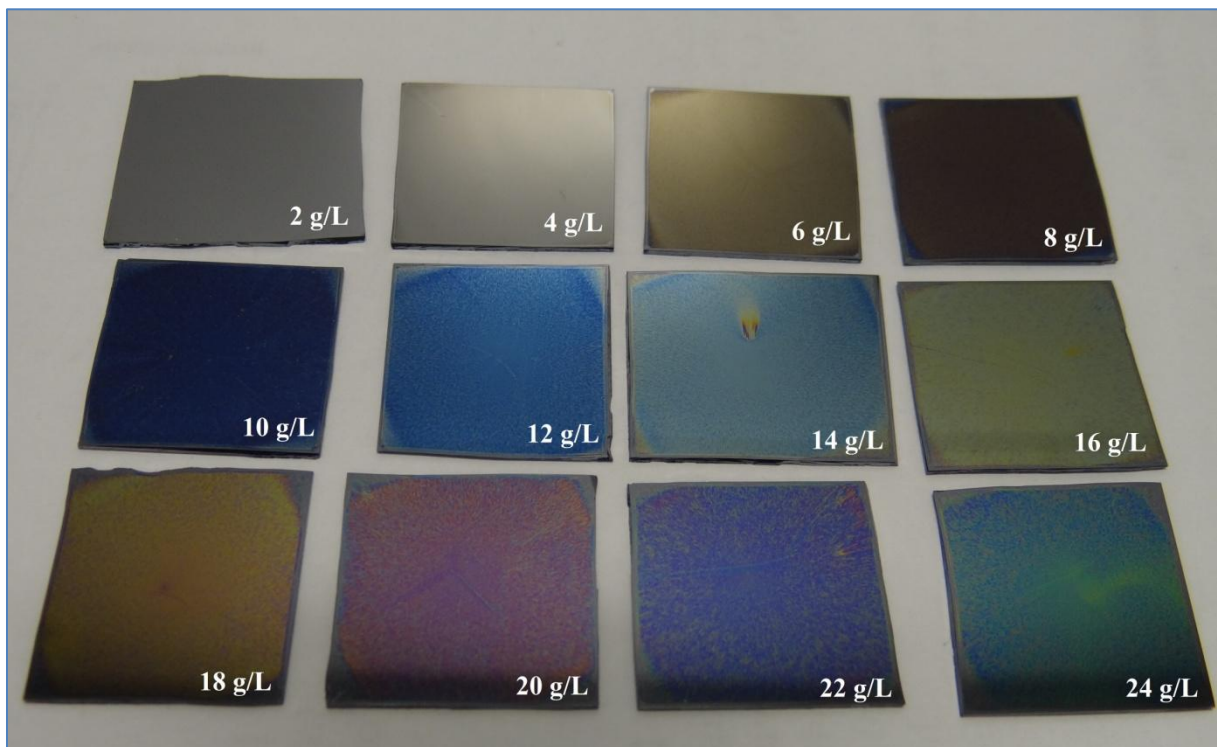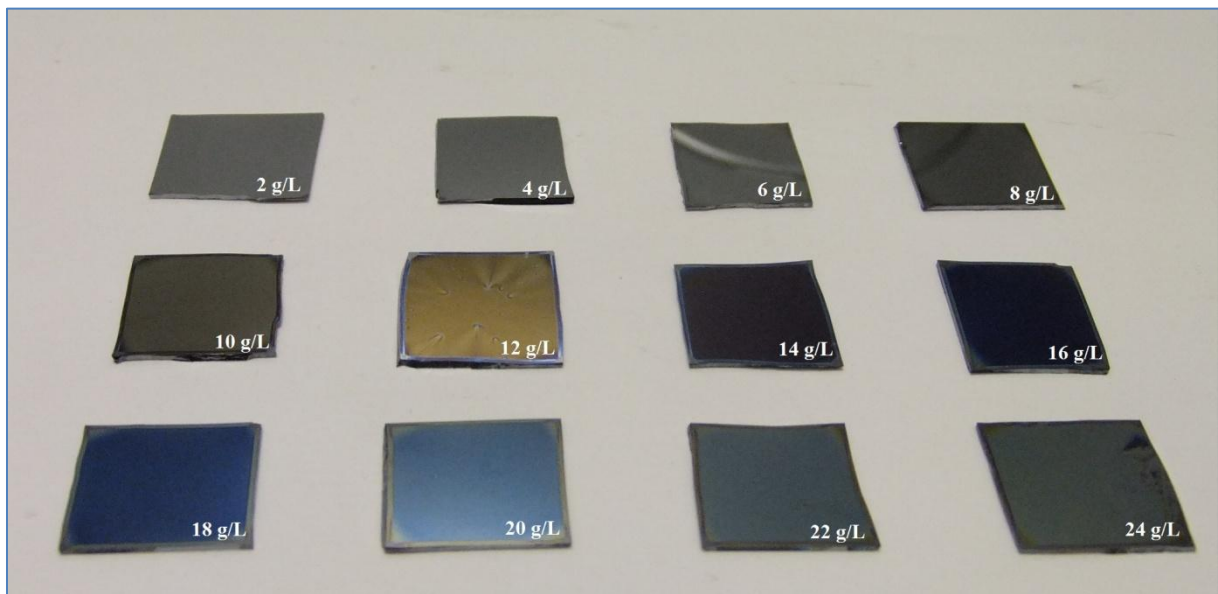
Figure 5.2 Photographs of SBS thin films from chloroform (above) and toluene (bottom) for 2-24 g/L concentrations.
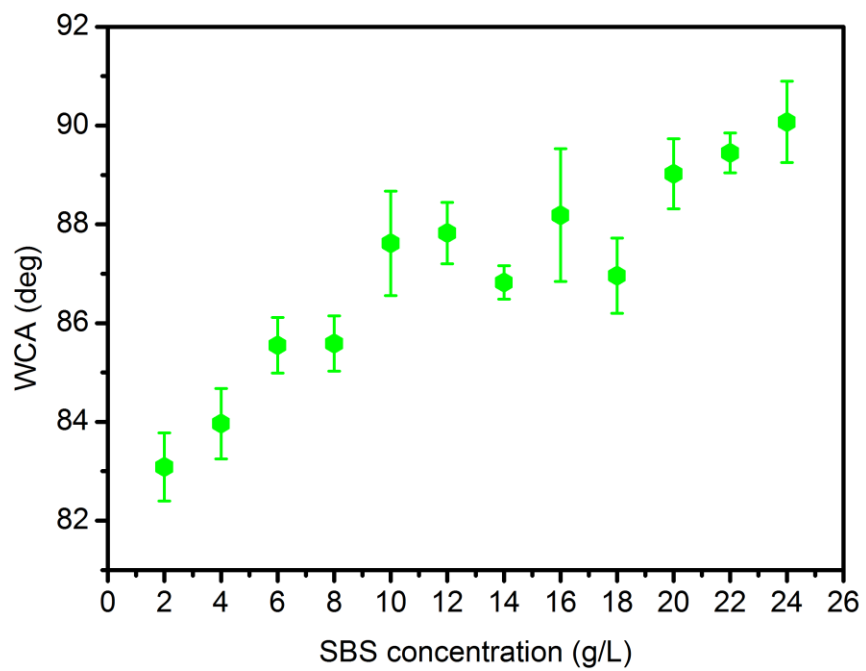
Figure 5.1.1 Water contact angles of different concentration SBS thin films.

5.2 Wettability of silica nanoparticle/SBS composite thin films

The contact angles of composite thin films were measured to understand the effect of hydrophobic silica nanoparticles on the wettability. Figure 5.2.1 shows the effect of nanoparticle inclusion on water contact angle of coatings. Water contact angle increases up to 135° by addition of nanoparticles. The reason of this increment is methyl groups attached to silica core of nanoparticles give hydrophobicity to surface and additionally nanoparticle assembly on surface provides roughness. When the surface is rough, there are two predominant models to describe contact angle. In Wenzel Model, liquid is assumed to wet the rough surface completely and roughness factor (ratio of the actual area to the projected area) is related to contact angle with the following formula [81]

$$cos\theta^W = rcos\theta$$

Where θ^W is the apparent contact angle in Wenzel state, r is the roughness factor of the surface which can be obtained from dividing the actual area by the projected area, and θ is the contact angle. Other model is Cassie-Baxter and according to this model liquid partially wets the rough surface. Impinged water droplets are suspended by air between grooves [82]

$$cos\theta^{CB} = f_1cos\theta - f_2$$

Where θ^{CB} is the apparent contact angle in the Cassie- Baxter state, f_1 is the area of the liquid in contact with the solid divided by the projected area, and f_2 is the area of the liquid in contact with the air divided by the projected area.

The interesting thing in Figure 5.2.1 is the presence of upper limit for the water contact angle. The water contact angles of the coatings increase up to 135° from 88° and stays constant. According to Wenzel model surface roughness increases the WCA of the surfaces. Our results showed that roughness increases up to 50 % (wt.) nanoparticle fraction (10 g/L nanoparticle concentration). Above 50 % the WCA stays constant which indicates surface roughness does not change significantly beyond a certain value.
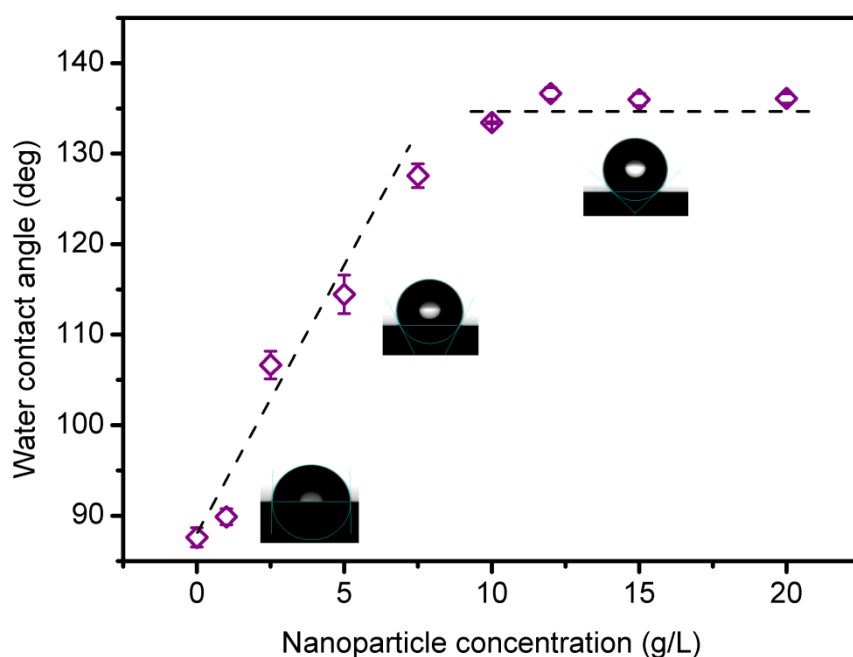
Figure 5.2.1 Change in water contact angle with increasing nanoparticle concentration. Inclusion of hydrophobic nanoparticles increase water contact angle of the coating.

SEM pictures of coatings were taken to analyze the effect of nanoparticles on the surface morphology. Figure 5.2.2 shows the SEM pictures of coatings with varying nanoparticle concentrations. It is obviously seen that nanoparticle addition contributes to the surface roughness of the coatings and nanoparticles dispersed homogenously on the surface. However, surface morphology shows differences for each nanoparticle concentrations. Figure 5.2.3 shows magnified versions of SEM pictures. For the lowest nanoparticle concentration, 2.5 g/L, nanoparticles are seen to embed into SBS matrix and rarely form islands. The coatings from nanoparticle concentrations of 5 and 7.5 g/L showed nanoparticle aggregates on the surface. These aggregates vary in size. Multi-size aggregates form micro and nano roughness. Nevertheless, large aggregates are more pronounced for the 7.5 g/L nanoparticle concentration. When nanoparticle concentration equals (10 g/L) and exceeds polymer matrix concentration (12-20 g/L), nanoparticles form a network throughout the surface. The network consists of small voids as seen in Figure 5.2.3 d), e) and f). After the surface is completely covered with nanoparticles voids become smaller.

a)

b)

c)

d)

e)

f)
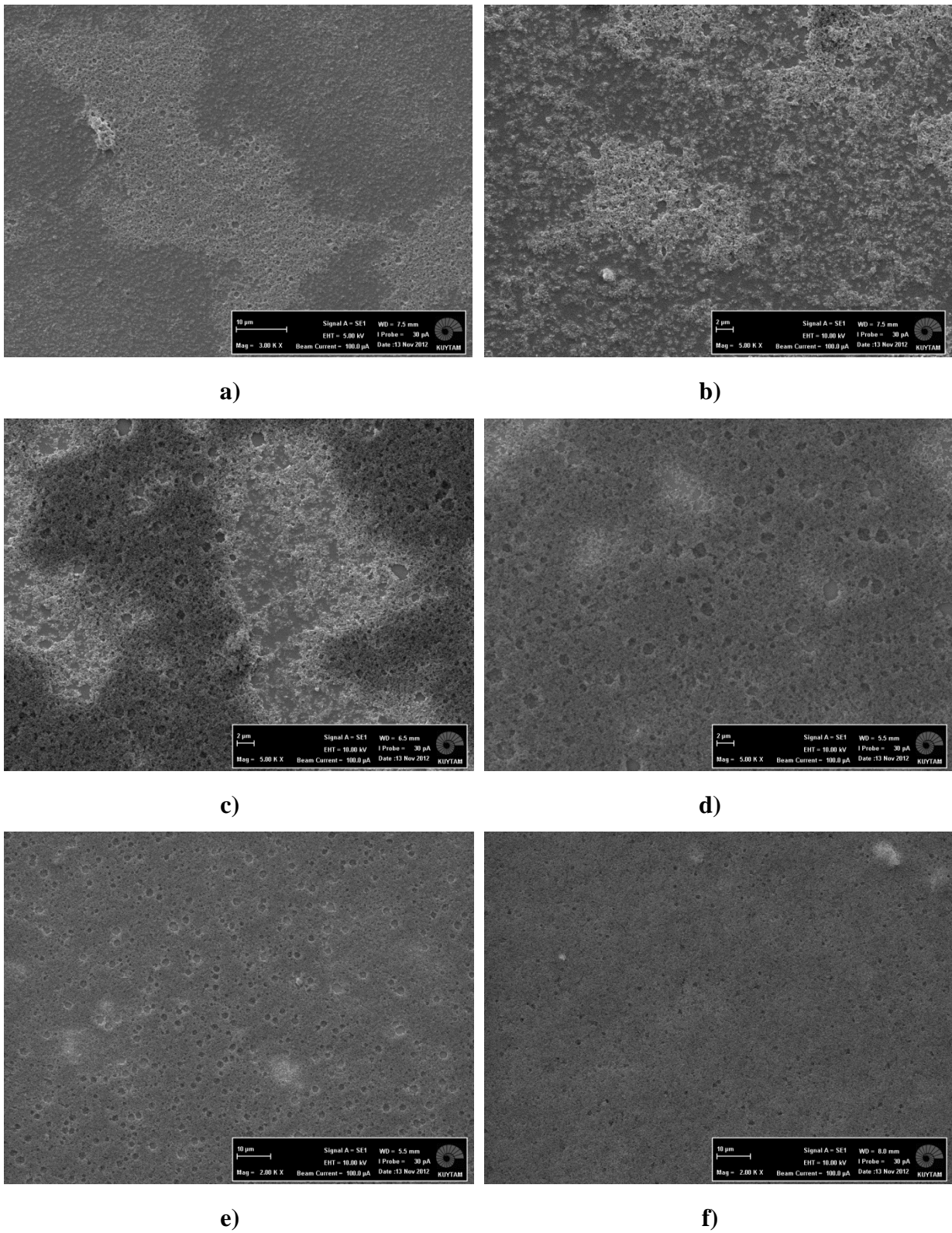
Figure 5.2.2 SEM pictures of SBS/Hydrophobic silica nanoparticle coatings. Nanoparticle concentrations from a) to f) are 2.5, 5, 7.5, 10, 12, 20 g/L. Magnification varies between 2K and 5K.
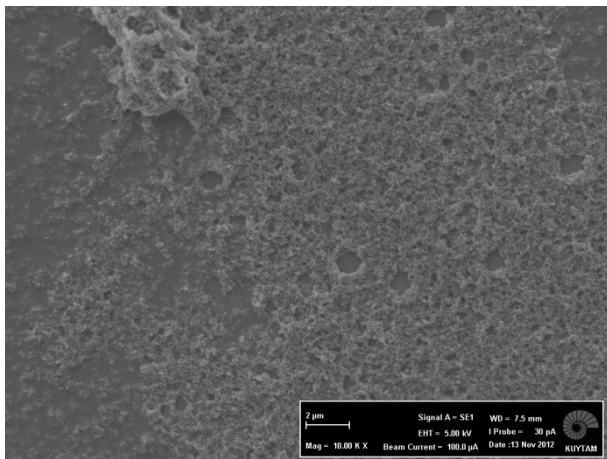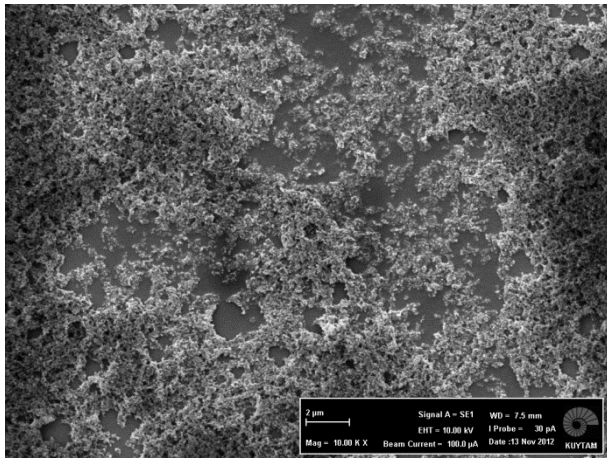
a)
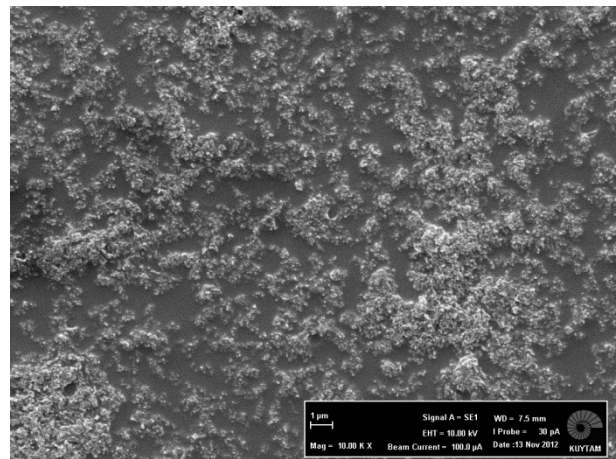
b)

c)

d)

e)

f)

Figure 5.2.3 SEM pictures of SBS/Hydrophobic silica nanoparticle coatings. Nanoparticle concentrations from a) to f) are 2.5, 5, 7.5, 10, 12, 20 g/L. Magnification varies between 10K and 15K.
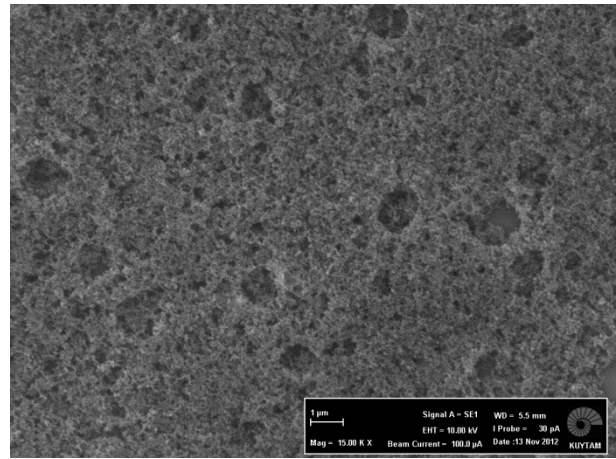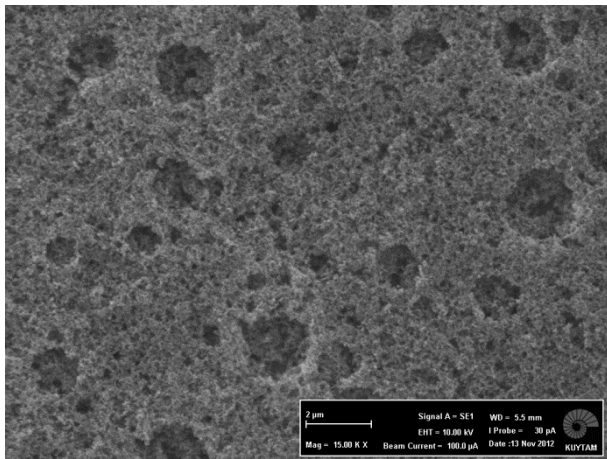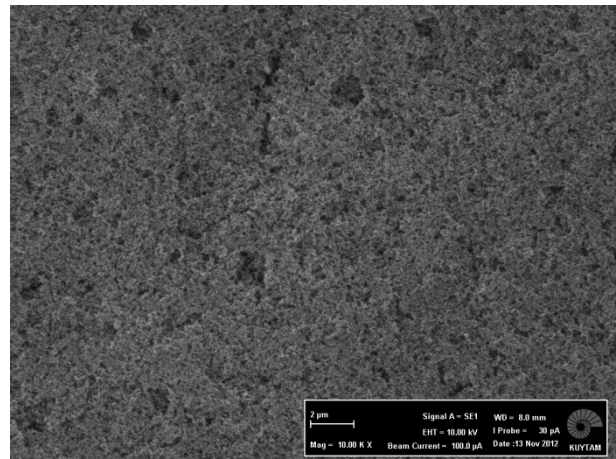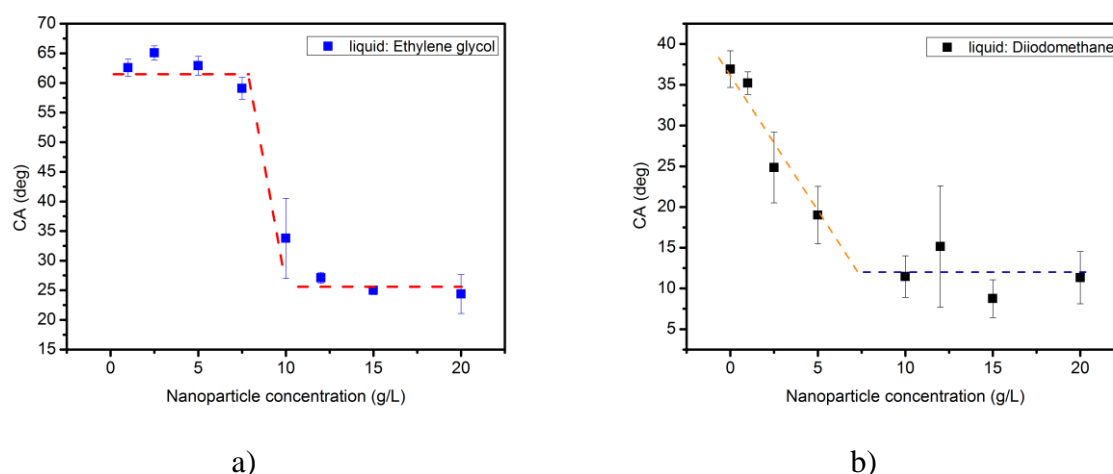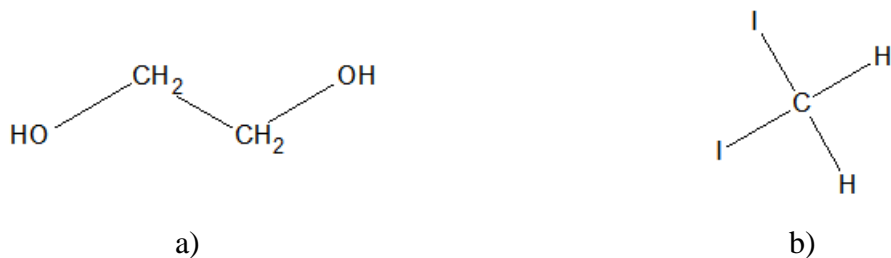
The contact angles of ethylene glycol and diiodomethane droplets also give additional information about surface wettability. Figure 5.2.4 shows change in ethylene glycol and diiodomethane contact angles on films spin coated from solution containing 10 g/L SBS at room temperature. Contrary to the increase in water contact angles with addition of nanoparticles, we see steady values until 7.5 g/L nanoparticle concentration and a sudden decrease to 35° from 60°. Surface tension of ethylene glycol at room temperature is 47.3 mN/m [83]. The contact angles of ethylene glycol droplets do not change much until 7.5 g/L. The presence of fewer nanoparticles on the surface does not prevent ethylene glycol to be in contact with SBS matrix. So, similar contact angles are obtained for the nanoparticle concentrations of 2.5, 5.0, 7.5 g/L. A pronounced decline is observed for the 10 g/L nanoparticle concentration. Since the surface is completely covered by a network of hydrophobic nanoparticles, the hydrophobic CH2 groups of ethylene glycol molecules can spread on nanoparticle network and displays low contact angle values. CH_2 groups of EG may also promote its penetration into pores of hydrophobic silica nanoparticles (Figure 5.2.5). Diiodomethane is a non-polar molecule and only van der Waals interactions exist. It lacks of hydrogen bonding and has lower surface tension (50.8 mN/m) [83]. For the case of diiodomethane, decrease in contact angle is gradual (orange line in Figure 5.2.1.3, b)) and later follows the same trend as in ethylene glycol case (blue line in Figure 5.2.1.3, b)). These results clearly indicate that a significant wettability change occurs when the nanoparticle concentration switched to 10 g/L from 7.5 g/L.

a)   b)

Figure 5.2.4 Contact angles of ethylene glycol a) and diiodomethane b) droplets. A sharp decrease is seen for ethylene glycol contact angles whereas gradual decrease is seen for diiodomethane droplets. However, the transition from 7.5 g/L to 10 g/L nanoparticle concentration is obvious for both cases.

a)   b)

Figure 5.2.5 Chemical structures of ethylene glycol a) and diiodomethane b).

5.3 Wettability of polymer/silica nanoparticle thin films at lower temperatures

Water contact angles of the coatings were measured at lower temperatures to understand how the surface wettability changes towards freezing temperatures of water. Figure 5.3.1 shows evolution of water contact angles at temperatures below room temperature. It is seen that contact angle increase is preserved at each temperature with the addition of nanoparticles
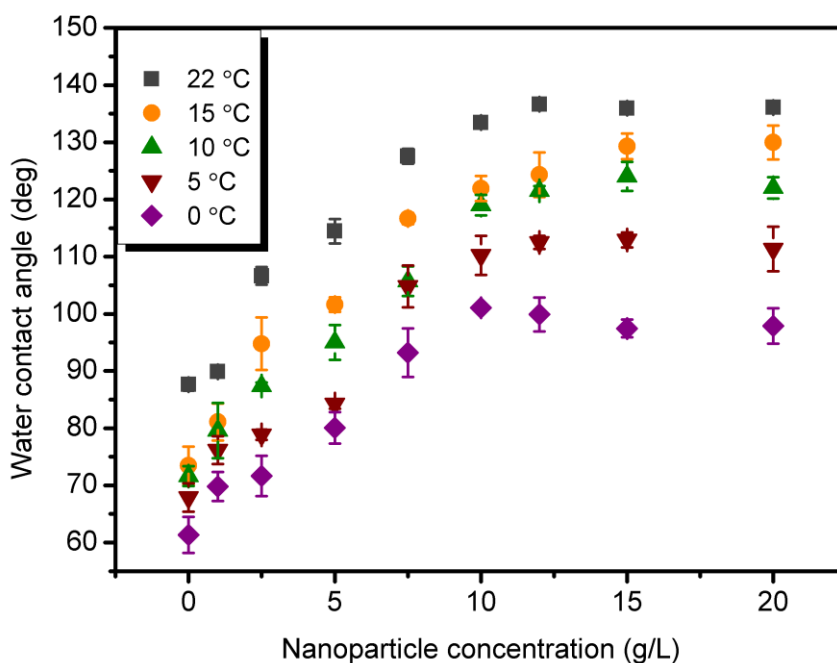
Figure 5.3.1 The change in water contact angles on composite films with the underlying plate temperature.
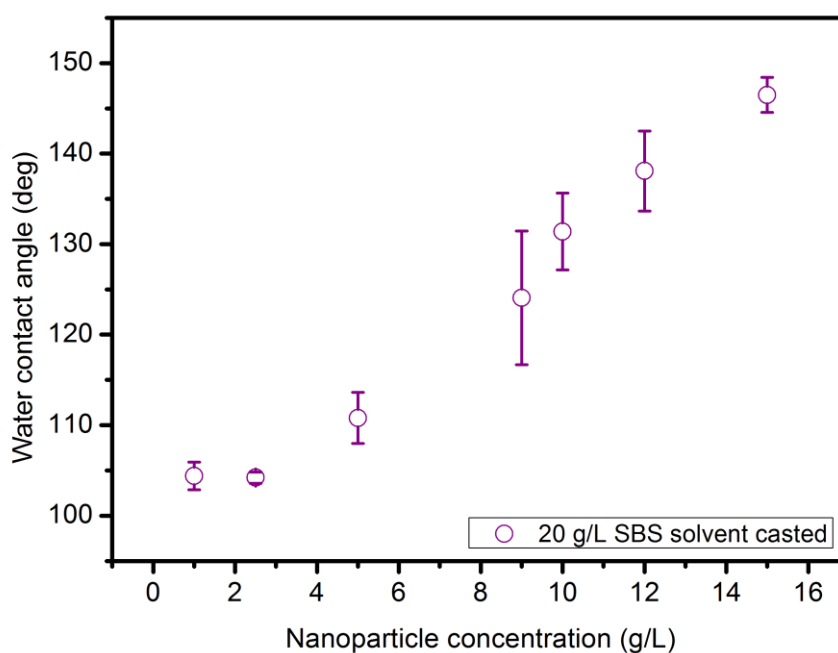
Figure 5.3.2 Water contact angles of 20 g/L SBS solvent cast film with varying hydrophobic silica nanoparticle concentrations at room temperature.

However, the contact angle values decrease with decreasing temperature. Nevertheless, contact angle values are ~ 90 ° on the coatings of 7.5-20 g/L nanoparticle concentration which means that coatings are still hydrophobic at low temperatures. The reason of decrease in contact angles is the formation of thin water film on the surface. Due to water condensation, water adsorbs in cavities between asperities. When droplet is deposited onto film, it coalesces with the existing water film resulting in low water contact angle values. The relationship between freezing time and contact angle is an ongoing debate [84]. It is also previously reported that superhydrophobic surfaces lose their hydrophobicity at low temperatures [40]. Our coatings show promising results since they do not lose their hydrophobicity at low temperatures.

From the application point of view solvent cast is a facile method to prepare polymer films. In order to see whether the solvent cast films also show similar properties as spin cast films water contact angles were measured. Figure 5.3.2 shows water contact angles of solvent cast films. As we see in spin cast films water contact angle increases with nanoparticle addition. To test solvent cast films' humidity resistance we put solvent cast film that contains 20 g/L SBS and 15 g/L hydrophobic silica nanoparticle in the humidity and temperature control cell. Plate temperature was decreased to 0 °C, air temperature and relative humidity were 20 °C

and 48 %, respectively. Figure 5.3.3 shows photographs of the coating at zeroth, 10th and 30th minutes. The photographs indicate that water condensation is prohibited on the coating whereas water condenses on the part without coating. Even at 30th minute, condensed water droplets are not seen on the coating.
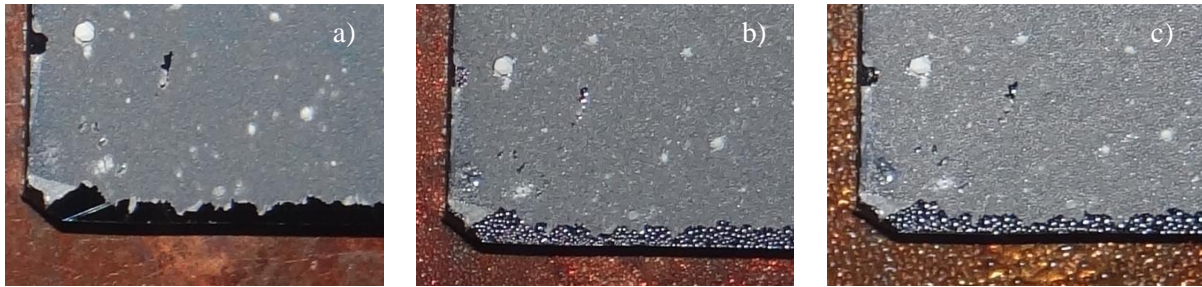
Figure 5.3.3 Photographs of solvenst cast film that contains 20 g/L SBS and 15 g/L hydrophobic silica nanoparticle. in the humidity and temperature control cell. Plate temperature is 0 °C, air temperature is 20 °C and relative humidity is % 48. a) Zeroth minute in the cell, b) 10th minute, c) 30th minute.

5.3.1 Freezing of water droplets on polymer/silica nanoparticle thin films

We tested anti-icing properties of the coatings at – 4 °C and – 8 °C plate temperatures. Figure 5.3.1.1 shows the results of freezing experiments at – 4 °C and – 8 °C plate temperatures. At – 4 °C all nanoparticle containing films showed much longer freezing times compared to SBS films. The freezing time was ~ 50 s for SBS films and ~ 1000 s or more for nanoparticle containing films. The longest freezing time was seen for 43 % and was 3718 s. At – 8 °C films from larger nanoparticle concentrations (43 % and 50 %) were more effective compared to 20 % and 33 %. The longest freezing time belonged to 43 % and was 980 s. This indicates that more nanoparticle is more effective at lower temperatures for the composites.
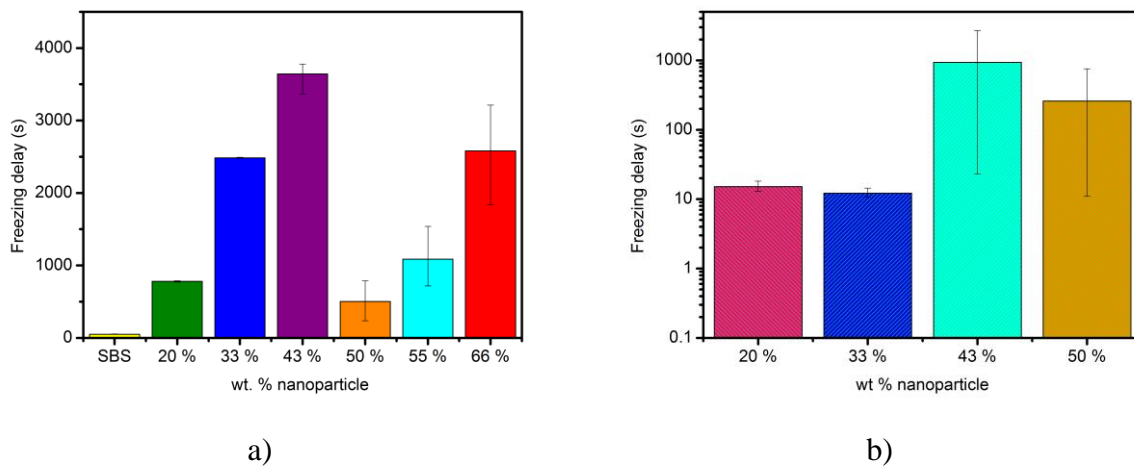
Figure 5.3.3.1 Freezing delays of water droplets on the coatings at – 4 °C a) and – 8 °C b) plate temperatures.
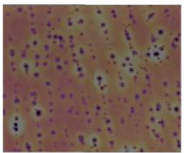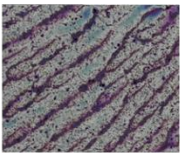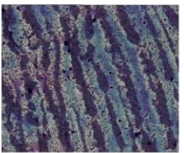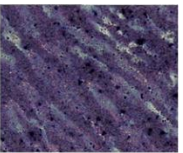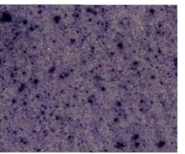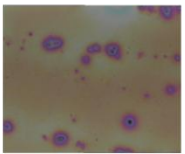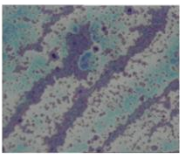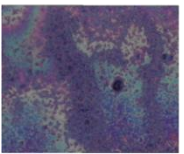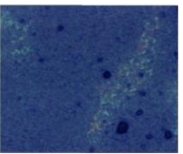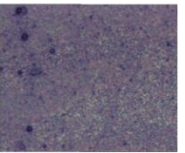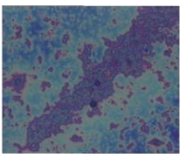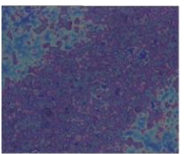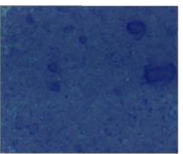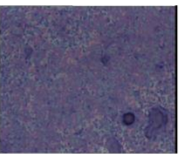
5.4 An application: Incorporation of NP/SBS into bitumen

Bitumen is the major component of asphalt that is used for road pavement. Modification of bitumen by SBS to improve its mechanical properties has long been known [85][86]. However, anti-icing bitumen has not yet been reported. In this section, anti-icing properties of SBS/NP composite containing bitumen thin films will be presented in comparison to those of bare bitumen.

5.4.1 Compatibility of polymer/hydrophobic silica nanoparticle composite with bitumen

As we discussed earlier, homogenous dispersion of nanoparticles is crucial to have micro and nano roughness on the surface and therefore have freezing delay. We took optical microscopy images of the films in order to see the compatibility of bitumen and polymer/hydrophobic nanoparticle composite. Table 5.4.1.1 shows these images with varying nanoparticle-SBS triblock copolymer ratio (0-50 % by weight). It is seen that with nanoparticle addition surface becomes rough. Coatings with 20 and 33 % nanoparticle by weight show lines of nanoparticle aggregates which provide micro roughness. Coating that contains 43 % nanoparticle has nearly nanoparticle covered surface. But still, SBS-bitumen matrix is seen below nanoparticles. For the coating that contains 50 % nanoparticle we can say that surface is completely covered by nanoparticles and still maintain the homogeneity.

Table 5.4.1.1 Optical microscope images of bare bitumen and composite modified bitumen. With increasing nanoparticle concentration surface totally becomes covered with nanoparticles. Homogeneity and uniformity of the surfaces indicate that bitumen and hydrophobic nanoparticles are chemically compatible.

Magnification \ Sample	Bitumen	Bitumen + SBS + 20 % NP (wt.)	Bitumen + SBS + 33 % NP (wt.)	Bitumen + SBS + 43 % NP (wt.)	Bitumen + SBS + 50 % NP (wt.)
5x 960 x 720 µm²					
20x 240 x 180 µm²					
50x 96 x 72 µm²					

5.4.1.1 Rheology measurements of modified bitumen

In order to understand compatibility between polymer/hydrophobic silica nanoparticle composite and bitumen the change in complex modulus with respect to frequency and temperature was measured. Figure 5.4.1.1.1 shows the complex modulus change with applied frequency for bare bitumen a) and BC25 modified bitumen b). BC25 stands for 5 % (wt.) SBS of SBS/bitumen mixture and 20 % nanoparticle (wt.) of SBS/nanoparticle mixture. The complex modulus values for the bare bitumen are consistent with the literature [85]. From the graph b) it is seen that even the small addition of nanoparticle increased the complex modulus of bitumen from ~ 9x 10^5 to 4 x 10^6 Pa for the temperature of 30 °C and the frequency of 10 Hz. Complex modulus contains elastic (G') and viscous (G'') components and is defined as the ratio of maximum stress to maximum strain. It provides the measure of the total resistance to deformation [85].
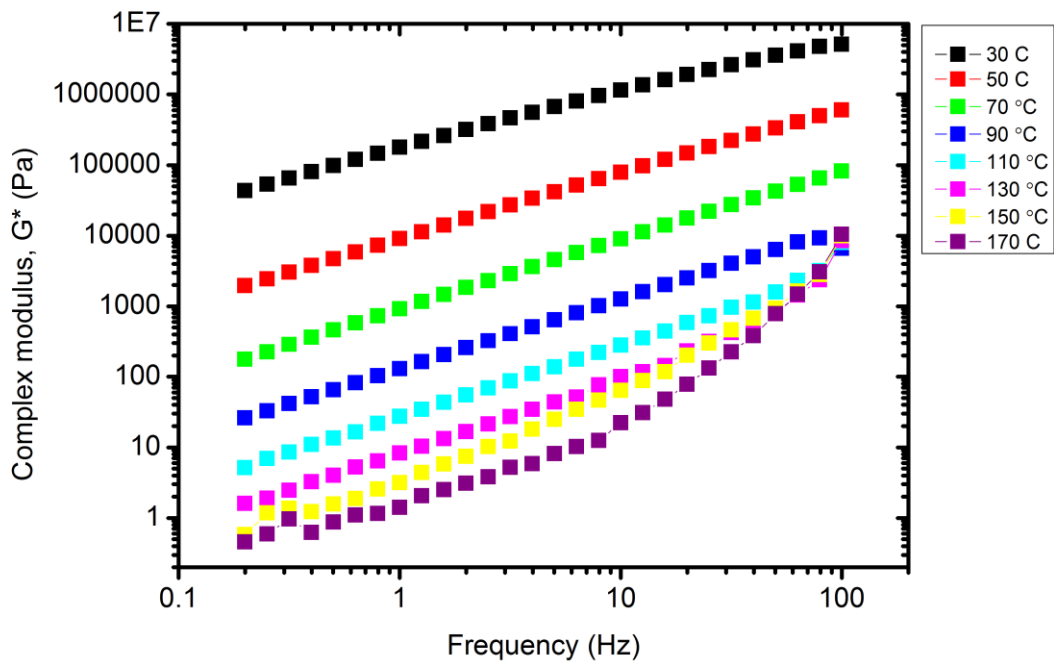
a)
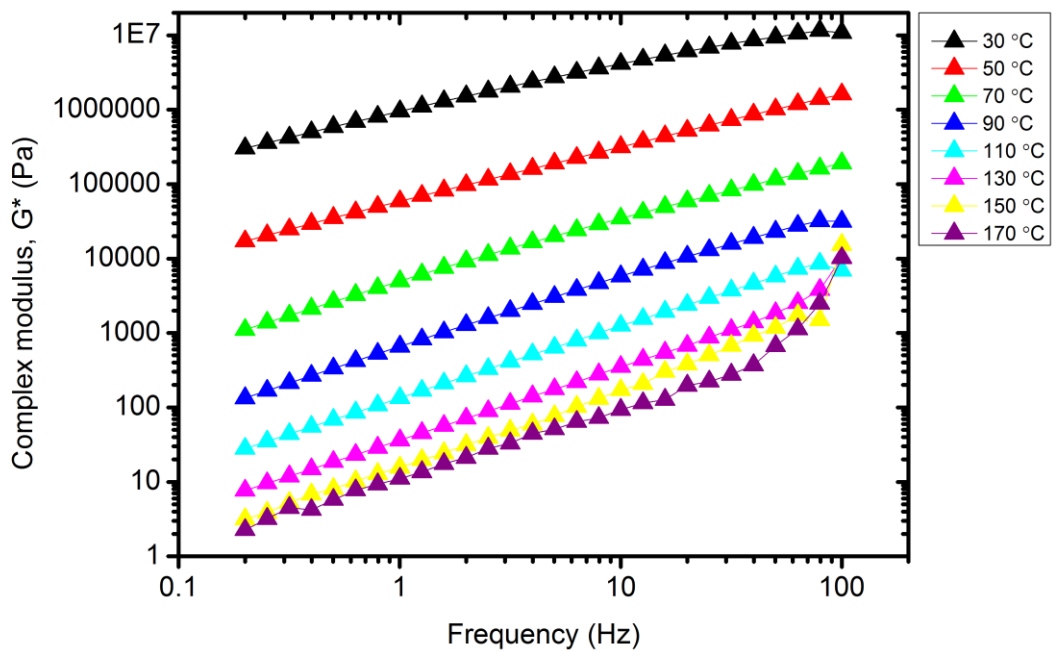
b)

Figure 5.4.1.1.1 The change in complex modulus with respect to frequency at temperatures between 30 and 170 °C a) bare bitumen, b) BC25.

Figure 5.4.1.1.2 shows that change in complex modulus with temperature at 10 Hz applied frequency. BP5 stands for the 5 % by mass SBS in bitumen. All of three samples showed decrease in complex modulus with increasing temperature. It is seen that even slight nanoparticle addition increased the complex modulus of bitumen in addition to the effect of SBS. This also shows the good compatibility of polymer/nanoparticle composite with bitumen.
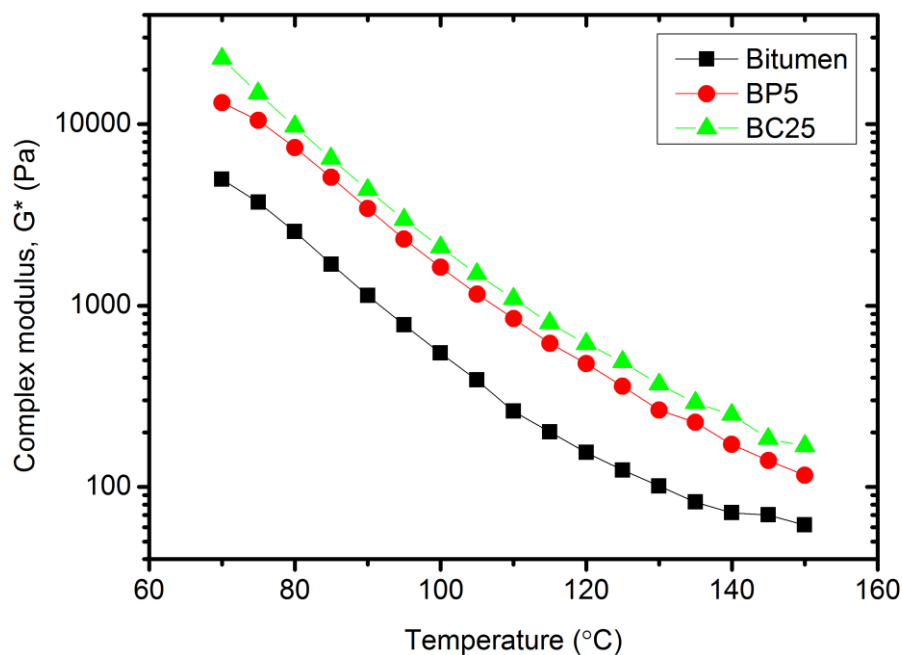
Figure 5.4.1.1.2 Complex modulus of bitumen mixtures with increasing temperatures. Black line represents bare bitumen, red line is 5 % by mass SBS in bitumen mixture and BCP25 is 5 % (wt.) SBS of SBS/bitumen mixture and 20 % nanoparticle (wt.) of SBS/nanoparticle mixture.

The viscosity of the bitumen is another important factor in road pavement applications. To see the effect of composite inclusion the dynamic viscosity of the bitumen and modified bitumens were measured. Figure 5.4.1.1.3 shows the change in dynamic viscosity with respect to frequency for bare bitumen and modified bitumen. It is seen that bare bitumen behaves like Newtonian fluid except at 30 °C. For the case of modified bitumen, however, non-Newtonian behavior is observed at temperatures 30 °C, 50 °C and 70 °C.
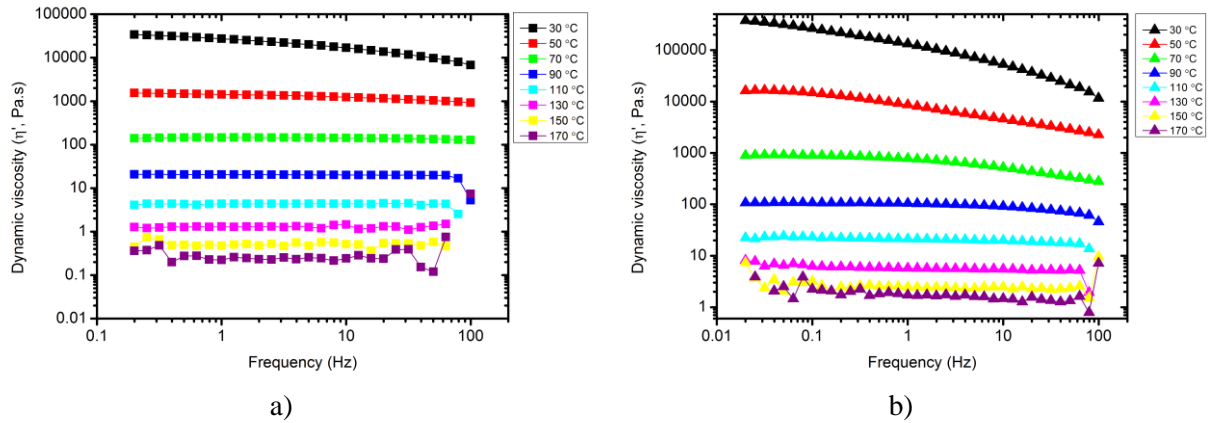
Figure 5.4.1.1.3 Change of dynamic viscosity with frequency at temperatures 30-170 °C for a) bare bitumen b) modified bitumen.

Figure 5.4.1.1.4 shows the change in dynamic viscosity with temperature for bitumen and modified bitumens at 10 Hz. In this graph it is clearly seen that addition of SBS and SBS/nanoparticle composite increased the viscosity of bitumen at all temperatures. Bitumen temperature is increased to roughly 150 °C before being paved. The dynamic viscosity of bare bitumen at this temperature is 0.74 Pa.s whereas addition of composite increased the value to 2.93 Pa.s. This increase does not bring any disadvantage in terms of the storing and laying bitumen on roads.
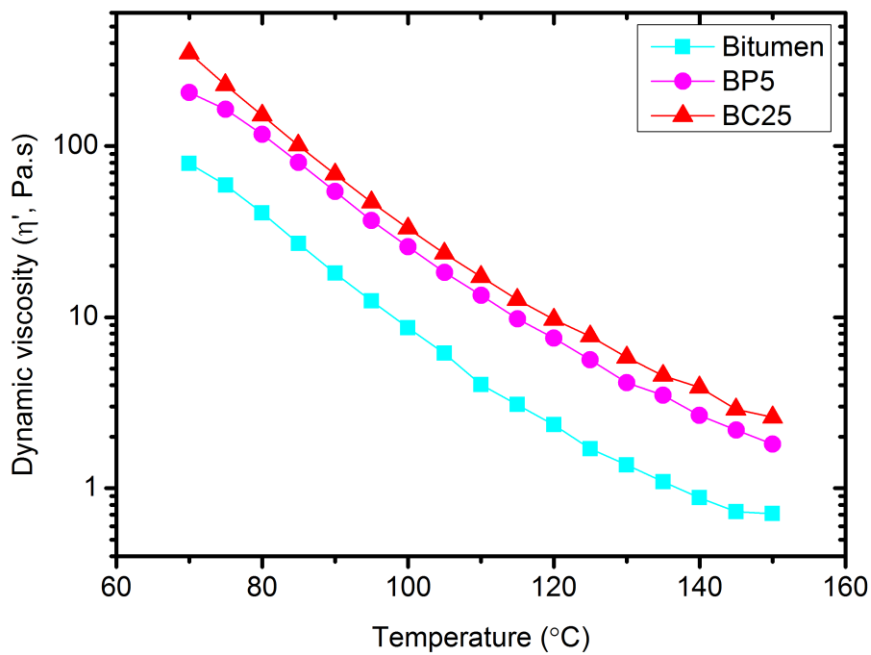
Figure 5.4.1.1.4 Change in dynamic viscosity with temperature for bare bitumen and modified bitumens. Addition of composites increased the viscosity of bitumen at every temperature.

The phase angle of the bitumen and modified bitumens were measured in order to analyze the elasticity of bitumen after modified with composite. Phase angle is the ratio of the viscous modulus to storage modulus (tanδ = G''/G'). Figure 5.4.1.1.5 shows the change in phase angle with respect to increasing temperatures. The addition of SBS decreased the phase angle which means that it increased the elasticity of bitumen. With the addition of nanoparticles the decrease in the phase angles continued. This indicates that elasticity of bitumen increased since tanδ equals to the ratio of G'' to G'. The peak temperature of tanδ is 80 °C for bare bitumen. It increased to 100 °C for SBS modified bitumen and to 125 °C for composite modified bitumen. It shows that the viscosity of bitumen increases and therefore higher temperatures might be required for the pavement.
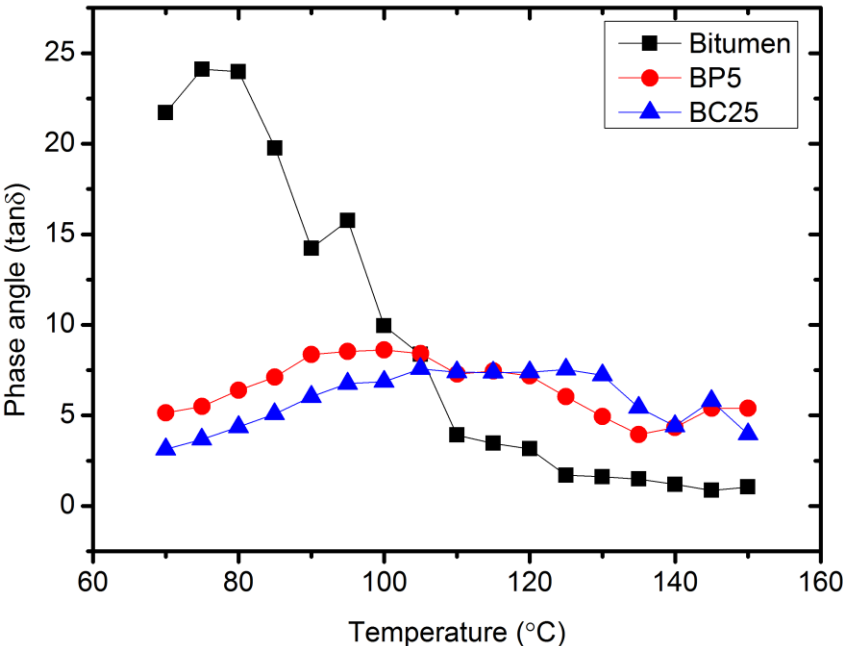
Figure 5.4.1.1.5 Change of phase angle with respect to temperature for bitumen, SBS and composite modified bitumen.

5.3.2 Wettability of polymer/hydrophobic silica nanoparticle-bitumen thin films

To find the effect of composite addition into bitumen on wettability of films we measured water contact angles of the films. Figure 5.3.2.1 shows change in water contact angle with the addition of nanoparticles to constant SBS (pink circles) and bitumen-SBS (green squares) concentrations. Water contact angle of modified bitumen increases slowly compared to SBS/hydrophobic silica nanoparticle composite. It shows that hydrophobic silica nanoparticles are compatible with bitumen and dispersed well in bitumen/SBS solution. Although water contact angle values are lower for the case of modified bitumen, still, coating has micro and nano roughness as seen clearly under optical microscope. The homogeneous formation of thin composite film is expected to delay the freezing of water.
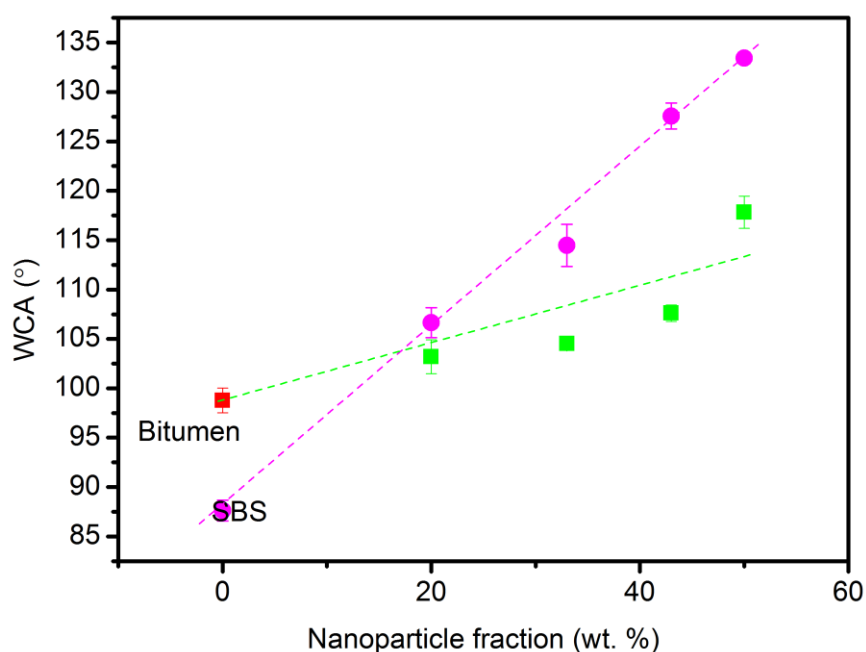
Figure 5.3.2.1 Water contact angles of modified bitumen (green squares) and composite (pink circles). Water contact angle increases slowly with the addition of nanoparticle in case of bitumen. This may indicate that bitumen and hydrophobic silica nanoparticles homogenously mixed in the solution state.

To understand the humidity effect on freezing we put bare bitumen and modified bitumen with varying nanoparticle concentrations in humidity and temperature controlled cell. We increased relative humidity from 30 % to 80 % at − 14 °C plate temperature. Figure 5.3.2.2

shows photographs of the coatings at different relative humidity conditions. From top left to bottom right, it is seen that water condenses on the coatings and freeze. However, freezing pattern differs for different nanoparticle concentrations. At conditions where bitumen surface is completely frozen, nanoparticle coated surfaces display rather less frozen parts. It indicates that even at higher relative humidity conditions, modified bitumen surfaces prevent icing to form on surfaces.
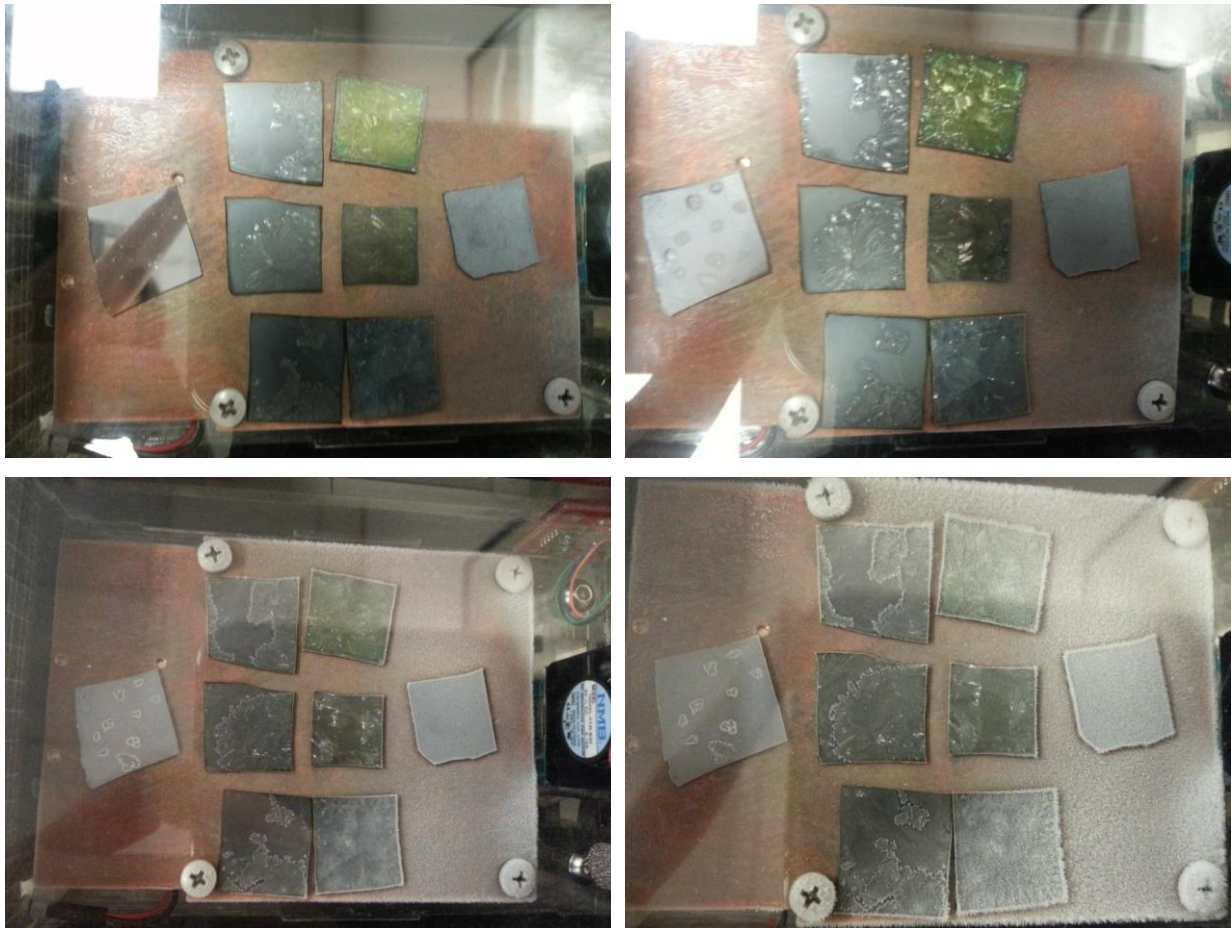
Figure 5.3.2.2 From top right to bottom 40 g/L bitumen, 20 g/L SBS + 40 g/L bitumen, 20%, 33%, 43% and 50% y weight hydrophobic silica coatings. The silicon wafer at right and left is for reference.

5.3.3 Freezing delay on modified bitumen films

Freezing delay ability of the coatings was tested by impinging water droplets having volumes between 3-5 µL. We gave codes to each location where samples were placed. Figure 5.3.3.1 shows the location codes and the photograph from one of the experiments. In order to see whether freezing times have location dependence, each sample were placed in different locations at – 10 °C plate temperature and freezing times for the boundary locations (first row

(A1, B1, C1 and D1) and for the A4 and D4) were recorded. The locations of the samples for three experiments are given in Figure 5.3.3.2. B stands for the bitumen sample and numbers show the mass percentage of nanoparticles in the composites.
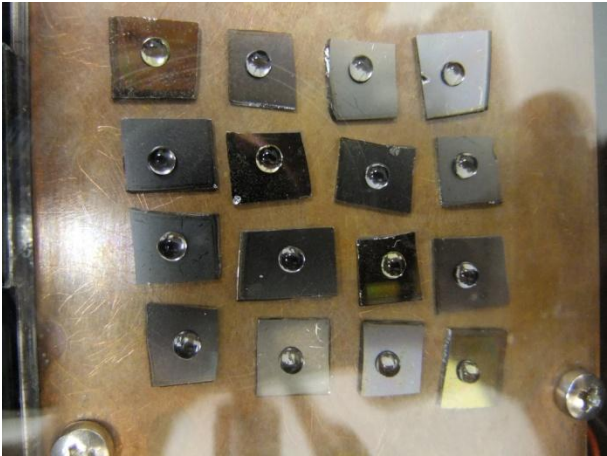
a)   b)

Figure 5.3.3.1 The location codes a) and the photograph of placed samples in the cell b). Each sample was cut into four pieces and placed in the cell.

a)   b)   c)
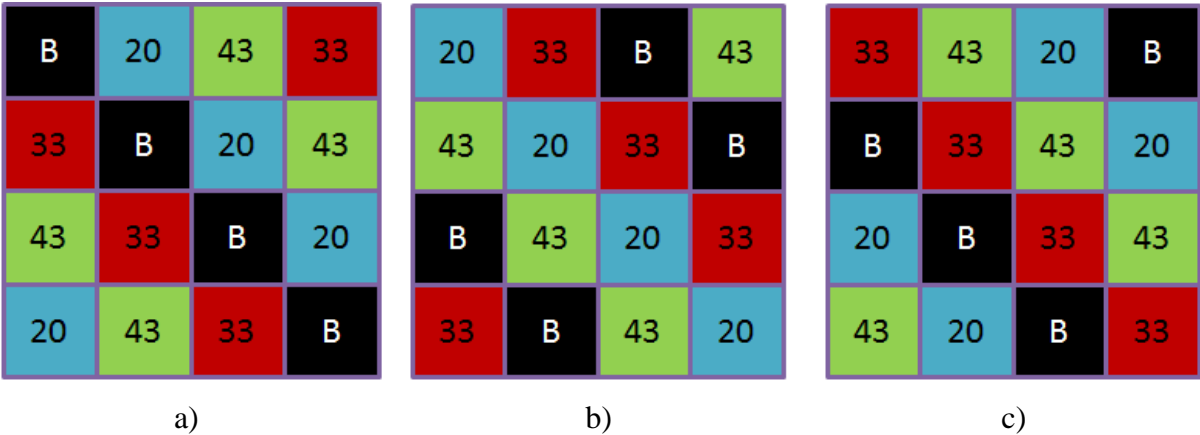
Figure 5.3.3.2 The sample placement for the measurement of location dependence. B stands for bitumen and the numbers indicate percentage of nanoparticle by mass.
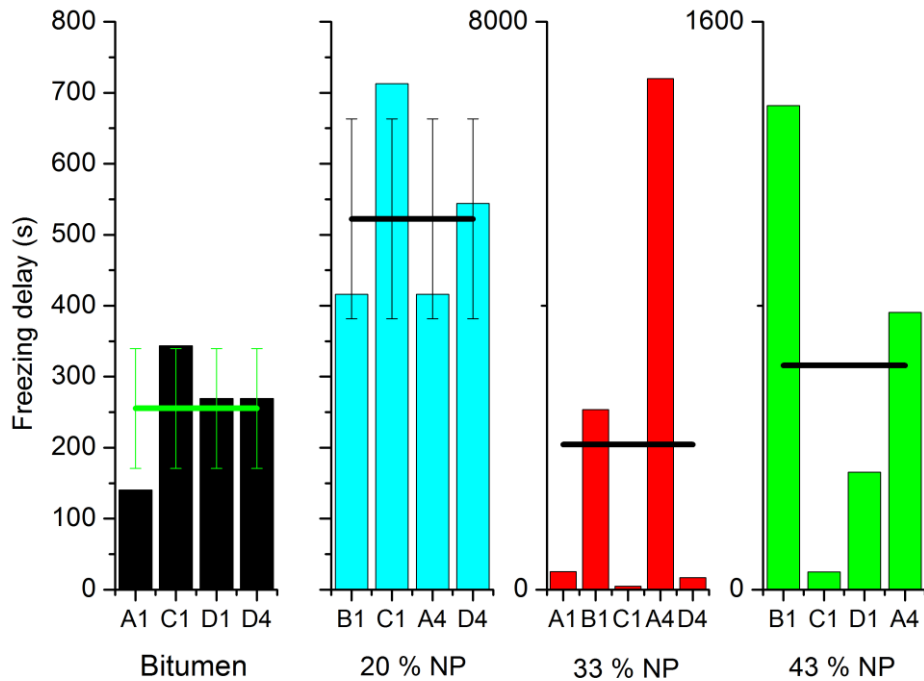
Figure 5.3.3.3 Freezing times of each sample at different locations in the cell. It is seen that the freezing times on bitumen and 20 % nanoparticle coating are not location dependent. The coatings of 33 and 43 % nanoparticle, on the other hand, show scattered results.

The freezing times of each droplet for each sample at different locations are given in Figure 5.3.3.3. It is seen that the freezing times on bitumen and 20 % nanoparticle coating were not location dependent since the standard deviation is in the range. However, for the coatings containing 33 % and 43 % nanoparticle, freezing times scattered. The lines are the mean values of each sample. It is our opinion that the reason of the scatter cannot be the location variance of the coatings. As nanoparticle concentration increase, the surface contains more nanoparticles. So the scatter must reflect the effect of surface morphology on freezing delay.
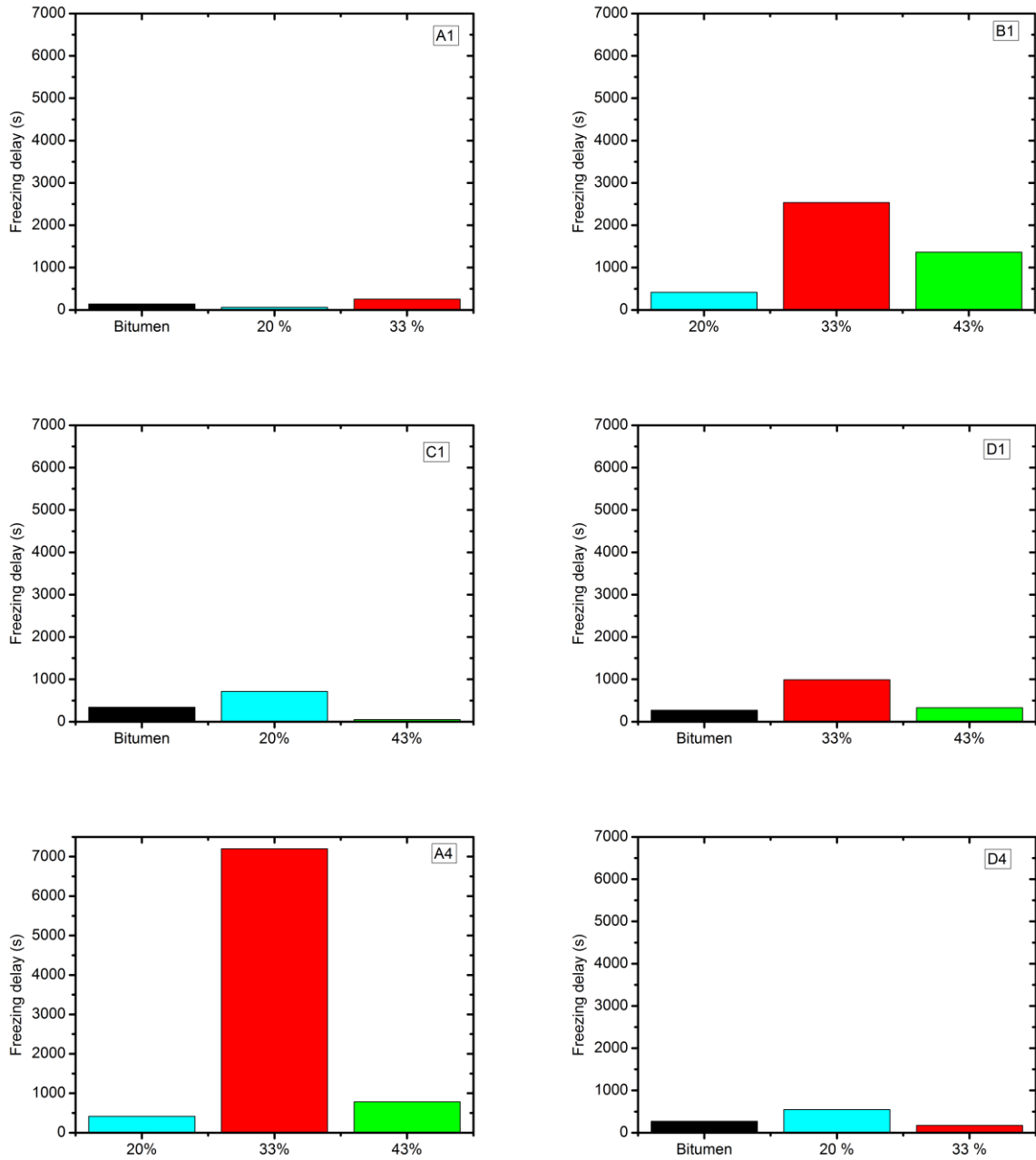
Figure 5.3.3.4 Freezing times of water droplets on each sample with different locations. It is seen that 33 % nanoparticle by mass showed the location dependence whereas other samples gave similar freezing times.

Figure 5.3.3.4 shows the freezing delay graphs of each location. It is seen that 33 % nanoparticle fraction gave the longest delays (~ 7000 s) for the A4 location. Also 20 % nanoparticle gave longer delays compared to bitumen surfaces.

After being sure of the location independence of the coatings we performed freezing experiments at – 8 °C, – 10 °C, – 12 °C and – 15 °C plate temperatures. The air temperature cannot be controlled separately, but by the Peltier element under the plate. The relative humidity values vary between 40 and 50 %. The freezing times for the given plate temperatures are listed below.
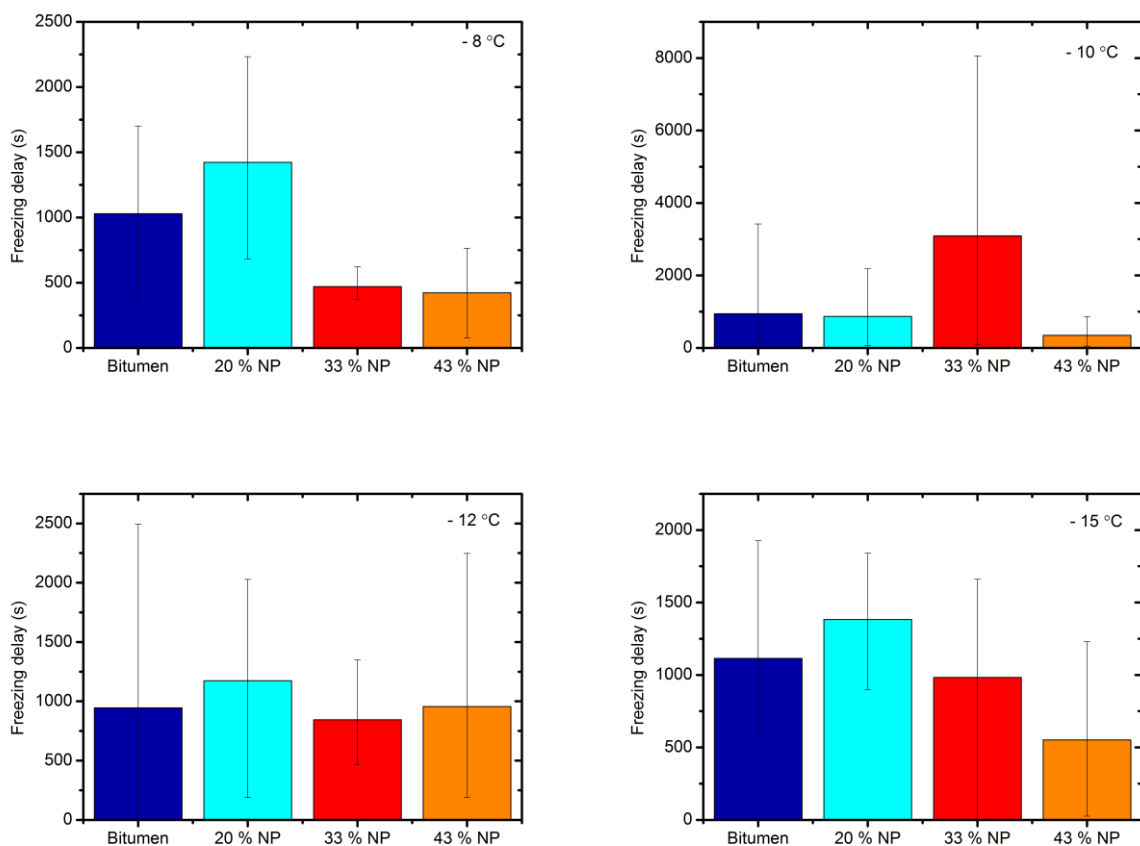
Figure 5.3.3.4 In all of the graphs it is seen that 20 % nanoparticle fraction freezes delayed late than bitumen.

Figure 5.3.3.4 shows the freezing times of all samples at different plate temperatures. Relevant air temperatures and relative humidity values are given below (Table 5.3.3.1). At the plate temperature larger than – 10 °C, 20% and 33 % nanoparticle coatings gave significantly larger freezing times (~ 1500 s at – 8 °C and ~ 4000 s at – 10 °C). At temperatures lower than – 10 °C all samples gave similar freezing times on average. This indicates that the surface

contribution to freezing is negligible at these surface temperatures. The reason is the domination of the homogenous nucleation at these temperatures rather than heterogenous nucleation.

Table 5.3.3.1 Air temperatures and relative humidity values at the times droplets freeze.

PT = - 8 °C	Bitumen	Bitumen + SBS + 20 % NP	Bitumen + SBS + 33 % NP	Bitumen + SBS + 43 % NP
Cell T (°C)	12.2 ± 1.5	12.1 ± 2.0	12.5 ± 2.4	13.2 ± 2.8
Relative Humidity %	42.7 ± 2.3	42.1 ± 3.5	42.2 ± 4.6	41.8 ± 1.7

PT = - 10 °C	Bitumen	Bitumen + SBS + 20 % NP	Bitumen + SBS + 33 % NP	Bitumen + SBS + 43 % NP
Cell T (°C)	7.9 ± 2.7	7.7 ± 2.0	8.4 ± 1.7	8.0 ± 3.1
Relative Humidity %	44.5 ± 7.0	43.8 ± 9.5	47.1 ± 6.4	41.4 ± 8.6

PT = - 12 °C	Bitumen	Bitumen + SBS + 20 % NP	Bitumen + SBS + 33 % NP	Bitumen + SBS + 43 % NP
Cell T (°C)	5.6 ± 2.4	4.9 ± 1.1	4.5 ± 0.4	5.0 ± 0.8
Relative Humidity %	45.5 ± 7.0	48.0 ± 2.7	48.8 ± 1.1	47.5 ± 2.5

PT = - 15 °C	Bitumen	Bitumen + SBS + 20 % NP	Bitumen + SBS + 33 % NP	Bitumen + SBS + 43 % NP
Cell T (°C)	5.2 ± 0.7	5.3 ± 0.7	6.4 ± 2.7	6.2 ± 2.2
Relative Humidity %	46.0 ± 1.2	46.5 ± 0.5	44.1 ± 4.7	42.2 ± 4.0

We also tested freezing delays of coatings between the relative humidity conditions of 20-30 %. We first expected to see the longest freezing time for 43 % by mass nanoparticle sample as we did in composites. Therefore, the experiment with − 15 °C plate temperature and ~ 30 % relative humidity was conducted for 43 % nanoparticle fraction, bare bitumen and silicon. Figure 5.3.3.5 shows the freezing times of coatings at − 15 °C a) and − 8 °C b) plate temperatures. It is seen that for both of the plate temperatures composite modified bitumen showed the longest delay of 800 s for − 15 °C and 3300 s for − 8 °C.

a)   b)
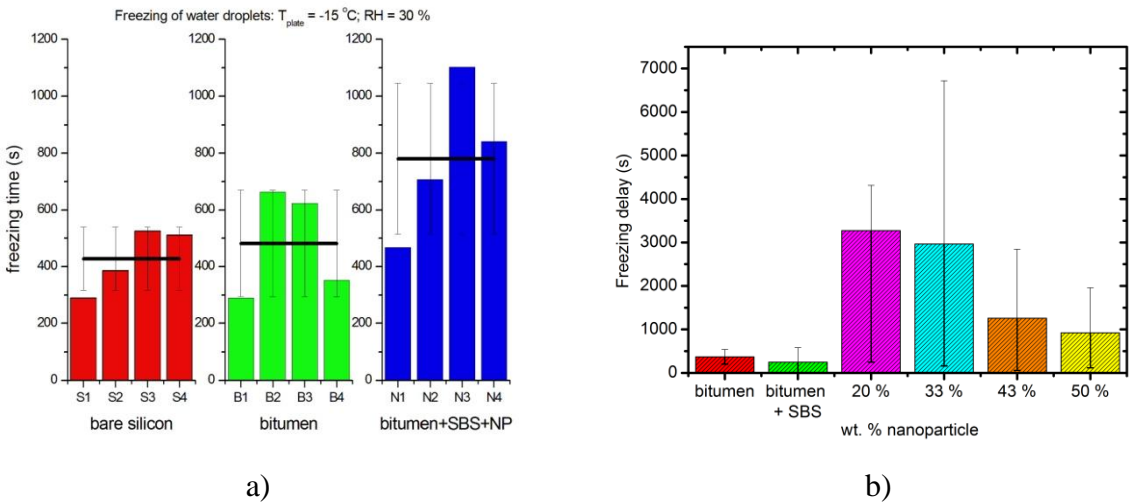
Figure 5.3.3.5 Freezing times of water droplets on bare bitumen and different nanoparticle fraction coatings. a) plate temperatures is − 15 C, relative humidity is ~ 30 % and droplet volume is 3 µL. b) relative humidity is ~ 26 % and cell temperature is ~ 12 °C and droplet volume is 3 µL.

Table 5.3.3.2 Relative humidity and room temperature values for the graph in Figure 5.3.3.1 b)

	Bitumen	Bitumen + SBS	Bitumen + SBS + 20 % NP	Bitumen + SBS + 33 % NP	Bitumen + SBS + 43 % NP	Bitumen + SBS + 50 % NP
T	14.4 ± 0.8	14.1 ± 0.4	14.2 ± 0.4	14.2 ± 0.2	14 ± 0.2	14.1 ± 0.3
H	25.5 ± 1.8	26.5 ± 0.5	26.5 ± 0.6	26.4 ± 1	26.8 ± 0.9	26.2 ± 0.8

0 s

50 s

84 s

140 s

186 s

242 s
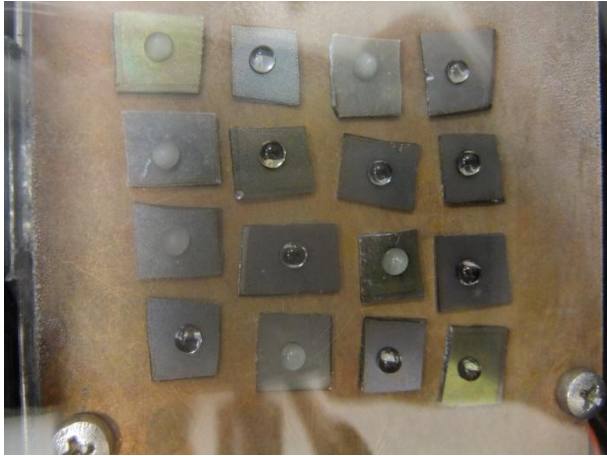
344 s

458 s

606 s

622 s

864 s
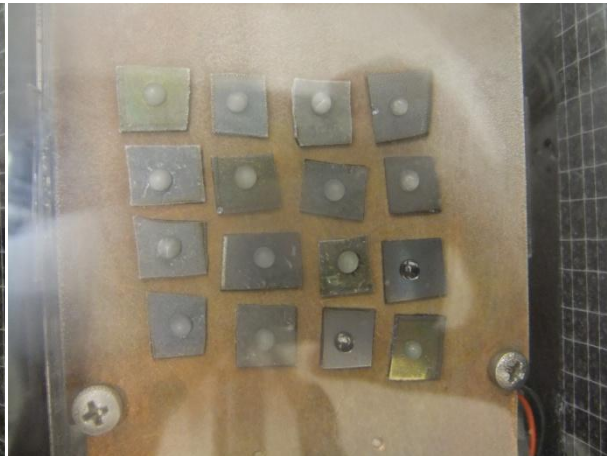
988 s

| 1442 s | 5018 s |
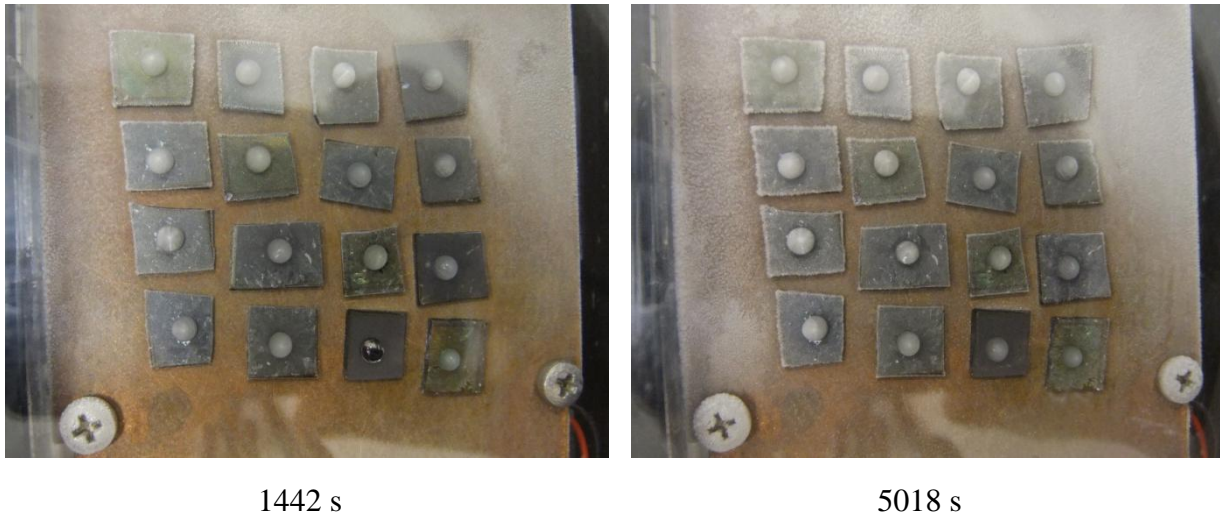
Figure 5.3.3.6 Photographs of droplets freezing for the experiment in which plate temperature was – 10 °C and relative humidity was ~ 50 %.

5.4 Conclusions

SBS/hydrophobic silica nanoparticle thin films that can be used as anti-icing coating on various surfaces were prepared. These surfaces have 145° water contact angle at most for the solvent cast films. We studied humidity effect on coatings and found that condensed air decrease water contact angles. However, our coatings still preserved hydrophobicity. One of the observations is the change in freezing time with the morphological differences of coatings. We found that freezing time changes significantly when the surface morphology evolved from micro-nano roughness to complete cover of nanoparticles. Pronounced surface morphology change occurred when the nanoparticle weight fraction exceeds 43 %. This is the result from the SEM pictures and also indirectly from the contact angle measurements of ethylene glycol and diiodomethane. The concentration just before the transition of morphology change has the longest freezing delay. At – 4 and – 8 °C plate temperatures 43 % nanoparticle by mass gave the longest freezing delay which are 3718 s and 980 s, respectively. There might be an optimum roughness i.e. optimum trapped air between grooves to prevent icing on surfaces.

We included bitumen to SBS/ hydrophobic silica nanoparticles and prepared spin casted thin films as an application part. We first tested the compatibility of composite and bitumen by rheometer. The increase in complex modulus of bitumen showed that addition of composite increases the resistance of bitumen to deformation. Dynamic viscosity and phase angle

measurements showed that inclusion of composite increased the viscosity of the bitumen end therefore higher temperatures might be required for the pavement.

The contact angle values of modified bitumen increased slowly with the nanoparticles. We attributed this tendency to the good compatibility of bitumen and hydrophobic silica nanoparticles. Humidity tests showed that a large part of coatings can become unaffected from the freezing at high humidity conditions. Since the surface morphology changed with the inclusion of bitumen, the effective nanoparticle fraction became 20 % by weight. Freezing experiments were performed at − 8 °C, − 10 °C, − 12 °C and − 15 °C plate temperatures having relative humidity values between 40 and 50 %. The coatings having 20-33 % nanoparticle showed significant freezing delays at the surface temperatures above − 10 °C. However, when the temperature is below − 10 °C no significant freezing delay difference observed among coatings. The homogenous nucleation at these temperatures might dominate and exclude the surface morphology difference of coatings.

When the relative humidity is ~ 20-30 % and the plate temperature is − 8 °C, again the coating having 20-33 % nanoparticle by mass showed the longest delay with 3330 s. These results show that composite modified bitumen is a promising candidate in terms of delaying icing.

CHAPTER VI

CONCLUSIONS

The goal of this work was to prepare novel anti-icing coatings. We divided our work into two tracks of studies. In one track, the effect of two water soluble polymers, PEG and PEOx, on the melting and freezing behavior of water was investigated. By doing this we were able to understand freezing and melting phenomenon of water at the molecular basis. These findings are important to improve the effectiveness of anti-icing coatings for future applications. In other track, silica nanoparticle/SBS composite thin films were prepared successfully for the first time. We analyzed the anti-icing ability of the coatings and later applied to bitumen, the main constituent of road pavement.

For the first track, it was found that aqueous solutions of PEG have low-T endotherm that can later be attributed to the melting of PEG-water complex. The melting temperature of low-T endotherm changed with the molecular weight of PEG. The temperatures of low-T endotherms of PEG-2K, PEG-10K, PEG-100K, PEG-200K and PEG-400K were found to be – 16.6 °C, – 11.1 °C, – 11.6 °C, – 10.6 °C, – 8.03 °C, respectively. It was previously known that DSC heating curves of aqueous solutions of PEG reveals secondary melting peak [69][33] but most of the studies did not include the molecular weight effect or wanted to omit the topic. We found that the temperature of low-T endotherm decreased with decreasing molecular weight of PEG. This finding is promising to use low molecular weight PEG as anti-icing agent in the coatings.

The aqueous solutions of PEOx, on the other hand, did not show low-T endotherm. Rather than that all PEOx solutions including 5K and 50K molecular weights displayed glass transition at around – 26 °C. This observation showed that there was still unfrozen water confined in PEOx chains. At the heating scan of the solutions confined water gave mobility to polymer chains and it was reflected as the glass transition in the DSC curves. No low temperature study of DSC was conducted before for aqueous solutions of PEOx. So, these findings not only helped us to understand water behavior in detail but also might open a new path for researchers to study low-T properties of PEOx aqueous solutions.

Analysis of DSC curves revealed that both PEG and PEOx solutions decrease the melting enthalpy of bulk water which indicates that with the addition of the polymers less ice is

formed. For the aqueous solutions of PEG, some portion of the bulk water became bound to polymer chains and therefore melting enthalpy decreases. We clearly observed this as an increase of melting enthalpy of bound water-PEG complex. Although PEOx solutions also decreased the melting enthalpy of ice, low-T endotherm was not observed. It is our opinion that we were unable to freeze bound water down to -60 °C. The water stayed as bound to polymer but was unable to freeze. Therefore, the melting enthalpy decrease was still observed. The melting enthalpy calculations are present in the literature for aqueous solutions of PEG [29][87] but the relation with the low-T endotherm either do not exist or the relation is unclear. Our work contributed to the elucidation of the relationship between low-T and the 0 °C ice melting endotherms.

The refreezing experiments revealed that PEOx has ability to delay the ice nucleation growth. Also refreezing enthalpies of PEG and PEOx solutions at -1 °C showed that with the addition of polymer more water can coexist with ice indicating that polymers are effective in melting the ice. Comparison of two polymers showed that PEOx is better in terms of melting the ice at -1 °C. The refreezing enthalpy was 163 J/g sample for the concentration of 40 g/L PEOx-50K which is equivalent to 0.008 molal. On the other hand, 40 g/L PEG-10K which is equivalent to 0.04 molal had 140 J/g sample refreezing enthalpy. PEOx, although at five times lower molality had nearly same effectiveness to melt the ice. In our opinion, this is the result of high probability of hydrogen-bonding ability of PEOx monomers. Previously, the same DSC procedure was applied to natural anti-freeze proteins [88] but for the first time it was applied to synthetic polymers and showed promising results regarding of anti-icing effect.

In other track, as a part of anti-icing coatings, we prepared silica nanoparticle/SBS composite thin films for the first time in the literature. By including hydrophobic silica nanoparticles we were able to increase contact angles from 87° to 135° and 145° for the spin cast and solvent cast films, respectively. The surface morphology changed dramatically with the addition of nanoparticle concentration. SEM pictures showed that the surface morphology from 43 % to 50 % by weight nanoparticle showed drastic changes. At 43 % nanoparticle fraction surface contained both micro and nano roughness. But, after 50 %, surface was completely covered with nanoparticles and formed network of nanoparticle rich areas. The control on surface morphology by changing the concentration is reported previously [89]. However, the preparation of silica nanoparticle/SBS composite thin films and the morphology control of these films by concentration have not been studied. Our work filled the gap in the literature and contributed to the preparation of polymer/nanoparticle composites.

On the road to anti-icing coatings, humidity effect on the wettability of coatings was also studied. We concluded that solvent cast films prohibited the water condensed on the surfaces compared to bare surfaces. However, the condensed water still adversely affected the water contact angles of spin cast films. The contact angle was decreased from 132.5° to 100° for 50 % wt. nanoparticle fraction. After studying humidity effect we came to the conclusion that humidity plays great role on the wettability of surfaces even if the surface is hydrophobic. Therefore, the utilization of the anti-icing coatings should be done with great caution.

The freezing experiments on the coatings showed that 43 % nanoparticle fraction gave the longest delay times for the plate temperatures of – 4 °C and – 8 °C. The freezing delays were 3718 s and 980 s for – 4 °C and – 8 °C, respectively. Figure 6.1.1 shows the place of our coating among others. It is clearly seen that our results left behind most of the counterparts.
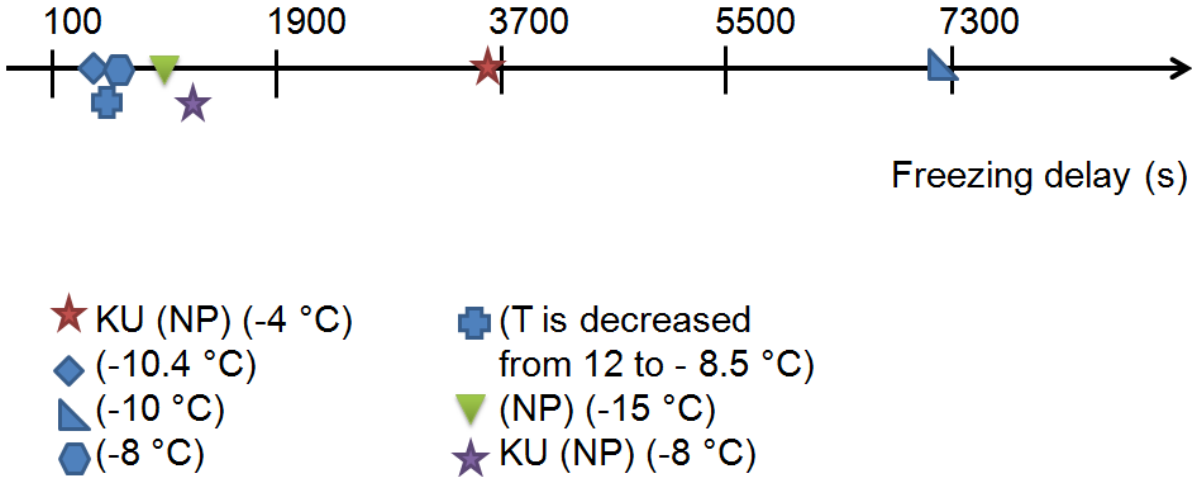
Figure 6.1.1 The freezing delays of our coating and its counterparts. The results are indicative that anti-icing coating was successfully prepared.

SBS/NP composite coatings containing bitumen was successfully prepared as a part of an application. We performed contact angle measurements on the coatings and found that addition of bitumen decreased the water contact angles. The good compatibility between SBS and nanoparticles led to this result. We also saw from rheology measurements that addition of SBS and nanoparticles increased the complex modulus of bitumen. It means that we did not lose the mechanical strength of bitumen while modifying it with anti-icing property.

The freezing delay of the modified bitumen surfaces are 3290 s when the plate temperature is – 8 °C and humidity is 26 % for the 20 % by weight nanoparticle fraction and 1425 s when the plate temperature is again – 8 °C and humidity is 42 %. As we concluded before the

humidity is a crucial factor to determine freezing delays. Additional experiments at higher humidity conditions such as 40-50 % and -8 °C, -10 °C, -12 °C and -15 °C plate temperatures revealed that the coatings having 20-33 % nanoparticle are effective at plate temperatures above -10 °C. Below this temperature coatings lost their property and similar freezing delays were obtained. It is our opinion that homogenous nucleation is the driving force of losing the effect of surface morphology and reason of similar freezing times below -10 °C.

All of these results showed that the inclusion of composite to bitumen functioned the anti-icing property and thus modified bitumen is a good candidate to become a commercial anti-icing product for the surface temperatures above -10 °C. For the temperatures below -10 C, PEG inclusion to modified bitumen might be very successful in delaying the freezing since PEG has ability to make bonds with water and prevent it to freeze until -11 °C.

BIBLIOGRAPHY

[1]   L. Cao, A. K. Jones, V. K. Sikka, J. Wu, and D. Gao, "Anti-icing superhydrophobic coatings," *Langmuir*, vol. 25, no. 21, pp. 12444–8, Nov. 2009.

[2]   S. Farhadi, M. Farzaneh, and S. A. Kulinich, "Anti-icing performance of superhydrophobic surfaces," *Applied Surface Science*, vol. 257, no. 14, pp. 6264–6269, May 2011.

[3]   M. He, J. Wang, H. Li, and Y. Song, "Super-hydrophobic surfaces to condensed micro-droplets at temperatures below the freezing point retard ice/frost formation," *Soft Matter*, vol. 7, no. 8, pp. 3993–4000, 2011.

[4]   M. He, J. J. Wang, H. Li, X. Jin, B. Liu, and Y. Song, "Super-hydrophobic film retards frost formation," *Soft Matter*, vol. 6, no. 11, pp. 2396–2399, 2010.

[5]   R. Jafari, R. Menini, and M. Farzaneh, "Superhydrophobic and icephobic surfaces prepared by RF-sputtered polytetrafluoroethylene coatings," *Applied Surface Science*, vol. 257, no. 5, pp. 1540–1543, Dec. 2010.

[6]   Z. Liu, Y. Gou, J. Wang, and S. Cheng, "Frost formation on a super-hydrophobic surface under natural convection conditions," *International Journal of Heat and Mass Transfer*, vol. 51, no. 25–26, pp. 5975–5982, Dec. 2008.

[7]   P. Tourkine, M. Le Merrer, and D. Quéré, "Delayed freezing on water repellent materials," *Langmuir*, vol. 25, no. 13, pp. 7214–7216, Jul. 2009.

[8]   S. a Kulinich, S. Farhadi, K. Nose, and X. W. Du, "Superhydrophobic surfaces: are they really ice-repellent?," *Langmuir*, vol. 27, no. 1, pp. 25–29, Jan. 2011.

[9]   S. Jung, M. Dorrestijn, D. Raps, A. Das, C. M. Megaridis, and D. Poulikakos, "Are superhydrophobic surfaces best for icephobicity?," *Langmuir*, pp. 3059–3066, Feb. 2011.

[10]   A. L. DeVries, "Glycoproteins as biological antifreeze agents in antarctic fishes," *Science*, vol. 172, no. 3988, pp. 1152–1155, Jun. 1971.

[11]   A. L. DeVries and D. E. Wohlschlag, "Freezing resistance in some antarctic fishes," *Science*, vol. 163, no. 3871, pp. 1073–1075, Mar. 1969.

[12]   E. Baruch and Y. Mastai, "Antifreeze properties of polyglycidol block copolymers," *Macromolecular Rapid Communications*, vol. 28, no. 23, pp. 2256–2261, Oct. 2007.

[13]   P. L. Davies and C. L. Hew, "Biochemistry of fish antifreeze proteins.," *FASEB journal : official publication of the Federation of American Societies for Experimental Biology*, vol. 4, no. 8, pp. 2460–2468, May 1990.

[14]   M. Gibson, "Slowing the growth of ice with synthetic macromolecules: beyond antifreeze(glyco) proteins," *Polymer Chemistry*, vol. 1, no. 8, p. 1141, 2010.

[15]   H. Cölfen, "Double-hydrophilic block copolymers: Synthesis and application as novel surfactants and crystal growth modifiers," *Macromolecular Rapid Communications*, vol. 22, no. 4, pp. 219–252, Feb. 2001.

[16] Y. E. Yagci, M. Antonietti, and H. G. Börner, "Synthesis of Poly(tartar amides) as Bio-Inspired Antifreeze Additives," *Macromolecular Rapid Communications*, vol. 27, no. 19, pp. 1660–1664, Oct. 2006.

[17] C. a Knight, C. C. Cheng, and A. L. DeVries, "Adsorption of alpha-helical antifreeze peptides on specific ice crystal surface planes," *Biophysical journal*, vol. 59, no. 2, pp. 409–18, Feb. 1991.

[18] C. a Knight, E. Driggers, and a L. DeVries, "Adsorption to ice of fish antifreeze glycopeptides 7 and 8.," *Biophysical journal*, vol. 64, no. 1, pp. 252–9, Jan. 1993.

[19] J. A. Raymond and A. L. DeVries, "Adsorption inhibition as a mechanism of freezing resistance in polar fishes," *PNAS*, vol. 74, no. 6, pp. 2589–93, Jun. 1977.

[20] A. L. DeVries, S. K. Komatsu, and R. E. Feeney, "Chemical and physical properties of freezing point depressing glycoproteins from Antarctic Fishes," *The Journal of biological chemistry*, vol. 245, no. 11, pp. 2901–2908, Jun. 1970.

[21] J. a Raymond, P. Wilson, and A. L. DeVries, "Inhibition of growth of nonbasal planes in ice by fish antifreezes," *Proceedings of the National Academy of Sciences of the United States of America*, vol. 86, no. 3, pp. 881–5, Feb. 1989.

[22] Y. Tachibana, G. L. Fletcher, N. Fujitani, S. Tsuda, K. Monde, and S. Nishimura, "Antifreeze glycoproteins: elucidation of the structural motifs that are essential for antifreeze activity.," *Angewandte Chemie (International ed. in English)*, vol. 43, no. 7, pp. 856–62, Feb. 2004.

[23] Z. Jia and P. L. Davies, "Antifreeze proteins: an unusual receptor-ligand interaction.," *Trends in biochemical sciences*, vol. 27, no. 2, pp. 101–6, Feb. 2002.

[24] J. G. Duman and A. L. DeVries, "Freezing behavior of aqueous solutions of glycoproteins from the blood of an Antarctic fish," *Cryobiology*, vol. 9, no. 5, pp. 469–472, Oct. 1972.

[25] M. Gibson, C. A. Barker, S. G. Spain, L. Albertin, and N. R. Cameron, "Inhibition of ice crystal growth by synthetic glycopolymers: Implications for the rational design of antifreeze glycoprotein mimics.," *Biomacromolecules*, vol. 10, no. 2, pp. 328–33, Feb. 2009.

[26] C. Budke and T. Koop, "Ice recrystallization inhibition and molecular recognition of ice faces by poly(vinyl alcohol)," *Chemphyschem*, vol. 7, no. 12, pp. 2601–6, Dec. 2006.

[27] B. Wowk, E. Leitl, C. M. Rasch, N. Mesbah-Karimi, S. B. Harris, and G. M. Fahy, "Vitrification enhancement by synthetic ice blocking agents," *Cryobiology*, vol. 40, no. 3, pp. 228–236, May 2000.

[28] A. Hillgren and M. Alde, "Differential Scanning Calorimetry Investigation of Formation of Poly (ethylene glycol) Hydrate with Controlled Freeze – Thawing of Aqueous Protein Solution," 2013.

[29] B. S. Bhatnagar, S. M. Martin, D. L. Teagarden, E. Y. Shalaev, and R. A. J. Suryanarayanan, "Investigation of PEG Crystallization in Frozen PEG – Sucrose – Water Solutions : II . Characterization of the Equilibrium Behavior During Freeze-Thawing," vol. 99, no. 11, pp. 2609–2619, 2010.

[30]   T. Inada, T. Koyama, F. Goto, and T. Seto, "Inactivation of ice nucleating activity of silver iodide by antifreeze proteins and synthetic polymers.," *The journal of physical chemistry. B*, vol. 116, no. 18, pp. 5364–71, May 2012.

[31]   L. Huang and K. Nishinari, "Interaction between poly(ethylene glycol) and water as studied by differential scanning calorimetry," *Journal of Polymer Science Part B: Polymer Physics*, vol. 39, no. 5, pp. 496–506, Mar. 2001.

[32]   R. W. Michelmore and F. Franks, "Nucleation rates of ice in undercooled water and aqueous solutions of polyethylene glycol," *Cryobiology*, vol. 19, no. 2, pp. 163–171, Apr. 1982.

[33]   T. De Vringer, J. G. H. Joostenl, and H. E. Junginger, "A study of the hydration of polYoxyethylene _ at low temperatures by differential scanning calorimetry," vol. 630, pp. 623–630, 1986.

[34]   Z. Liu, X. Zhang, H. Wang, S. Meng, and S. Cheng, "Influences of surface hydrophilicity on frost formation on a vertical cold plate under natural convection conditions," *Experimental Thermal and Fluid Science*, vol. 31, no. 7, pp. 789–794, Jul. 2007.

[35]   Z. Liu, Y. Gou, J. Wang, and S. Cheng, "Frost formation on a super-hydrophobic surface under natural convection conditions," *International Journal of Heat and Mass Transfer*, vol. 51, no. 25–26, pp. 5975–5982, Dec. 2008.

[36]   H. Wang, L. Tang, X. Wu, W. Dai, and Y. Qiu, "Fabrication and anti-frosting performance of super hydrophobic coating based on modified nano-sized calcium carbonate and ordinary polyacrylate," *Applied Surface Science*, vol. 253, no. 22, pp. 8818–8824, Sep. 2007.

[37]   M. He, J. Wang, H. Li, X. Jin, J. Wang, B. Liu, and Y. Song, "Super-hydrophobic film retards frost formation," *Soft Matter*, vol. 6, no. 11, pp. 2396–2399, 2010.

[38]   L. Cao, A. K. Jones, V. K. Sikka, J. Wu, and D. Gao, "Anti-icing superhydrophobic coatings.," *Langmuir : the ACS journal of surfaces and colloids*, vol. 25, no. 21, pp. 12444–8, Nov. 2009.

[39]   L. Yin, Q. Xia, J. Xue, S. Yang, Q. Wang, and Q. Chen, "In situ investigation of ice formation on surfaces with representative wettability," *Applied Surface Science*, vol. 256, no. 22, pp. 6764–6769, Sep. 2010.

[40]   R. Karmouch and G. G. Ross, "Experimental study on the evolution of contact angles with temperature near the freezing point," *The Journal of Physical Chemistry C*, vol. 114, no. 9, pp. 4063–4066, Mar. 2010.

[41]   A. Alizadeh, M. Yamada, R. Li, W. Shang, S. Otta, S. Zhong, L. Ge, A. Dhinojwala, K. R. Conway, V. Bahadur, A. J. Vinciquerra, B. Stephens, and M. L. Blohm, "Dynamics of ice nucleation on water repellent surfaces," *Langmuir*, vol. 28, no. 6, pp. 3180–6, Feb. 2012.

[42]   S. Suzuki, A. Nakajima, N. Yoshida, M. Sakai, A. Hashimoto, Y. Kameshima, and K. Okada, "Freezing of water droplets on silicon surfaces coated with various silanes," *Chemical Physics Letters*, vol. 445, no. 1–3, pp. 37–41, Sep. 2007.

[43]   L. Zheng, Z. Li, S. Bourdo, K. R. Khedir, M. P. Asar, C. C. Ryerson, and A. S. Biris, "Exceptional superhydrophobicity and low velocity impact icephobicity of acetone-functionalized carbon nanotube films," *Langmuir : the ACS journal of surfaces and colloids*, vol. 27, no. 16, pp. 9936–43, Aug. 2011.

[44] H. Mei, D. Luo, P. Guo, C. Song, C. Liu, Y. Zheng, and L. Jiang, "Multi-level micro-/nanostructures of butterfly wings adapt at low temperature to water repellency," *Soft Matter*, vol. 7, no. 22, pp. 10569–10573, 2011.

[45] P. Guo, Y. Zheng, M. Wen, C. Song, Y. Lin, and L. Jiang, "Icephobic/anti-icing properties of micro/nanostructured surfaces," *Advanced materials*, vol. 24, no. 19, pp. 2642–2648, Apr. 2012.

[46] P. Guo, Y. Zheng, M. Wen, C. Song, Y. Lin, and L. Jiang, "Supporting information of icephobic/anti-icing properties of micro/nanostructured surfaces," *Advanced materials*, 2012.

[47] A. J. Meuler, J. D. Smith, K. K. Varanasi, J. M. Mabry, G. H. McKinley, and R. E. Cohen, "Relationships between water wettability and ice adhesion," *ACS Applied Materials & Interfaces*, vol. 2, no. 11, pp. 3100–10, Nov. 2010.

[48] A. Dotan, H. Dodiuk, C. Laforte, and S. Kenig, "The relationship between water wetting and ice adhesion," *Journal of Adhesion Science and Technology*, vol. 23, no. 15, pp. 1907–1915, Sep. 2009.

[49] S. A. Kulinich and M. Farzaneh, "How wetting hysteresis influences ice adhesion strength on superhydrophobic surfaces," *Langmuir*, vol. 25, no. 16, pp. 8854–8856, Aug. 2009.

[50] L. Mishchenko, B. Hatton, V. Bahadur, J. A. Taylor, T. Krupenkin, and J. Aizenberg, "Design of ice-free nanostructured surfaces based on repulsion of impacting water droplets," *ACS Nano*, vol. 4, no. 12, pp. 7699–7707, Dec. 2010.

[51] D. K. Sarkar and M. Farzaneh, "Superhydrophobic coatings with reduced ice adhesion," *Journal of Adhesion Science and Technology*, vol. 23, no. 9, pp. 1215–1237, Jun. 2009.

[52] S. A. Kulinich and M. Farzaneh, "Ice adhesion on super-hydrophobic surfaces," *Applied Surface Science*, vol. 255, no. 18, pp. 8153–8157, Jun. 2009.

[53] K. K. Varanasi, T. Deng, J. D. Smith, M. Hsu, and N. Bhate, "Frost formation and ice adhesion on superhydrophobic surfaces," *Applied Physics Letters*, vol. 97, no. 23, p. 234102, 2010.

[54] S. A. Kulinich, S. Farhadi, K. Nose, and X. W. Du, "Superhydrophobic surfaces: Are they really ice-repellent?," *Langmuir*, vol. 27, no. 1, pp. 25–9, Jan. 2011.

[55] S. A. Kulinich and M. Farzaneh, "On ice-releasing properties of rough hydrophobic coatings," *Cold Regions Science and Technology*, vol. 65, no. 1, pp. 60–64, Jan. 2011.

[56] J. F. Rabolt and M. Carlo, "Application Issues for in Structure Spin-Cast Thin and Polymer Ultrathin Films," vol. 273, no. 5277, pp. 912–915, 2012.

[57] H. Butt, K. Graf, and M. Kappl, *Physics and Chemistry of Interfaces*. Weinheim, FRG: Wiley-VCH Verlag GmbH & Co. KGaA, 2003.

[58] P. Atkins and J. D. E. Paula, *CHEMISTRY*. .

[59] A. I. Norman, Y. Fei, D. L. Ho, and S. C. Greer, "Folding and Unfolding of Polymer Helices in Solution," *Macromolecules*, vol. 40, no. 7, pp. 2559–2567, Apr. 2007.

[60] P. Tatar Güner and A. L. Demirel, "Effect of anions on the cloud point temperature of aqueous poly(2-ethyl-2-oxazoline) solutions," *The journal of physical chemistry B*, vol. 116, no. 49, pp. 14510–4, Dec. 2012.

[61] P. W. Wilson, J. W. Arthur, and A. D. J. Haymet, "Ice premelting during differential scanning calorimetry," *Biophysical Journal*, vol. 77, no. 5, pp. 2850–2855, Nov. 1999.

[62] B. a. Miller-Chou and J. L. Koenig, "A review of polymer dissolution," *Progress in Polymer Science*, vol. 28, no. 8, pp. 1223–1270, Aug. 2003.

[63] F. Meeussen, Y. Bauwens, R. Moerkerke, E. Nies, and H. Berghmans, "Molecular complex formation in the system poly(vinyl methyl ether)/water," *Polymer*, vol. 41, no. 10, pp. 3737–3743, May 2000.

[64] J. Zhang, B. Berge, F. Meeussen, and E. Nies, "Influence of the Interactions in Aqueous Mixtures of Poly (vinyl methyl ether) on the Crystallization Behavior of Water," pp. 9145–9153, 2003.

[65] C. J. Capicciotti, M. Doshi, and R. N. Ben, "Ice Recrystallization Inhibitors : From Biological Antifreezes to Small Molecules," 2013.

[66] T. Hatakeyama, H. Kasuga, M. Tanaka, and H. Hatakeyama, "Cold crystallization of poly(ethylene glycol)–water systems," *Thermochimica Acta*, vol. 465, no. 1–2, pp. 59–66, Dec. 2007.

[67] T. Nakaoki and H. Yamashita, "Bound states of water in poly(vinyl alcohol) hydrogel prepared by repeated freezing and melting method," *Journal of Molecular Structure*, vol. 875, no. 1–3, pp. 282–287, Mar. 2008.

[68] "Read on Feb 4th 2013 . Very nice review on bound water . Interaction between water and hydrophilic polymers l oda sıcakligi ne," vol. 1, no. 97, 2013.

[69] Z. H. Ping, Q. T. Nguyen, S. M. Chen, J. Q. Zhou, and Y. D. Ding, "States of water in different hydrophilic polymers Ð DSC and FTIR studies," vol. 42, no. 2001, 2012.

[70] J. Wolfe, G. Bryant, and K. L. Koster, "What is 'unfreezable water', how unfreezable is it, and how much is there?," *Cryo letters*, vol. 23, no. 3, pp. 157–66, 2002.

[71] S. L. Hager, T. B. Macrury, and U. C. Corporation, "Investigation of Phase Behavior and Water Binding in Poly (alkylene Oxide) Solutions," vol. 25, pp. 1559–1571, 1980.

[72] a. Herrera-Gómez, G. Velázquez-Cruz, and M. O. Martín-Polo, "Analysis of the water bound to a polymer matrix by infrared spectroscopy," *Journal of Applied Physics*, vol. 89, no. 10, p. 5431, 2001.

[73] F. Meeussen, Y. Bauwens, R. Moerkerke, E. Nies, and H. Berghmans, "Molecular complex formation in the system poly(vinyl methyl ether)/water," *Polymer*, vol. 41, no. 10, pp. 3737–3743, May 2000.

[74] M. Nagura, N. Takagi, and H. Katakami, "States of water in poly (viny1 alcohol) hydrogels," vol. 5, no. 1997, pp. 455–468, 1998.

[75] P. T. Güner, A. Mikó, F. F. Schweinberger, and a. L. Demirel, "Self-assembled poly(2-ethyl-2-oxazoline) fibers in aqueous solutions," *Polymer Chemistry*, vol. 3, no. 2, p. 322, 2012.

[76] H. Schlaad, C. Diehl, A. Gress, M. Meyer, a L. Demirel, Y. Nur, and A. Bertin, "Poly (2-oxazoline) s as Smart Bioinspired Polymers," *Macromolecular rapid communications*, vol. 31, no. 6, pp. 511–525, Mar. 2010.

[77] M. L. Huang, D. Ehre, Q. Jiang, C. Hu, K. Kirshenbaum, and M. D. Ward, "Biomimetic peptoid oligomers as dual-action antifreeze agents.," *Proceedings of the National Academy of Sciences of the United States of America*, vol. 109, no. 49, pp. 19922–7, Dec. 2012.

[78] C. Antonini, M. Innocenti, T. Horn, M. Marengo, and a. Amirfazli, "Understanding the effect of superhydrophobic coatings on energy reduction in anti-icing systems," *Cold Regions Science and Technology*, vol. 67, no. 1–2, pp. 58–67, Jun. 2011.

[79] T. Young, "An Essay on the Cohesion of Fluids," *Philosophical Transactions of the Royal Society of London*, vol. 95, pp. 65–87, Jan. 1805.

[80] X. Li, Y. Han, and L. An, "Surface Morphology Evolution of Thin Triblock Copolymer," no. 7, pp. 5293–5298, 2002.

[81] R. N. Wenzel, "Resistance of Solid Surfaces to Wetting by Water," *Industrial & Engineering Chemistry*, vol. 28, no. 8, pp. 988–994, Aug. 1936.

[82] A. B. D. Cassie and S. Baxter, "Wettability of porous surfaces," *Transactions of the Faraday Society*, vol. 40, no. 5, p. 546, 1944.

[83] A. W. Adamson and A. P. Gast, *Physical chemistry of surfaces*, 6th ed. New York, USA: John Wiley & Sons, Inc., 1997, p. 804.

[84] L. Huang, Z. Liu, Y. Liu, Y. Gou, and L. Wang, "Effect of contact angle on water droplet freezing process on a cold flat surface," *Experimental Thermal and Fluid Science*, vol. 40, pp. 74–80, Jul. 2012.

[85] G. Airey, "Rheological properties of styrene butadiene styrene polymer modified road bitumens," *Fuel*, vol. 82, no. 14, pp. 1709–1719, Oct. 2003.

[86] X. Lu and P. Redelius, "SBS Modified Bitumens : Does Their Morphology and Storage Stability Influence Asphalt Mix Performance ?"

[87] K. Pielichowski and K. Flejtuch, "Differential Scanning Calorimetry Studies on Poly (ethylene Glycol) with Different Molecular Weights for Thermal Energy Storage Materials †," vol. 696, no. February 2002, pp. 690–696, 2003.

[88] J. G. Boast, "Differential scanning calorimetric analys | s of antifreeze protein activity in the common mealworm , Tenebrio molitor," vol. 957, pp. 217–221, 1988.

[89] S. S. Latthe and A. L. Demirel, "Polystyrene/octadecyltrichlorosilane superhydrophobic coatings with hierarchical morphology," *Polymer Chemistry*, vol. 4, no. 2, p. 246, 2013.

VITA

Bilge Ercan was born in 1989 in Istanbul, Turkey. She received BSc degree in Chemistry and minor in Anthropology in 2011 from Hacettepe University in Ankara, Turkey. In same year, she started MSc in Materials Science and Engineering program in Koc University. After completing her MSc, Bilge is going to pursue a PhD in Chemistry at National University of Singapore with a concentration in biochemistry of the bacterial membrane formation mechanism.